Unione Europea

Ministero dell'Istruzione
dell'Università e della Ricerca

Università degli
Studi di Palermo

Tesi Di Dottorato

Environmental Noise in Classical and Quantum Systems

Rumore Ambientale in Sistemi classici e Quantistici

Dottorando

Angelo La Cognata

Tutor

Prof. Bernardo Spagnolo

Coordinatore

Prof. Bernardo Spagnolo

SSD: ***Fis03***

Università degli Studi di Palermo
Dipartimento di Fisica

Corso di DOTTORATO INTERNAZIONALE DI RICERCA
in FISICA APPLICATA (XXII CICLO) – 2011

To all whom the science
attracts them, destroys them and abandons them
To all whom the science
makes them happy, deceives them and embitters them
To all whom the science
enlightens them, warms them and raises them
To all who are finding in science
the lymph of their life.

Acknowledgements

My first and sincere thank for the transmission of knowledge and scientific curiosity, goes to my tutor professor Bernardo Spagnolo. Without his organizational skills and contacts with the multidisciplinary scientific community I would not have had the opportunity to exploit my abilities as a researcher. Soon after, I would like to thank Davide Valenti, for his endless willingness to support me from a technical and scientific point of view. Thanks to him I have become able to develop and carry out various researching reported in this thesis. I wish to thanks also professor Alexander Dubkov of Nizhniy-Novgorod University and professor Giuseppe Falci of Catania University for fruitful scientific discussions on the topic of this thesis. Then I would like remind my fellows who have been tackling with me this PhD experience for three years, beginning with Pasquale Caldara. He has been an irreplaceable colleague whom I have debated on many topics with (not only on physics), and I have established a strong friendship with him. Continuing with the young promise of physics research Stefano Spezia, who had been a budding engineer when he started the PhD studies and now he knows more things than a physicist. I would like to thank Giovanni Denaro too, because he has been a guiding light in my labor struggle and he will be the next PhD student of professor Spagnolo. I would like to mention together with Pasquale Caldara, the other XXII-cicle's colleagues, Rosita Barraco and Giuseppe Cannella, whom I have shared the tough exam preparations of PhD with and all the seminar and post seminar moments. I would like to extend my thanks to all DIFTER's colleagues I have shared something with, beginning from Giuseppe Augello, who has been my tireless fellow of swimming, following with Nicola Pizzolato, Dominique Persano Adorno, Luciano Curcio, Davide Gurrera, Fabio Vizzini, Rosario Grammauta, Francesca Alberghina, Anna Longo and Benedetto Schiavo. A special thank goes to Maria Antonietta Lodato for her inexhaustible tenacity against the daily challenges. Finally I would like to cuddle the love of my life for the moral supports during the most dramatic moments of my PhD.

Commonly Used Abbreviations

Stochastic Differential Equation - SDE
Fokker-Planck equation - FPE
Fractional Fokker-Planck equation - FFPE
Probability Density Functions - PDFs
Mean First Passage Time - MFPT
Nonlinear Relaxation Time - NLRT
Noise Enhanced Stability - NES
Stochastic Resonance - SR
Signal-to-Noise Ratio - SNR
Spectral Power Amplification - SPA (in Chapter 2)
Single Path Approximation - SPA (in Chapter 3)
Stimulated Raman Adiabatic Passage - STIRAP
Discrete Variable Representation - DVR
Feynman-Vernon functional - FV functional
Non-Interacting Cluster Approximation - NICA
Rotating-Wave Approximation - RWA

Contents

Introduction

In the last two decades, complexity is bringing biology together with mathematics, engineering, computer science and physics in an interdisciplinary interest. The complexity is one of the most exciting and fast growing branches of modern science. This research area is at the forefront in interdisciplinary research and it has an increasingly important impact on a variety of applied subjects ranging from the study of turbulence and the behavior of the weather, through the investigation of electrical and mechanical oscillations in macroscopic system physics and the emergence of ordered structures in condensed matter physics, to the physics of nano-structures and nano-devices, and to the analysis of biological and economic phenomena. Complex system behavior cannot be predicted by standard deterministic linear equations and their properties are not fully explained by an understanding of its interacting components parts. These systems can be modelled as open systems in which the interaction between the components is nonlinear and the interaction with the environment is noisy. This intrinsic nonlinearity can give rise to the complex behavior of the system, which becomes very sensitive to initial conditions, various deterministic external perturbations, and to fluctuations always present in nature. The performance of any complex system depends on a correct information exchange between its components. In most natural systems, a signal carrying informations is often mixed with noise. The comprehension of noise role in the dynamics of nonlinear systems plays a key aspect in the efforts devoted to understand and model so-called complex systems. Understanding of biological systems indeed may be enhanced by analysis of their complex nature. One approach to understanding the complexity is to start with a conceptually simple view of the system and add details that introduce new levels of complexity. In general the effects of small perturbations and noise, which is ubiquitous in real systems, can be quite difficult to predict and often yield counterin-

tuitive behavior. Transport in ion-channels, synchronization/coherence in biological extended systems, virus propagation, forecasting protocols are just a few examples that illustrate the subtle beneficial synergy between noise and nonlinearity. Complex systems may have extremely rich coherent dynamics due to the environmental noise and, in specific points of their phase space, are extremely sensitive to external perturbations.

Usually the contamination by the noise makes it difficult to detect signals, but in some cases noise induced effects known as *stochastic resonance*, *resonant activation* and *noise enhanced stability* improve conditions for signal detection when noise and system parameters become optimal [1]-[4]. Moreover the noise through its interaction with the nonlinearity of the system can give rise to new phenomena such as *noise induced transitions* [5] *noise delayed extinction*, *temporal oscillations* [6] and *spatial patterns* [7]. The combined action of external deterministic or random driving forces and the environmental noise can given rise to new phenomena with a rich scenario of far-from equilibrium effects. To describe complex systems, it is in fact fundamental to understand the interplay between noise, periodic and random driving forces and the intrinsic nonlinearity of the system itself [8].

Two kinds of motions can easily be observed in Nature: smooth, regular and quasi-regular motion, like Newtonian motion of planets, and random, highly irregular motion, like Brownian motion of small specks of dust in the air. The first kind of motion can be predicted and consequently, described in the frame of deterministic approach. The second one demands the statistical approach [9]. The idea of an effective stochastic motion of a particle in a surrounding heat bath has been a triumph of statistical approach of complex systems. The description of Brownian motion in Einstein's work of 1905 relies on the assumption of the existence of a time-interval τ , such that the particle's motion during different τ-intervals is independent. The coarse-grained version of this motion leads then to the known diffusion equation. Classical Brownian motion of a particle is distinguished by the linear growth of the mean-square displacement of its position coordinate x,

$$\langle x^2(t)\rangle \propto t.$$

However, in many cases the Einstein's assumption is violated, and many systems exhibit deviations from the linear time dependence. Often, a nonlinear scaling of

the form

$$\langle x^2(t)\rangle \propto t^s$$

is observed. In the last 15 years, this type of diffusion, named *anomalous diffusion* is being used to describe several phenomena observed in complex systems. From a probability theory point view, such behavior corresponds to the limiting distribution of the sum of positive, independent and identically distributed random variables [10]. The noise source generated by this random variable give rises to the Lévy motion, characterized by Lévy flights, that is extremely long jumps. The length of these jumps is distributed according to a Lévy stable statistics with a power law tail, divergence of the second moment and heavy tails. This peculiar property strongly contradicts the ordinary Brownian motion, for which all the moments of the particle coordinate are finite. The presence of anomalous diffusion can be explained as a deviation of the real statistics of fluctuations from the Gaussian law, giving rise to the generalization of the central limit theorem [11]. Lévy flights have been observed in many physical, natural and social complex systems, where scale-invariance phenomena take place or can be suspected [12]-[15]. Recently noise-induced ordering phenomena, such as dynamic hysteresis, stochastic resonance, resonant activation, and double stochastic resonance phenomenon were observed in a bistable system, in the presence of Lévy noise [16]-[19]. Of course, anomalous diffusion has a lot of peculiarities different from those observed in normal Brownian motion [20]. The main difference from ordinary diffusion consists in replacing the white Gaussian noise source in the underlying Langevin equation with a Lévy stable noise.

Another important problem within complex systems is the matastability together with nonequilibrium dynamics. The metastable state is a local minimum in the potential profile of the physical system considered. The action on the system of deterministic and/or stochastic driving forces produces typical scenario of out of equilibrium dynamics. The presence of the noise source in the escape of the system from a matastable state through a potential barrier could increase the crossing time and then the lifetime of the system in the metastable state [3, 4]. The first scientist who studied this problem was Kramers [21]. He proposed to model the chemical reaction kinetics as the diffusion of a Brownian particle, initially located in a potential well, across a potential barrier of finite height. Kramers's theory has been applied to a much more general range of processes associated with the barrier

crossing of a physical entity experiencing random kicks fueled by its contact to a thermal bath [22]-[24]. If the random processes in complex systems violate the rules of Brownian motion, the Kramer's theory cannot to be applied [25]-[27].

In standard quantum mechanics, instead, the systems mainly deals with closed physical systems that can be considered isolated from any external environment, the latter being generically a larger system consisting of (infinitely) many degrees of freedom. The time-evolution of closed systems is described by one-parameter groups of unitary operators embodying the reversible character of the dynamics. On the contrary, when a system interacts with an environment in a non-negligible way, it must be treated as an open quantum system, namely as a subsystem embedded within environment, exchanging with it energy and entropy, and whose time-evolution is irreversible [28]-[38]. In general, the time-evolution of the system is inextricably linked to that of the environment. The compound system plus environment is closed and develops reversibly in time; however, the global time-evolution rarely permits the extraction of a meaningful dynamics for the system alone. This can be done if the coupling among subsystem and environment is sufficiently weak, in which case physically plausible approximations lead to reduced dynamics that involve only the degrees of freedom of the system and are generated by master equations. Such reduced dynamics provide effective descriptions of how the environment affects the time-evolution of the system which, on time-scales that are specific of the given physical contexts, typically incorporates dissipative and noisy effects. Classical Brownian motion indicates that, when the typical time-scale of the system is much larger than the time-scale governing the decay of time-correlations of the environment, then the environment can be described as an effective source of damping and noise. In the framework of open quantum systems, this possibility is technically implemented either by letting the typical variation time of the system, τ_S, go to infinity, while the environment correlation time τ_E stays finite, or by letting τ_E go to zero, while τ_S stays finite [39]. As we shall see, these two regimes give rise to two different procedures to arrive at a reduced dynamics: the so-called *weak coupling* and *singular coupling* limits.

Since their first appearance, open quantum systems have been providing models of non-equilibrium quantum systems in diverse fields as chemical-physics, quantum optics and magnetic resonance. Recently, the rapid development of the theory of

quantum information, communication and computation [40]-[42] has revived the interest in open quantum systems in relations to their decoherence properties, but also in their capacity of creating entanglement in multi-partite systems immersed in certain environments. The observation of coherent dynamics in nanodevices is an important achievement towards quantum control in solid state devices. In the last decade superconducting nanocircuits exhibiting the dynamics of single artificial atoms [43]-[45], two coupled artificial atoms [46, 47] and artificial atoms coupled to electromagnetic resonators [48, 49] have been demonstrated. This development opens new perspectives to study quantum phenomena in solid-state devices that traditionally have been part of quantum optics [50].

The typical open quantum systems in these contexts are n-level systems, like atoms, photons or neutrons embedded in optical cavities or heat baths consisting of bosonic or fermionic degrees of freedom.

Focus of this thesis is to analyze the role of the environmental noise in classical and quantum systems. We focus on two classical systems and two quantum ones. In particular, we want to pay attention on the role of Lévy noise in a metastable state and in populations dynamics [51]-[53]. We investigate the effects of low-frequency quantum noise on a particular nanodevice (the Quantronium) and the role of noise in an asymmetric quantum bistable system interacting with thermal bath [54, 55].

In the first classical system, we investigate the barrier crossing event in the presence of Lévy noise, by focusing on the nonlinear relaxation time (NLRT) for a metastable cubic potential. In the second one, we start to consider two competing species subject to multiplicative α-stable Lévy noise. Studying the species dynamics, which is characterized by two different regimes, exclusion of one species and coexistence of both, and analysing the role of the Lévy noise sources, we find quasi-periodic oscillations and stochastic resonance phenomenon in the dynamics of the species.

The population dynamics is that part of life science that studies the space-time evolution of certain variables describing the population itself (eg size, age, weight). All those biological and environmental processes that influence this development are of paramount importance. Historically this area was of interest in mathematical biology, just think of the Gompertz, Verhulst and Malthusian models, or the famous Lotka and Volterra equations [56, 57]. Today, all these models are widely used in

various researche fields. Among the most important are the epidemiological ones, for the study of viral transmission [58] and the zoological concerning migration and foraging strategies [59].

Concerning the two open quantum systems, first we propose a way to analyze low frequency noise in terms of fictitious correlated fluctuations of external parameters, showing that optimizing the trade-off between efficient coupling and protection against noise may allow to observe coherent population transfer in a particular nanodevice, namely the Quantronium [44, 60]. Recent experiments have demonstrated coherent phenomena in three-level systems based on superconducting nanocircuits. This opens the possibility to detect Stimulated Raman Adiabatic Passage (STIRAP) [50] in artificial atoms.

Subsequently, we study the relaxation time of an open quantum system with asymmetric bistable potential and interacting with a thermal reservoir. We obtain the time evolution of the population distributions in both energy and position eigenstates of the system, for different values of the coupling strength with the thermal bath.

The plan of this thesis is as follows. In chapter 1 we give a very short introduction to stochastic processes and Lévy processes in a mathematical framework. In chapter 2, we analize the effect of Lévy noise in a barrier crossing problem and in a population dynamics model. Finally, in chapter 3 we investigate the role of the environmental noise in two open quantum systems.

Chapter 1

Stochastic Processes and Lévy Processes

In this chapter we introduce the basic mathematical concepts to address the aforementioned research topics, namely the stochastic processes, the Wiener and the Lévy processes.

1.1 Stochastic Processes

The triple $(\Omega, \mathcal{F}, P)$ is called a probability space if Ω is a set, $\mathcal{F}$ is a family of subset of Ω such that:

(i) $\emptyset \in \mathcal{F}$

(ii) $F \in \mathcal{F} \Rightarrow F^C \in \mathcal{F}$, where F^C is the complement of F

(iii) $A_1, A_2, \ldots \in \mathcal{F} \Rightarrow A := \bigcup_{i=0}^{\infty} A_i \in \mathcal{F}$;

and the probability measure P is a function $P : \mathcal{F} \to [0, 1]$ such that:

(iv) $P(\emptyset) = 0, \quad P(\Omega) = 1$

(v) if $A_1, A_2, \ldots \in \mathcal{F}$ and $\{A_i\}_{i=1}^{\infty}$ is disjoint then $P\left(\bigcup_{i=1}^{\infty} A_i\right) = \sum_{i=1}^{\infty} P(A_i)$.

In this given probability space $(\Omega, \mathcal{F}, P)$, a *random variable* X is a function $X : \Omega \to \mathbf{R}^n$. Every random variable induces a probability measure μ_X on $B \subseteq \mathbf{R}^n$

(Borel set), defined by

$$\mu_X(B) = P\left(X^{-1}(B)\right)$$

and called the *distribution* of X.

A *stochastic process* is a parametrized collection of random variables

$$\{X_i\}_{t\in T}$$

defined on a probability space $(\Omega, \mathcal{F}, P)$ and assuming values in $\mathbf{R}^n$. The parameter space T is usually the half-line $[0; +\infty)$, but it may also be an interval $[a; b]$. Note that for each $t \in T$ fixed we have a random variable

$$\omega \to X_t(\omega); \qquad \omega \in \Omega.$$

On the other hand, fixing $\omega \in \Omega$ we can consider the function

$$t \to X_t(\omega); \qquad t \in T$$

which is called a *path* of X_t. It is simple for the intuition to imagine t as "time" and each ω as an individual "particle" ("experiment"). Within picture $X_t(\omega)$ would represent the position (result) at time t of the particle (experiment) ω. The finite-dimensional distributions of the stochastic process $X = X_{t\in T}$ are the measures $\mu_{t_1,\ldots,t_k}$ defined on $\mathbf{R}^{nk}$, $k = 1, 2, \ldots$ by

$$\mu_{t_1,\ldots,t_k}(F_1 \times F_2 \times \cdots \times F_k) = P[X_{t_1}, \cdots, X_{t_k}]; \qquad t_i \in T. \tag{1.1}$$

Here $F_1, \ldots, F_k$ denote Borel sets in $\mathbf{R}^n$. The family of all finite-dimensional distributions determine many important properties of the process X, therefore, given a family of probability measures in $\mathbf{R}^{nk}$ is important to be able to construct a corresponding stochastic process (see the Kolmogorov's extension theorem [61]).

1.1.1 Wiener process

A landmark example of stochastic process is that describing the Brownian motion. In 1828 the Scottish botanist Robert Brown observed that pollen grains suspended in liquid performed an irregular motion. The motion was later explained by the random collisions with the molecules of the liquid. To describe the motion mathematically it is natural to use the concept of stochastic process $X_t(\omega)$, interpreted as the position

at time t of the pollen grain ω. In this case we have $x, y \in \mathbf{R}^3$ $0 \leq t_1 \leq t_2 \leq \cdots \leq t_k$ and the measure (1.1) becomes

$$\mu_{t_1,\ldots,t_k}(F_1 \times F_2 \times \cdots \times F_k) = \int_{F_1 \times F_2 \times \cdots \times F_k} p(t_1, |x - x_1|) \\ p(t_2 - t_1, |x_1 - x_2|) \cdots p(t_k - t_{k-1}, |x_{k-1} - x_k|) dx_1 dx_2 \cdots dx_k \tag{1.2}$$

where the distribution $p(t, |x - y|)$ is a Gaussian:

$$p(t, |x - y|) = (2\pi t)^{-3/2} \cdot \exp\left(-\frac{|x - y|^2}{2t}\right).$$

Here, note that the standard deviation of the distribution is $\sqrt{t}$. Indeed all the processes described by this distribution are characteristic of so-called normal or Gaussian or Brownian diffusion. Moreover, from Eq. (1.2) we deduce that all the increment $|x_i - x_{i+1}|$ are independent each other. If we require that the trajectory is continuous in $\mathbf{R}^3$ (see Kolmogorov's continuity theorem [61]) we have constructed the so-called *Wiener process* $(W_t)_{t \geq 0}$. A very important property of the Wiener process is that its trajectories are not differentiable at any point for $t > 0$ [62].

1.2 Lévy Processes and Lévy Distributions

Two important properties are intrinsic to the homogeneous Brownian motion: the diffusion packet initially concentrated at a point takes later the Gaussian form, whose width grows in time as $t^{1/2}$. This kind of diffusion was called the normal diffusion. In 1926 Richardson [63] published the article where he presented empirical data being in contradiction with the normal diffusion: the size Δ of an admixture cloud in a turbulent atmosphere grows in time proportionally to $t^{3/2}$, that is much faster than in the normal case ($t^{1/2}$). This turbulent diffusion was the first example of *superdiffusion processes*, when $\Delta \propto t^{\gamma}$ with $\gamma > 1/2$.

A random process $\{X(t)\}_{t \geq 0}$ is called a *Markovian process*, if for any $n \geq 1$ and $t_1 < t_2 < \ldots < t_n < t \Rightarrow P(X(t) < x | X(t_1) = x_1, \ldots, X(t_t) = x_n) = P(X(t) < x | X(t_n) = x_n)$. The Markovian property is interpreted as independence of future from the past for the known present.

A random process with independent increments is called *homogeneous or stationary*, if the random variables $X(t + \tau) - X(t) = \Delta X$ have distributions which are

independent of t:$P(\Delta X < x) = F(x, \tau)$.
$\{X(t)\}_t \geq 0$ is a *Lévy process* if, for every $t, \tau \geq 0$, the increment $X(t+\tau) - X(t)$ is independent of the process $\{X(t')\}_{0 \leq t' < t}$ and has the same law as $X(\tau)$. In particular,$X(0) = 0$.

We will denote the Lévy process $L(t)$. As it follows from the evident decomposition [9]

$$L(t) = L\left(\frac{t}{n}\right) + \left[L\left(\frac{2t}{n}\right) - L\left(\frac{t}{n}\right)\right] + \cdots + \left[L\left(\frac{nt}{n}\right) - L\left(\frac{(n-1)t}{n}\right)\right]$$

the random variable $L(t)$ can be divided into the sum of an arbitrary number of independent and identically distributed random variables. In other words, the probability distribution of $L(t)$ belongs to the class of infinitely divisible distributions [10, 64]. Hence, we can express the *second characteristics*, i.e. the logarithm of characteristic function of the random variable $L(t)$ in the Lévy-Khinchine form [65]

$$\begin{aligned} \phi(k,t) &\equiv \ln \widetilde{P}(k,t) = \ln\langle e^{ikL(t)}\rangle \\ &= t\int_{-\infty}^{+\infty}(e^{ikx} - 1 - ik\sin x)\frac{\rho(x)}{x^2}dx, \end{aligned} \tag{1.3}$$

where $\rho(x) \geq 0$ is the canonical measure density. Note that the last term in the bracket, $-iksinx$, serves to ensure the convergence of the integral and can be omitted if the integral converges itself. Choosing

$$\rho(x) = \delta(x)$$

and taking into account that

$$e^{ikx} - 1 - ik\sin x = -\frac{k^2x^2}{2}, \qquad x \to 0,$$

we arrive at the normalized Brownian motion (Wiener process) with characteristic function

$$\widetilde{P}(k,t) = \exp\left\{-\frac{tk^2}{2}\right\}. \tag{1.4}$$

Lévy processes that have the scale invariant property are called *Lévy flights*. The distributions that describe these processes are called *stable distributions* and can be indexed via the parameter α [11, 65].

The random process $\{Y(t)\}_{t\geq 0}$ is a *stable process* if for any positive $a, b \in \mathbf{R}$ there are positive number $c, d \in \mathbf{R}$, such that the independent copies Y_1, Y_2 of Y are in relation

$$aY_1 + bY_2 \doteq cY + d.$$

The symbol $\doteq$ means the equality of distributions of the corresponding random variables. Moreover if $d = 0$, the process Y is *strictly stable*. The random process $\{L^{(\alpha,\beta)}(t)\}_{t\geq 0}$ is called α-stable Lévy motion with parameters $0 < \alpha \leq 2, \quad -1 \leq \beta \leq 1$, if

(i) $L^{(\alpha,\beta)}(0) = 0$ almost certainly;

(ii) $L^{(\alpha,\beta)}(t)_{t\geq 0}$ is a process with independent increments;

(iii) $L^{(\alpha,\beta)}(t+\tau) - L^{(\alpha,\beta)}(t) \doteq \tau^{1/\alpha} Y^{(\alpha,\beta)}$ at any t and τ (with Y stable process).

The condition

$$L^{(\alpha,\beta)}(t) = \tau^{1/\alpha} Y^{(\alpha,\beta)}$$

is the *self-similarity condition.*

The characteristic function $\widetilde{P}^{(\alpha,\beta)}(k)$ of the strictly stable probability distribution $P^{(\alpha,\beta)}(x)$, with parameters α and β, is given by the formula [11],[66]-[68]

$$\widetilde{P}^{(\alpha,\beta)}(k) = \begin{cases} \exp\left\{-|k|^\alpha \left[1 - i\beta \mathrm{sign}(k) \tan\frac{\pi\alpha}{2}\right]\right\} & \alpha \neq 1, \\ \exp\left\{-|k| \left[1 + i\beta \mathrm{sign}(k) \frac{2}{\pi} \ln|k|\right]\right\} & \alpha = 1, \end{cases} \tag{1.5}$$

The characteristic index $\alpha \in (0, 2]$ determines the decreasing rate of the large values probability for stable distributions. For $\alpha = 2$ the variance of distribution is finite, while for $\alpha < 2$ the variance is infinite. Moreover, when $\alpha < 1$ also the expectation value does not exists. The parameter $\beta \in [-1, 1]$ characterizes the asymmetry of the distributions: for $\beta = 0$ the stable distribution is symmetric.

For $\alpha = 1, \beta = 0$ we find the Cauchy distribution

$$P^{(1,0)}(x) = \frac{1}{\pi(1 + x^2)} \tag{1.6}$$

with the characteristic function

$$\widetilde{P}^{(1,0)}(k) = \exp\{-|k|\}. \tag{1.7}$$

For $\alpha = 1/2, \beta = 1$ we find an one-side distribution known as the Lévy-Smirnov distribution [67, 68]

$$P^{(1/2,1)}(x) = \frac{1}{\sqrt{2\pi}} x^{-3/2} \exp\left(-\frac{1}{2x}\right), \quad x \geq 0. \tag{1.8}$$

Lévy flights are characterized by many small movements and few large displacements (see Fig. 1.1) which correspond to the parametrized stable distribution (see Fig.1.2).

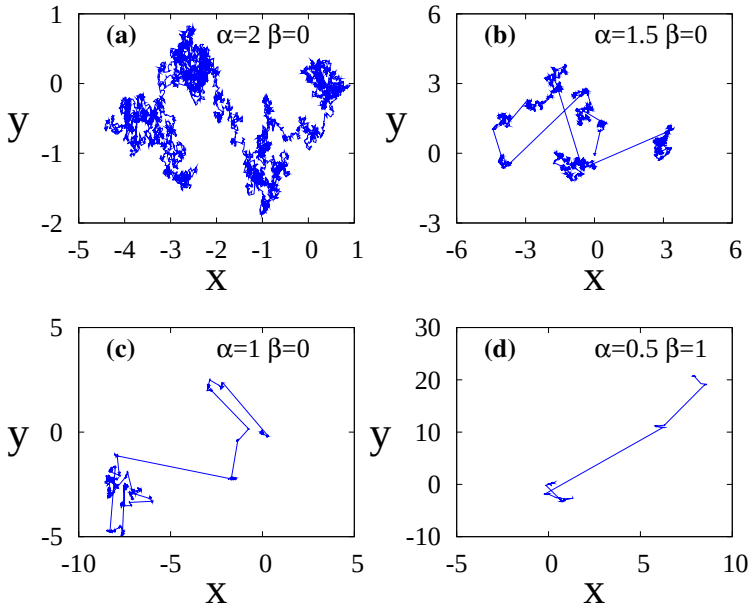

Figure 1.1: Two dimensional trajectories of free diffusion of a particle subjected to noise sources with Gaussian ($\alpha = 2, \beta = 0$), Cauchy-Lorentz ($\alpha = 1, \beta = 0$), Lévy ($\alpha = 1.5, \beta = 0$), and Lévy-Smirnov ($\alpha = 0.5, \beta = 1$) distributions. The values of the other parameters are $\mu = 0$, $\sigma = 1$.

We underline here only the fact that all members of the set of stable distributions are characterized by the presence of 'heavy' (power-type) tails and, as a consequence, of infinite variance, and that concerns all of them, except the Gaussian (normal) distribution. That is, we want to remark that the whole set of stable laws appear as limiting distributions in the *generalized central limiting theorem*. This is, certainly, the most important advantage for these distributions.

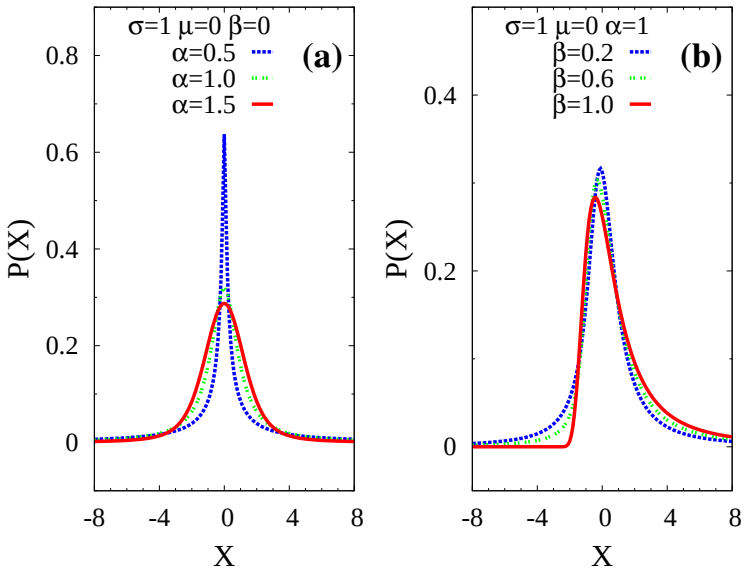

Figure 1.2: PDFs of stable Lévy distribution for different values of the parameters α, β, μ and σ. Namely, (left panel) $\sigma = 1$, $\mu = 0$, $\beta = 0$, and $\alpha = 0.5, 1.0, 1.5$; (right panel) $\sigma = 1$, $\mu = 0$, $\alpha = 1$, and $\beta = 0.2, 0.6, 1.0$

1.2.1 Generalized Central Limiting Theorem

The central limit theorem states that let $(X_1, X_2, \ldots, X_n)$ be n random variable independent and identically distributed (i.i.d), with mean μ and variation σ^2, then the variable sum standardized

$$\widetilde{S_n} = \frac{S_n - \mu}{\sigma\sqrt{n}} = \frac{X_1 + X_2 + \cdots + X_n}{\sigma\sqrt{n}}$$

for n large is standard normal distributed $\widetilde{S_n} \cong N(0, 1)$. The Gaussian distribution is an attractor in the functional space of probability density functions (pdfs). When the conditions of independence and finite variance are not satisfied, other limit theorems must be considered. We can generalize the central limit theorem within stable distributions [69], accordingly, also the non-Gaussian stable distributions are attractors in the functional space of pdfs; the Gaussian distribution is the only stable distribution having all its moments finite (see Fig. 1.3). For more details see also [70]-[73].

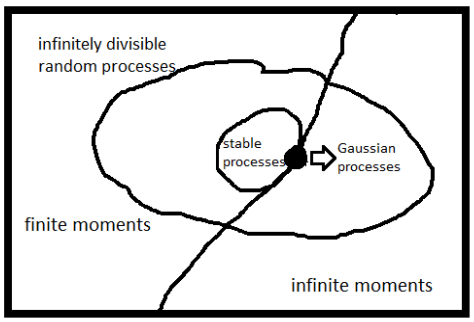

Figure 1.3: Illustration scheme of the classes of random processes.

1.2.2 Lévy Flight Superdiffusion

As it was seen above, if $\alpha = 2$ the Lévy motion becomes the Brownian motion with characteristic function, see (1.4)

$$\widetilde{P}^{(2,0)}(k,t) = e^{-tk^2}, \tag{1.9}$$

obeying the differential equation

$$\frac{\partial \widetilde{P}^{(2,0)}(k,t)}{\partial t} = -k^2 \widetilde{P}^{(2,0)}(k,t) \tag{1.10}$$

under initial condition $\widetilde{P}^{(2,0)}(k,0) = 1$. Factor $-k^2$ is the Fourier image of the one-dimensional Laplace operator $\Delta_1 = \partial^2/\partial x^2$. The inverse transformation yields the partial differential equation

$$\frac{\partial P^{(2,0)}(x,t)}{\partial t} = \frac{\partial^2 P^{(2,0)}(x,t)}{\partial x^2}, \tag{1.11}$$

with initial condition $P^{(2,0)}(x,0) = \delta(x)$. For the symmetric Lévy motion with $\beta = 0$ and arbitrary α, the corresponding expression of the characteristic function reads

$$\widetilde{P}^{(\alpha,0)}(k,t) = e^{-t|k|^\alpha}, \tag{1.12}$$

and

$$\frac{\partial \widetilde{P}^{(\alpha,0)}(k,t)}{\partial t} = -|k|^\alpha \widetilde{P}^{(\alpha,0)}(k,t). \tag{1.13}$$

Here taking into account that $-|k|^\alpha$ is the Fourier image of the Riesz [74] fractional operator $\Delta_1^{\alpha/2} = \partial^\alpha/\partial|x|^\alpha$, we arrive at the fractional differential equation

$$\frac{\partial P^{(\alpha,0)}(x,t)}{\partial t} = \frac{\partial^\alpha P^{(\alpha,0)}(x,t)}{\partial |x|^\alpha}. \tag{1.14}$$

The Riesz operator has an integral representation as follows

$$\frac{\partial^\alpha f(x)}{\partial |x|^\alpha} = -\frac{1}{K(\alpha)} \int_0^{+\infty} \frac{2f(x) - f(x-y) - f(x+y)}{y^{1+\alpha}} dy, \tag{1.15}$$

where

$$K(\alpha) = \frac{\pi}{\Gamma(\alpha+1)\sin(\pi\alpha/2)}$$

(with Γ gamma function). If the Lévy motion is in a potential $U(x)$, the above Eq. (1.14) becomes the *fractional Fokker-Planck equation* (FFPE)

$$\frac{\partial P^{(\alpha,0)}(x,t)}{\partial t} = -\frac{\partial}{\partial x}[U'(x)P]\frac{\partial^\alpha P^{(\alpha,0)}(x,t)}{\partial |x|^\alpha}. \tag{1.16}$$

Finally, in the case of the asymmetric Lévy motion, the equation for probability distribution becomes

$$\frac{\partial P^{(\alpha,\beta)}(x,t)}{\partial t} = D_x^{(\alpha,\beta)} P^{(\alpha,\beta)}(x,t). \tag{1.17}$$

This equation contains the Feller fractional space derivative $D_x^{(\alpha,\beta)}$, which is determined by the relation

$$\begin{array}{l} D_x^{(\alpha,\beta)} f(x) = -\frac{A(\alpha,\beta)}{K(\alpha)} \\ \int_0^{+\infty} \frac{2f(x) - (1+\beta)f(x-y) - (1-\beta)f(x+y)}{y^{1+\alpha}} dy, \end{array} \tag{1.18}$$

where

$$A(\alpha,\beta) = 1 + \beta^2 \tan(\pi\alpha/2).$$

A more detailed consideration of fractional differential equation for the description of Lévy motion can be found in [12],[75]-[82].

The time derivative of the Lévy process is called *Lévy noise*

$$\xi^{(\alpha,\beta)}(t) = \dot{L}^{(\alpha,\beta)}(t). \tag{1.19}$$

This is a stationary random process and has analogy to the Gaussian white noise, which is the time derivative of the Wiener process. The Lévy process, in fact, is a

generalized Wiener process. We can write directly the Langevin equation associated to FPPE (1.16)

$$\dot{X} = -U'(x) + \xi^{\alpha}(t) \tag{1.20}$$

by replacing the white Gaussian noise $\xi(t) = \xi^{(2)}(t)$ with the symmetric Lévy α-stable noise $\xi^{(\alpha)}(t)$. Both of these equations (1.16) and (1.20) for $\alpha < 2$ describe the so-called *anomalous diffusion*, in particular superdiffusion processes. From a theoretical point of view, the Lévy flights result from a Langevin equation (1.20) driven by α-stable noise, giving rise to the scaling property $\Delta r(\lambda t) \sim \lambda^{1/\alpha}\Delta r(t)$, with λ a positive parameter. The exponent $1/\alpha$ is related to the scaling of the tail of the probability distribution for the increments of the random walk, $P(r \to \infty) \sim |r|^{-(1+\alpha)}$. For $\alpha < 2$ the process is super-diffusive, the probability density function follows a power law with heavy tails and the generalized cental limit theorem is valid [70, 72, 73]; for $\alpha = 1$ the probability density function is a Cauchy-Lorentz function. For $\alpha = 2$, the second moment exists and because of the central limit theorem the random walk reduces, in the continuum limit, to a Gaussian random process. Lévy flights are a special case of Markovian processes. As a consequence the Markovian analysis can be used to derive the generalized Kolmogorov equation directly from the Langevin equation with Lévy noise [9, 83]. We wanted to give these concepts on anomalous diffusion and its related processes, because all studies on classical systems addressed in this thesis are concerned specifically with the Lévy noise and its implications.

Chapter 2

Classical System

In this chapter we focus our attention on two classical systems, the first regards the problem of crossing barrier from a metastable state in the presence of Lévy noise, the second, instead, the time evolution of two competing species subject to Lévy noise. Here we follow closely the three recent published papers [84, 85, 86].

In the first system, starting from the backward fractional Fokker-Planck equation we investigate the barrier crossing event in the presence of Lévy noise, by focusing on the nonlinear relaxation time. In the follows sections we shortly review some recent results on barrier crossing problems with different approaches. Then the generalized equations useful to calculate the nonlinear relaxation time (NRLT) are presented. The NRLT for free Lévy flights and for a cubic potential profile are obtained.
The second one is a Lotka-Volterra system of two competing species subject to multiplicative α-stable Lévy noise. The interaction parameter between the species is a random process which obeys a stochastic differential equation with a generalized bistable potential in the presence both of a periodic driving term and an additive α-stable Lévy noise. We study the species dynamics, which is characterized by two different regimes, exclusion of one species and coexistence of both. Finally, we find quasi-periodic oscillations and stochastic resonance phenomenon in the dynamics of the competing species, analysing the role of the Lévy noise sources.

2.1 Barrier crossing with Lévy flights

The problem of escape from a metastable state, first investigated by Kramers [21], is ubiquitous in almost all scientific areas (see, for example the reviews [3, 23] and Ref. [4, 87]). Since many stochastic processes do not obey the Central Limit Theorem, the corresponding Kramers escape behavior will differ. An interesting example is given by the α-stable noise-induced barrier crossing in long paleoclimatic time series [88, 89]. Another new application is the escape from traps in optical or plasma systems [90].

The main tool to investigate the barrier crossing problem remains the first passage times technique. But for anomalous diffusion in the form of Lévy flights this procedure meets with some difficulties. First of all, the fractional Fokker-Planck equation describing the Lévy flights is integro-differential, and the conditions at absorbing and reflecting boundaries differ from those using for ordinary diffusion. Lévy flights are characterized by the presence of long jumps, and, as a result, a particle can reach instantaneously a boundary from arbitrary position.

2.1.1 Barrier crossing

The particle escape from a metastable state, and the first passage time probability density have been recently analyzed for Lévy flights in Refs. [9, 14, 88], [93]-[103]. The main focus in these papers is to understand how the barrier crossing behavior, according to the Kramers law [21], is modified by the presence of the Lévy noise. Here we discuss briefly some results on the barrier crossing events with Lévy flights, recently obtained with different approaches.

The main tools to investigate the barrier crossing problem for Lévy flights are the first passage times, crossing times, arrival times and residence times. We should emphasize that the problem of mean first passage time (MFPT) meets with some difficulties because free Lévy flights represent a special class of discontinuous Markovian processes with infinite mean squared displacement. As already mentioned, the anomalous diffusion in the form of Lévy flights, for a particle moving in a potential profile $U(x)$, is described by the fractional Fokker-Planck equation (see 1.16) for the probability density function $W(x,t)$ [9]

$$\frac{\partial W}{\partial t} = \frac{\partial}{\partial x}\left[U'(x)\, W\right] + D\frac{\partial^{\alpha} W}{\partial |x|^{\alpha}} \tag{2.1}$$

Due to the integro-differential nature of the equation (2.1), we cannot apply the usual boundary conditions at the reflecting and absorbing barriers of the system investigated. The particle, in fact, can reach instantaneously the boundaries from any position.

The numerical results for the first passage time of free Lévy flights confined in a finite interval were presented in Ref. [14]. There, the complexity of the first passage time statistics (mean first passage time and cumulative first passage time distribution) was elucidated together with a discussion of the proper setup of corresponding boundary conditions, that correctly yield the statistics of first passages for these non-Gaussian noises. In particular, it has been demonstrated by numerical studies that the use of the local boundary condition of vanishing probability flux in the case of reflection, and vanishing probability in the case of absorbtion, valid for normal Brownian motion, no longer apply for Lévy flights. This in turn requires the use of nonlocal boundary conditions. Dybiec with co-authors in [100] found a nonmonotonic behavior of the MFPT as a function of the Lévy index α for two absorbing boundaries, with the maximum being assumed for $\alpha = 1$, in contrast with a monotonic increase for reflecting and absorbing boundaries.

According to the Kramers law, the probability distribution of the escape times from a potential well with the barrier of height U_0, has the exponential form

$$p(t) = \frac{1}{T_c} \exp\left\{-\frac{t}{T_c}\right\} \tag{2.2}$$

with mean crossing time

$$T_c = C \exp\left\{\frac{U_0}{D}\right\}, \tag{2.3}$$

where C is some positive prefactor and D is the noise intensity. The barrier crossing behavior of the classical Kramers problem was investigated, both numerically and analytically, in Refs. [14], [96]-[100], where the role of the stable nature of Lévy flight processes on the barrier crossing event was analyzed. Authors considered Lévy flights in a bistable potential $U(x)$ by numerical solution of the Langevin equation associated to the fractional Fokker-Planck equation (2.1)

$$\dot{x} = -U'(x) + \xi^{(\alpha)}(t) \ , \tag{2.4}$$

where $\xi^{(\alpha)}(t)$ is the symmetric Lévy α-stable noise. It was shown that although the survival probability decays again exponentially as in Eq. (2.2), the mean escape time T_c has a power-law dependence on the noise intensity D

$$T_c \simeq \frac{C(\alpha)}{D^{\mu(\alpha)}} \, , \tag{2.5}$$

where the prefactor C and the exponent μ depend on the Lévy index α. Using the Fourier transform of the Eq. (2.1)

$$\frac{\partial \tilde{W}}{\partial t} = -ikU'\left(-i\frac{\partial}{\partial k}\right)\tilde{W} - D\,|k|^{\alpha}\,\tilde{W} \, , \tag{2.6}$$

the authors derived the mean escape rate for large values of $1/D$ in the case of Cauchy stable noise ($\alpha = 1$) in the framework of the constant flux approximation across the barrier. The probability law and the mean value of the escape time from a potential well for all values of the Lévy index $\alpha \in (0, 2)$, in the limit of small Lévy driving noise, were also determined in the paper [101] by purely probabilistic methods. The escape times have the same exponential distribution (2.2). The mean value depends on the noise intensity D, in accordance with Eq. (2.5) with $\mu(\alpha) = 1$, and the pre-factor C depends on α and the distance between the local extreme of the potential.

The barrier crossing of a particle driven by symmetric Lévy noise of index α and intensity D for three different generic types of potentials was numerically investigated in Ref. [98]. Specifically: (i) a bistable potential, (ii) a metastable potential, and (iii) a truncated harmonic potential, were considered. For the low noise intensity regime, the result of Eq. (2.5) was recovered. As it was shown, the exponent $\mu(\alpha)$ remains approximately constant, $\mu \approx 1$ for $0 < \alpha < 2$; at $\alpha = 2$ the power-law form of T_c changes into the exponential dependence (2.3). It exhibits a divergence-like behavior as α approaches 2. In this regime a monotonous increase of the escape time T_c with increasing α (keeping the noise intensity D constant) was observed. For low noise intensities the escape time process corresponds to the barrier crossing by multiple Lévy steps. For high noise intensities, the average escape time curves collapse into a single curve, for all values of α. At intermediate noise intensities, the

escape time exhibits non-monotonic dependence on the index α, while still retains the exponential form of the escape time density.

The first arrival time is an appropriate parameter to analyze the barrier crossing problem for Lévy flights. If we insert in fractional Fokker-Planck equation (2.1) a δ-sink of strength $q(t)$ in the origin we obtain the following equation for the non-normalized probability density function $W(x,t)$

$$\frac{\partial W}{\partial t} = \frac{\partial}{\partial x}\left[U'(x)\, W\right] + D\frac{\partial^{\alpha} W}{\partial |x|^{\alpha}} - q(t)\,\delta(x), \tag{2.7}$$

from which by integration over all space we may define the quantity

$$q(t) = -\frac{d}{dt}\int_{-\infty}^{+\infty} W(x,t)\, dx, \tag{2.8}$$

which is the negative time derivative of the survival probability. According to definition (2.8), $q(t)$ represents the probability density function of *the first arrival time*: once a random walker arrives at the sink it is annihilated. As it was shown in the paper [96] for free Lévy flights ($U(x) = 0$), the first arrival time distribution has a heavy tail

$$q(t) \sim t^{1/\alpha - 2} \tag{2.9}$$

with exponent depending on Lévy index α ($1 < \alpha < 2$) and differing from universal Sparre Andersen result [104, 105] for the probability density function of first passage time for arbitrary Markovian process

$$p(t) \sim t^{-3/2}. \tag{2.10}$$

In the Gaussian case ($\alpha = 2$), the quantity (2.9) is equivalent to the first passage time probability density (2.10). From a random walk perspective, this is due to the fact that individual steps are of the same increment, and the jump length statistics therefore ensures that the walker cannot hop across the sink in a long jump without actually hitting the sink and being absorbed. This behavior becomes drastically different for Lévy jump length statistics: there, the particle can easily cross the sink in a long jump. Thus, before eventually being absorbed, it can pass by the sink location numerous times, and therefore the statistics of the first arrival will be

different from that of the first passage. The result (2.10) for Lévy flights was also confirmed numerically in the paper [103].

2.1.2 Nonlinear relaxation time with Lévy flights

General equations

The nonlinear relaxation time technique is more suitable for analytical investigations of Lévy flights temporal characteristics, because does not request a constraint on the boundary conditions. According to definition, the nonlinear relaxation time (NLRT) reads

$$T(x_0) = \frac{\int_0^\infty [P(t, x_0) - P(\infty, x_0)]\, dt}{P(0, x_0) - P(\infty, x_0)}, \tag{2.11}$$

where $P(\infty, x_0) = \lim_{t\to\infty} P(t, x_0)$ and

$$P(t, x_0) = \int_{L_1}^{L_2} W(x, t|\, x_0, 0)\, dx \tag{2.12}$$

represents the probability to find a particle in the interval (L_1, L_2) at the time t, if it starts from point $x = x_0$. Let us use the same procedure as for calculating the first passage time probability density (see [106]). If the random process $x(t)$ is Markovian, the probability density of transitions obeys the following backward Kolmogorov's equation [107]

$$\frac{\partial W(x, t|\, x_0, 0)}{\partial t} = \hat{L}^+(x_0)\, W(x, t|\, x_0, 0) \tag{2.13}$$

with the initial condition

$$W(x, 0|\, x_0, 0) = \delta(x - x_0). \tag{2.14}$$

Here $\hat{L}^+(x_0)$ is the adjoint kinetic operator. After integration with respect to x from L_1 to L_2 directly in Eq. (2.13) and taking into account Eq. (2.12) we arrive at [84]

$$\frac{\partial P(t, x_0)}{\partial t} = \hat{L}^+(x_0)\, P(t, x_0). \tag{2.15}$$

The Eq. (2.15) should be solved with the initial condition following from Eq. (2.14)

$$P(0, x_0) = 1_{(L_1, L_2)}(x_0), \tag{2.16}$$

where $1_{(L_1,L_2)}(x)$ is indicator of the set (L_1, L_2).

According to Eq. (2.15) $\hat{L}^+(x_0) P(\infty, x_0) = 0$, and after integration of this equation with respect to t from 0 to ∞ we obtain (see Eq. (2.16))

$$\hat{L}^+(x_0) Q(x_0) = P(\infty, x_0) - 1_{(L_1,L_2)}(x_0), \tag{2.17}$$

where $Q(x_0)$ is the numerator of the expression (2.11), i.e.

$$Q(x_0) = \int_0^\infty [P(t, x_0) - P(\infty, x_0)]\, dt. \tag{2.18}$$

Finally, in accordance with Eqs. (2.11) and (2.18) the nonlinear relaxation time can be calculated as

$$T(x_0) = \frac{Q(x_0)}{1 - P(\infty, x_0)}. \tag{2.19}$$

with $x_0 \in (L_1, L_2)$. Although Eqs. (2.17) and (2.19) are a useful tool to analyze the temporal characteristics of Lévy flights in different potential profiles $U(x)$, obtaining the exact analytical results for the generic α parameter, characterizing the anomalous diffusion, is one of the unsolved problems in this research area. Even for some particular potential profile, like the cubic one, to derive a general expression of the NLRT as a function of the Lévy index α is a non trivial problem. In the next section we derive a general differential equation useful to calculate the NLRT for arbitrary Lévy index and we find a closed expression [84] for the case of Cauchy stable noise excitation ($\alpha = 1$).

Lévy flights in a cubic potential

The forward fractional Fokker-Planck equation for Lévy flights in the potential profile $U(x)$ reads

$$\frac{\partial W(x, t|\, x_0, 0)}{\partial t} = \frac{\partial}{\partial x}\left[U'(x)\, W(x, t|\, x_0, 0)\right] + D\frac{\partial^\alpha W(x, t|\, x_0, 0)}{\partial |x|^\alpha}, \tag{2.20}$$

where $0 < \alpha < 2$. It is easily to find from Eq. (2.20) the expression for the adjoint kinetic operator

$$\hat{L}^{+}(x_0) = -U'(x_0)\frac{\partial}{\partial x_0} + D\frac{\partial^{\alpha}}{\partial |x_0|^{\alpha}}. \tag{2.21}$$

Substituting Eq. (2.21) in Eq. (2.17) we arrive at

$$D\frac{d^{\alpha}Q(x_0)}{d|x_0|^{\alpha}} - U'(x_0)\frac{dQ(x_0)}{dx_0} = P(\infty) - 1_{(L_1,L_2)}(x_0), \tag{2.22}$$

because the probability $P(\infty, x_0)$ does not depend on the initial position of the particles.

The Fourier transform of Eq. (2.22) gives [84]

$$\left[U''\left(i\frac{d}{dk}\right) - ikU'\left(i\frac{d}{dk}\right)\right]\widetilde{Q}(k) - D|k|^{\alpha}\widetilde{Q}(k) = \\ = P(\infty)\delta(k) + \frac{e^{-ikL_2} - e^{-ikL_1}}{2\pi ik}, \tag{2.23}$$

where

$$\widetilde{Q}(k) = \frac{1}{2\pi}\int_{-\infty}^{+\infty} Q(x_0)\, e^{-ikx_0} dx_0 \tag{2.24}$$

and we took into account that in accordance with Eqs. (2.12) and (2.18) $Q(\pm\infty) = 0$.

Solving Eq. (2.23) and using the backward Fourier transform, we can calculate the nonlinear relaxation time as (see Eq. (2.19))

$$T(x_0) = \frac{1}{1 - P(\infty)}\int_{-\infty}^{+\infty} \widetilde{Q}(k)\, e^{ikx_0} dk, \tag{2.25}$$

where $x_0 \in (L_1, L_2)$. It is easily to check from Eq. (2.24) that $\widetilde{Q}(-k) = \widetilde{Q}^{*}(k)$. Dividing the integral in Eq. (2.25) on two parts for negative and positive variables k and using this relation we easily arrive at

$$T(x_0) = \frac{2}{1 - P(\infty)}\,\mathrm{Re}\left\{\int_0^{\infty} \widetilde{\mathrm{Q}}(\mathrm{k})\,\mathrm{e}^{\mathrm{ikx_0}}\mathrm{dk}\right\}. \tag{2.26}$$

As a result, it is sufficient to solve Eq. (2.23) only for positive values of k [84]

$$\left[U''\left(i\frac{d}{dk}\right) - ikU'\left(i\frac{d}{dk}\right)\right]\widetilde{Q}(k) - Dk^{\alpha}\widetilde{Q}(k) = \\ = P(\infty)\delta(k) + \frac{e^{-ikL_2} - e^{-ikL_1}}{2\pi ik}, \qquad (k > 0). \tag{2.27}$$

By solving Eq. (2.27) for a particular potential profile $U(x)$, we are able to calculate the NLRT by using Eq. (2.26), for a particle moving in that potential. However the general solution of this equation strictly depends on the functional form of the potential profile $U(x)$, and not for all the potential profiles there is a solution of this equation.

We now consider two cases: (a) a free anomalous diffusion, and (b) a cubic potential.

(a) For free Lévy flights ($U(x) = 0$): $P(\infty) = 0$, and from Eq. (2.27) we have

$$\widetilde{Q}(k) = \frac{e^{-ikL_1} - e^{-ikL_2}}{2\pi i D k^{\alpha+1}} \qquad (k > 0). \tag{2.28}$$

After substitution of Eq. (2.28) in Eq. (2.26) and evaluation of the integral we find finally for the case $0 < \alpha < 1$

$$T(x_0) = \frac{(x_0 - L_1)^{\alpha} + (L_2 - x_0)^{\alpha}}{2D\Gamma(\alpha+1)\cos(\pi\alpha/2)}. \tag{2.29}$$

As it is seen from Eq. (2.29), the nonlinear relaxation time decreases monotonically with increasing the noise intensity D and has a maximum as a function of initial position x_0 in the middle point of the interval (L_1, L_2). For Lévy index $1 \leq \alpha < 2$ the nonlinear relaxation time is infinite as for free Brownian motion ($\alpha = 2$).

(b) Lévy flights in a metastable cubic potential with a sink at $x = +\infty$

$$U(x) = -\frac{x^3}{3} + a^2 x. \tag{2.30}$$

Substituting this potential in Eq. (2.27) and taking into account that $P(\infty) = 0$ we obtain [84]

$$\frac{d}{dk}\left[k^2 \frac{d\widetilde{Q}(k)}{dk}\right] + \left(k^2 a^2 - iDk^{\alpha+1}\right)\widetilde{Q}(k) = \\ = \frac{e^{-ikL_2} - e^{-ikL_1}}{2\pi} \qquad (k > 0). \tag{2.31}$$

To solve Eq. (2.31) we introduce a new function $R(k) = k\widetilde{Q}(k)$. After substitution of this new function, Eq. (2.31) can be rearranged as

$$\frac{d^2 R(k)}{dk^2} + \left(a^2 - iDk^{\alpha-1}\right) R(k) = \frac{e^{-ikL_2} - e^{-ikL_1}}{2\pi k} \qquad (k > 0). \tag{2.32}$$

It is quite difficult to find an analytical solution of this equation for arbitrary Lévy index α. Thus, we limit our further considerations to the case $\alpha = 1$. Substituting $\alpha = 1$ in Eq. (2.32) and representing its right part in the form of integral, we arrive at

$$\frac{d^2R(k)}{dk^2} + \left(a^2 - iD\right) R(k) = -\frac{i}{2\pi}\int_{L_1}^{L_2} e^{-iky} dy \qquad (k > 0). \tag{2.33}$$

This linear differential equation can be exactly solved, and, as a result, we find (for any $k > 0$) the finite solution in the form

$$\widetilde{Q}(k) = \frac{1}{k}\left\{c_0\, e^{-\beta k - i\gamma k} + \frac{i}{2\pi}\int_{L_1}^{L_2} \frac{e^{-iky} dy}{y^2 + iD - a^2}\right\} \qquad (k > 0), \tag{2.34}$$

where

$$\begin{aligned} \beta &= a\left[1 + \left(\frac{D}{a^2}\right)^2\right]^{1/4} \sin\left[\frac{1}{2}\arctan\left(\frac{D}{a^2}\right)\right], \\ \gamma &= a\left[1 + \left(\frac{D}{a^2}\right)^2\right]^{1/4} \cos\left[\frac{1}{2}\arctan\left(\frac{D}{a^2}\right)\right]. \end{aligned} \tag{2.35}$$

Because of $\widetilde{Q}(0) < \infty$, the expression in curly brackets of Eq. (2.34) should be equal to zero, and we easily find the unknown constant c_0

$$c_0 = -\frac{i}{2\pi}\int_{L_1}^{L_2} \frac{dy}{y^2 + iD - a^2}. \tag{2.36}$$

Substitution of Eqs. (2.34) and (2.36) in Eq. (2.26) gives

$$T(x_0) = \frac{1}{\pi}\,\mathrm{Re}\left\{\int_0^\infty \frac{\mathrm{ie}^{\mathrm{ikx_0}}}{\mathrm{k}}\,\mathrm{dk}\int_{\mathrm{L_1}}^{\mathrm{L_2}} \frac{\mathrm{e}^{-\mathrm{iky}} - \mathrm{e}^{-\beta\mathrm{k} - \mathrm{i}\gamma\mathrm{k}}}{\mathrm{y}^2 + \mathrm{iD} - \mathrm{a}^2}\,\mathrm{dy}\right\}. \tag{2.37}$$

After changing the order of integration and evaluation of the integral on k we arrive at

$$T(x_0) = \frac{1}{\pi}\int_{L_1}^{L_2}\left\{\frac{D}{2}\ln\left[A(x_0, y)\right] + y_2 B(x_0, y)\right\}\frac{dy}{y_2^2 + D^2}, \tag{2.38}$$

where

$$A(x_0, y) = \frac{\beta^2 + (x_0 - \gamma)^2}{(x_0 - y)^2}; \;\; y_2 = y^2 - a^2; \tag{2.39}$$

and

$$B(x_0, y) = \arctan\left(\frac{x_0 - \gamma}{\beta}\right) - \frac{\pi}{2}\,\mathrm{sgn}(\mathrm{x_0 - y})\,. \tag{2.40}$$

In the following Fig. 2.1 we report the behavior of the nonlinear relaxation time $T(x_0)$, calculated by Eq. (2.38), as a function the initial position of the particle for different values of the noise intensity D, namely $D = 0.07, 0.35, 1.0, 3.0, 5.0$.

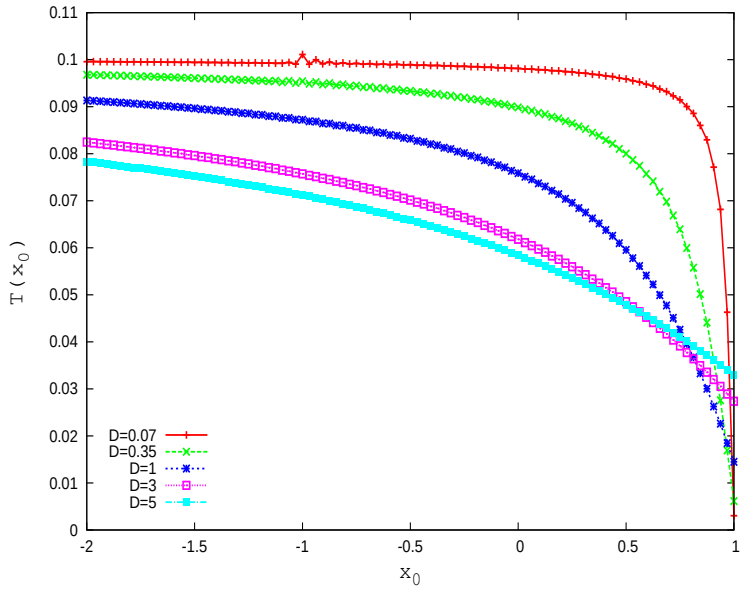

Figure 2.1: Nonlinear relaxation time, in arbitrary units (a. u.), as a function of the initial position x_0, for five values of the noise intensity D, namely: $D = 0.07, 0.35, 1.0, 3.0, 5.0$. The values of the parameters are: $a = 1$, $L_1 = -10$ and $L_2 = +10$.

The potential parameter a (see Eq. (2.30)) is $a = 1$, and the interval boundaries are $L_1 = -10$ and $L_2 = +10$. The integration step used to calculate $T(x_0)$ from Eq. (2.38) is $\Delta y = 10^{-4}$. For the initial position of the particle we focus on the range of values around the potential well, that is we consider $x_0 \in [-2, +1]$. A monotonic decreasing behavior of the nonlinear relaxation time is shown. The NLRT decreases with initial positions moving from the left of the minimum ($x_0 = -1$) towards the maximum ($x_0 = +1$) of the potential and with increasing noise intensity. An overlap of the different curves appears near the maximum of the potential. This behavior could be ascribed to the role of initial positions near the maximum. For initial positions that are close to the maximum of the potential ($x_0 = 1$) the height of the barrier to cross decreases considerably and the probability of the particle to fall

back into the potential well increases. For the role of the initial conditions in barrier crossing, with Gaussian noise, see Refs. [3, 87].

In Fig. 2.2 we report the log-log plot of the behavior of the NLRT as a function of the noise intensity D, for three initial positions of the particle, namely: $x_0 = -2.0, -1.0, 0$. As we can see the decreasing behavior of the NLRT with increasing noise intensity is recovered (see Ref. [98]).

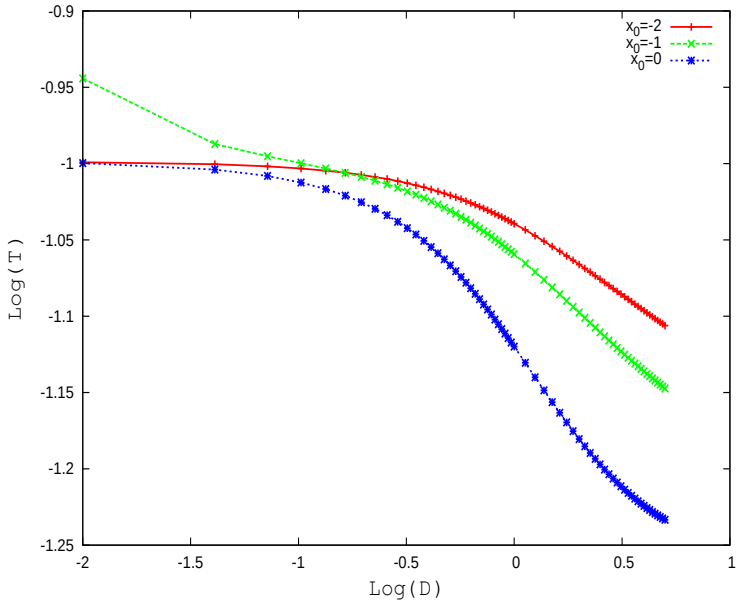

Figure 2.2: NLRT (a. u.) as a function of the noise intensity D, for three values of the initial position of the particle, namely: $x_0 = -2.0, -1.0, 0$. The parameter values are the same of Fig. 2.1.

2.2 Lévy flights in ecological systems

2.2.1 Some biological considerations of animal behavior

Animal movement and dispersal, which are major drivers of spatio-temporal patterns in ecosystems, have solicited in ecology questions difficult to answer for two main reasons. First, quantifying the precise distributions of populations interacting in time and space could be hard. Recent technological advances have to some extent changed this scenario, opening new perspectives for the future. A second aspect, which represents, at the moment, a stronger hurdle, is the lack of concepts and/or technical

tools for analysing the feedbacks between the properties of macroscopic ecosystems and their elementary parts. An evolutionary perspective, which takes into account the time evolution of the system and the contemporary presence of different "ecological" approaches, i.e. behavioural, landscape, and spatial ecology [108]-[110] could play a key-role in this matter. In particular, the understanding of the evolutionary components of large-scale and long-term properties of animal movement and dispersal allows to establish useful links across different scales, going from individuals to ecosystems and backwards [111]. Moreover, random fluctuations of environmental variables in ecosystems increase the unpredictability in resource availability throughout time. Thus, environmental stochasticity, together with inevitable biological constraints, could introduce randomness in many relevant ecological contexts: foraging, mating, dispersal, habitat colonization, etc [112]. Consequently, it is likely that an adaptive behaviour has been the response to environmental randomness, playing a fundamental role in animal survival and contributing to determine the spatiotemporal dynamics of processes and patterns in real ecosystems [113]. Random walks describe stochastic trajectories obtained when the system is uniquely "driven" by random forces. However, random walks could participate in dynamics of systems where deterministic forces are also present. Therefore, it is possible to introduce stochastic trajectories as results of richer dynamics, where deterministic and random components are present. In this context, random walks appear to be essential tools to model and describe the dynamics of real ecosystems, whose dynamics are affected both by deterministic and random forces. The Lévy flight theory has recently been borrowed by ecologists from the physical sciences to characterize the spatial distributions of predators or foragers and also to determine optimal search strategies for foragers looking for sparsely and randomly distributed targets. Models, in which Lévy noise sources are considered, have been successfully tested in different foraging animals such as bumble bees (*Bombus trifasciatus*) [114, 115], wandering albatrosses (*Diomedea exulans*) [116]-[119], reindeers (*Rangifer tarandus tarandus*), jackals (*Canis adustus*), grey seals (*Halichoerus grypus*), spider monkeys (*Ateles geoffroyi*) [120]. More recently, non-Gaussian noise has been used to describe the searching behaviour in the Peruvian anchovy (*Engraulis ringens*) fishery [121]-[125]. Noise-induced jumping between metastable states separated by potential barriers is common in physical systems. The time scale to overcome the barrier depends on

the noise source and potential profile. Most often the noise is Gaussian. However, non-Gaussian noises distributed with power law tails are found in different physical and biological systems such as turbulent diffusion, vortex dynamics, population dynamics, dynamical models and critical phenomena [88, 126]. The distributions observed appear to be well described by Lévy noise sources.

In this section we focus on the stochastic resonance phenomenon in a model of population dynamics. In particular, we investigate the stochastic dynamics of two competing species within the formalism of the generalized Lotka-Volterra equations. The interaction parameter between the species is a stochastic process which obeys a stochastic differential equation with a term of additive α-stable Lévy noise, which mimics the effects that environmental noise produces on the dynamical regime of an ecosystem [6, 127]. Moreover, we consider the generalized Lotka-Volterra equations in the presence of multiplicative α-stable Lévy noise, which models the direct interaction between species and environment. We analyse the role played by the Lévy noise on the system dynamics for different values of the index α. According to previous results obtained in the presence of Gaussian noise, we observe that the noise could have a constructive role. In particular, the additive noise is responsible for the generation of quasi-periodic oscillations in the time series of the species densities. Besides, the multiplicative noise, in the presence of two different dynamical regimes (coexistence and exclusion), produces the appearance of anticorrelated oscillations and stochastic resonance phenomenon.

2.2.2 Two Competing Species: Lotka-Volterra Model

Time evolution of two competing species is obtained by using a Lotka-Volterra model [128, 129] based on two stochastic differential equations in the presence of multiplicative Lévy noise [130]

$$\frac{dx}{dt} = mx(a - x - \gamma(t)y) + x\xi_x^{\alpha,\beta}(t), \tag{2.41}$$

$$\frac{dy}{dt} = my(a - y - \gamma(t)x) + y\xi_y^{\alpha,\beta}(t), \tag{2.42}$$

where a is the growth parameter and $\gamma(t)$ is the time dependent interaction parameter between the species. Here $\xi_x^{\alpha,\beta}(t)$ and $\xi_y^{\alpha,\beta}(t)$ are statistically independent α-stable Lévy noises with zero mean ($\mu = 0$) and intensity D equal for the two

noise sources. The time series for the two populations are obtained setting $m = 70$ and $a = 1$. It is known that for $\gamma < 1$ a coexistence regime takes place, while for $\gamma > 1$ an exclusion regime is established. Coexistence of the two species and exclusion of one of them correspond to stable states of the Lotka-Volterra's deterministic model [131]. Real ecosystems are open systems, which implies that they are immersed in a noisy nonstationary environment. Therefore, the interaction parameter $\gamma(t)$ is affected both by deterministic periodical "forces", e.g. temperature, and random fluctuations of environmental and natural variables such as the temperature itself and food resources, whose variations produce a competition between the species. Therefore noise together with periodic forces determines the crossing from one dynamical regime ($\gamma < 1 \rightarrow$ coexistence) to the other one ($\gamma > 1 \rightarrow$ exclusion). This continuous and noisy behaviour of the interaction parameter $\gamma(t)$ can be described by the stochastic differential equation

$$\frac{d\gamma(t)}{dt} = -\frac{\partial U(\gamma, t)}{\partial \gamma} + \xi_{\gamma}^{\alpha,\beta}(t), \tag{2.43}$$

where the time dependent bistable potential (see Fig. 2.3)

$$U(\gamma, t) = h(\gamma - 1)^4/\eta^4 - 2h(\gamma - 1)^2/\eta^2 + A\gamma \cos(\omega_0 t) \tag{2.44}$$

represents the effects of deterministic forces, and the term of additive noise $\xi_{\gamma}^{\alpha,\beta}(t)$ mimics the random fluctuations of environmental variables and natural resources. The oscillating driving force takes into account, for example, periodic variations of the temperature. In Eqs. (2.43) and (2.44), $h = 8$ is the height of the potential barrier, $A = 2h$ and $\omega_0 = \pi$ are the amplitude and the frequency of the driving force, respectively, and $\eta = 0.5$. The noise source $\xi_{\gamma}^{\alpha,\beta}(t)$ is given by a Lévy process with zero mean and intensity D_{γ}.

2.2.3 Deterministic stationary states

In the absence of multiplicative noise ($D = 0$) and for constant values of the interaction parameter γ, Eqs. (2.41), (2.42) describe the deterministic dynamics of two competing species. In these conditions the stationary values of the two species densities are given by

$$x^{st} = y^{st} = \frac{a}{1 + \gamma}. \tag{2.45}$$

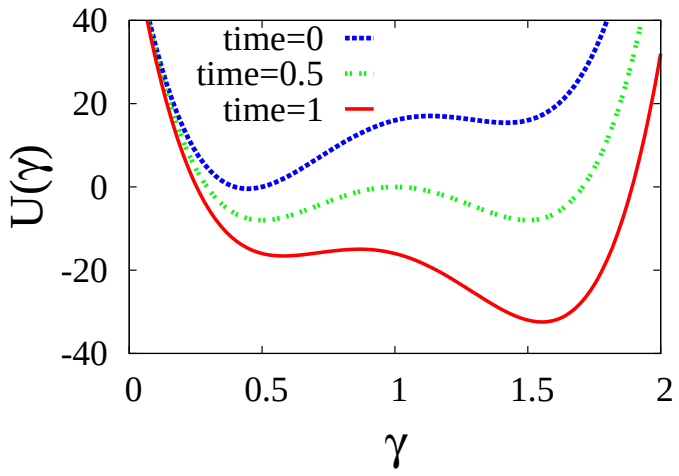

Figure 2.3: Three configurations of the time dependent bistable potential $U(\gamma, t)$ of Eq. (2.44) at times $t = 0, 0.5, 1$. The values of the potential parameters are $h = 8$, $\eta = 0.5$, $A = 2h$, $\omega_0 = \pi$.

In view of studying the system when a richer dynamics takes place, we introduced the interaction parameter $\gamma(t)$, as a stochastic process governed by Eq. (2.43). Here, $\gamma(t)$ takes values around the two minima, $\gamma = \gamma^{down} = 0.5$ (left-side well) and $\gamma = \gamma^{up} = 1.5$ (right-side well) corresponding to coexistence and exclusion regime, respectively. As a consequence, from Eq. (2.45) we get two different equilibrium points

$$\begin{aligned} x_1^{st} &= y_1^{st} = 2/3 \ \ (\gamma = 0.5 \ \rightarrow \ \text{coexistence}), \\ x_2^{st} &= y_2^{st} = 2/5 \ \ (\gamma = 1.5 \ \rightarrow \ \text{exclusion}). \end{aligned}$$

In order to determine the conditions for which the stationary states given in Eq. (2.45) correspond to a point of stable equilibrium in the phase space, we perform a stability analysis. Therefore, we consider the Jacobian matrix of the system given in Eqs. (2.41), (2.42)

$$J(\gamma) = \begin{pmatrix} -\frac{a}{1+\gamma} & -\frac{\gamma a}{1+\gamma} \\ -\frac{\gamma a}{1+\gamma} & -\frac{a}{1+\gamma} \end{pmatrix} \tag{2.46}$$

and obtain the corresponding eigenvalues

$$\lambda_1 = \frac{a\,(\gamma - 1)}{\gamma + 1} \tag{2.47}$$

$$\lambda_2 = -a. \tag{2.48}$$

Therefore, for $\gamma = 0.5$ we get

$$\lambda_1^s = -a/3,\ \lambda_2^s = -a, \tag{2.49}$$

and for $\gamma = 1.5$

$$\lambda_1^u = a/5,\ \lambda_2^u = -a, \tag{2.50}$$

where the apices 's' and 'u' indicate stable and unstable equilibrium, respectively. In fact, for $\gamma = 0.5$ the two eigenvalues are negative, which causes the equilibrium point to be unconditionally stable, while for $\gamma = 1.5$ one eigenvalue is positive and the other one negative, which implies that the equilibrium point corresponds to a saddle point in the phase space. Therefore, the stationary values $x_1^{st} = y_1^{st} = 2/3$ obtained for $\gamma = 0.5$ (coexistence regime) represent a stable equilibrium point for the Lotka-Volterra system considered (see Eqs. (2.41), (2.42)). Conversely, the stationary values $x_2^{st} = y_2^{st} = 2/5$ obtained for $\gamma = 1.5$ correspond to an unstable equilibrium (saddle point) and the system tends to exclude one of the two species (exclusion regime).

2.2.4 Stochastic Resonance

First, we investigate the effect of the noise on the time behaviour of $\gamma(t)$. Since the dynamics of the species strongly depends on the value of the interaction parameter, we initially analyze the time evolution of $\gamma(t)$ for different values of the intensity D_γ and index α, with $\beta = 0$, of the Lévy source $\xi_\gamma^{\alpha,\beta}(t)$ (see Eq. (2.43)).

Specifically, for $D_\gamma = 0$ and $\gamma(0) = 0.5$ we obtain a periodical behaviour of $\gamma(t)$ in the coexistence region (see Fig. 2.4). In the presence of non-Gaussian noise ($\alpha \neq 2$), for low noise intensity ($D_\gamma = 0.5 \ll h$), we can observe the effect of the noise on the time series of the interaction parameter (see Fig. 2.5). In particular, the noise is responsible not only for slight perturbations in the oscillating behaviour of $\gamma(t)$, but also for the appearance of jumps (Lévy flights) between $\gamma = 0.5$ (left well of the potential U) and $\gamma = 1.5$ (right well). These jumps, distributed according to a Lévy stable statistics, are known as Lévy flights and represent the effect of the heavy tails which characterize these non-Gaussian distributions. It is also evident how the distribution of these jumps changes for different values of α. This indicates that the alternating coexistence/exclusion regime can be modulated by the specific Lévy

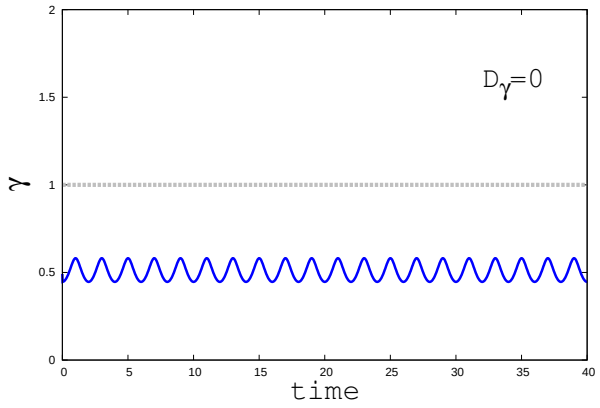

Figure 2.4: Time evolution of the interaction parameter $\gamma(t)$, by numerical integration of Eq. (2.43) with zero noise intensity D_γ.

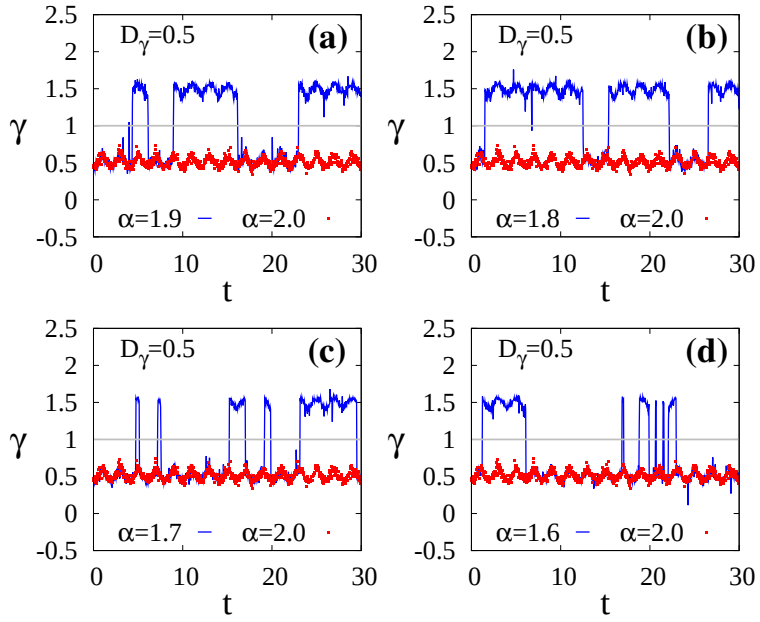

Figure 2.5: Time evolution of the parameter $\gamma(t)$, by numerical integration of Eq. (2.43) with noise intensity $D_\gamma = 0.5$, for five values of the index α, namely $\alpha = 1.6, 1.7, 1.8, 1.9, 2.0$, and $\beta = 0$.

noise source $\xi_{\gamma}^{\alpha,\beta}(t)$, varying both the intensity D_{γ} and the parameter α. It is then interesting to analyse the behaviour of $\gamma(t)$ for different levels of noise. Therefore,

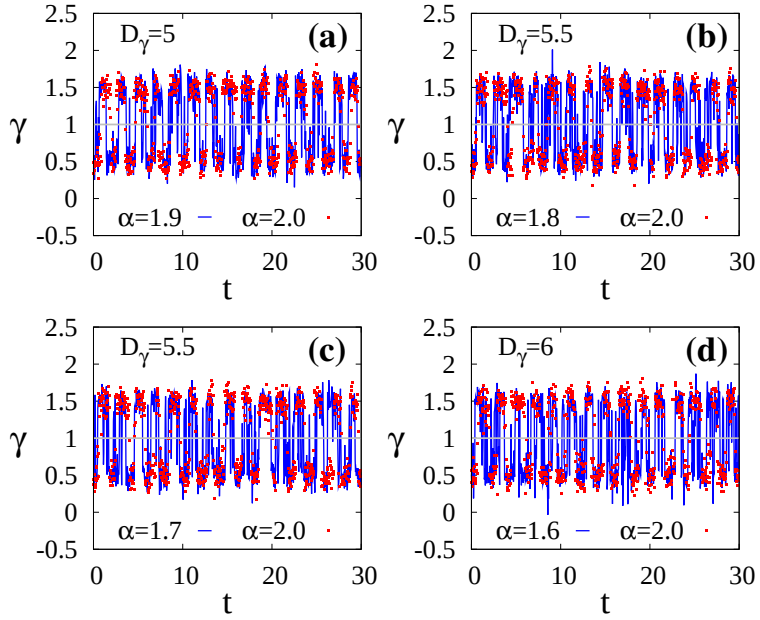

Figure 2.6: Time series of the parameter $\gamma(t)$ (from Eq. (2.43)), for suitable noise intensities ($D_{\gamma} = 5$, 5.5 and 6) and different values of the Lévy index α, namely $\alpha = 1.6, 1.7, 1.8, 1.9$ (blue dots), compared with the Gaussian case ($\alpha = 2.0$) (orange lines).

setting again $\beta = 0$, we obtain the time evolution of the interaction parameter for higher noise intensity ($D_{\gamma} \simeq h$). In particular, Fig. 2.6 shows the time series of $\gamma(t)$ with $D_{\gamma} = 5, 5.5, 6$ and for different values of α ($\alpha = 1.6, 1.7, 1.8, 1.9$), compared with those obtained for Gaussian noise ($\alpha = 2$) [6]. In the figure we see that the synchronization phenomenon between the Kramers time to overcome the potential barrier, starting from one of the two minima (see Fig. 2.3), and the periodical driving force is reduced in the presence of Lévy noise with respect to the Gaussian case. This indicates that the stochastic resonance effect, which can influence the dynamics of real ecosystems, results to be different in the presence of non-Gaussian noise source. A further increase of the noise intensity produces a loss of coherence and the dynamical behaviour is strongly controlled by the noise (see Fig. 2.7)).

A measure of the SR phenomenon and its intensity [1],[132]-[135] is provided by

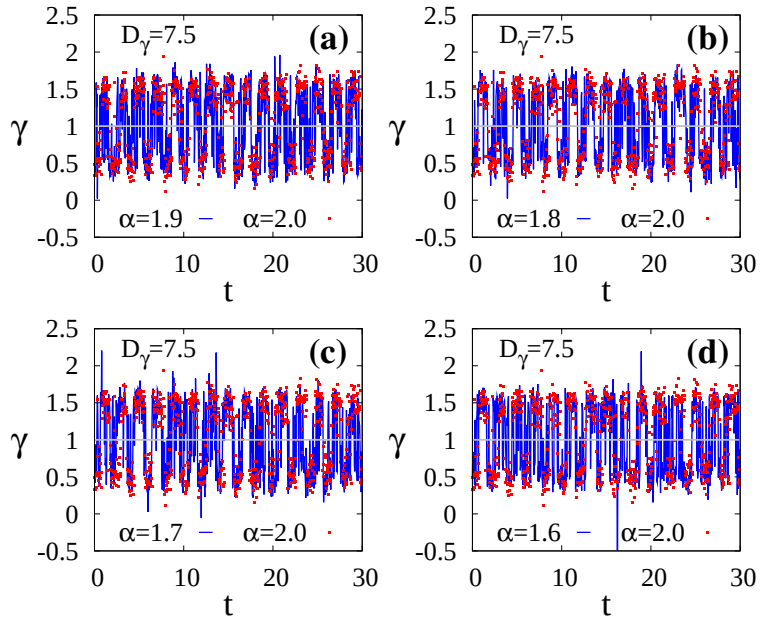

Figure 2.7: Time series of the parameter $\gamma(t)$ (from Eq. (2.43)), for noise intensity $D_\gamma = 7.5$ and different values of the Lévy index α, namely $\alpha = 1.6, 1.7, 1.8, 1.9$ (blue dots), compared with the Gaussian case ($\alpha = 2.0$) (orange lines).

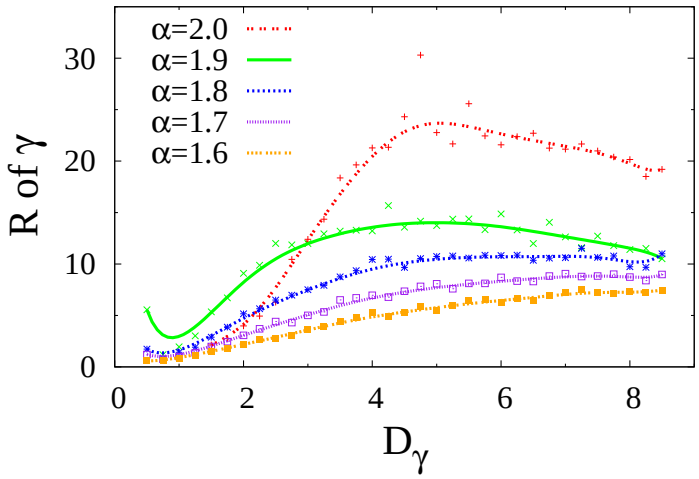

Figure 2.8: Signal-to-Noise Ratio of $\gamma(t)$ as a function of the noise intensity D_γ, for differen values of the index α of the symmetrical stable Lévy distribution, namely $\alpha = 1.6, 1.7, 1.8, 1.9, 2.0$.

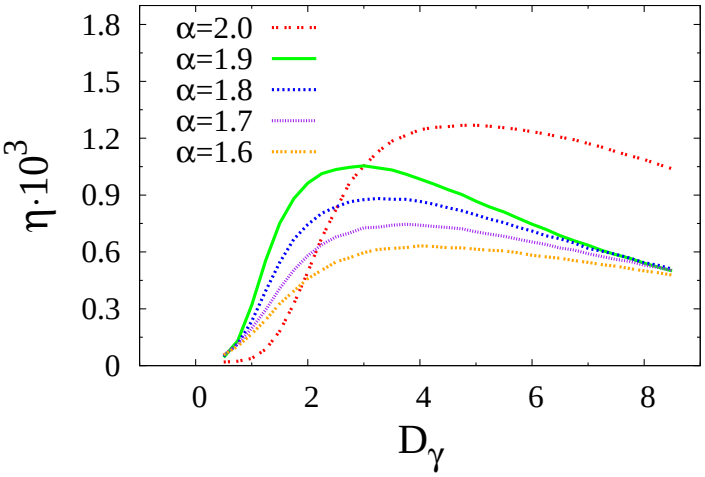

Figure 2.9: Spectral power amplification η of $\gamma(t)$ as a function of the noise intensity D_γ, for different values of the index α of the symmetrical stable Lévy distribution, namely $\alpha = 1.6, 1.7, 1.8, 1.9, 2.0$.

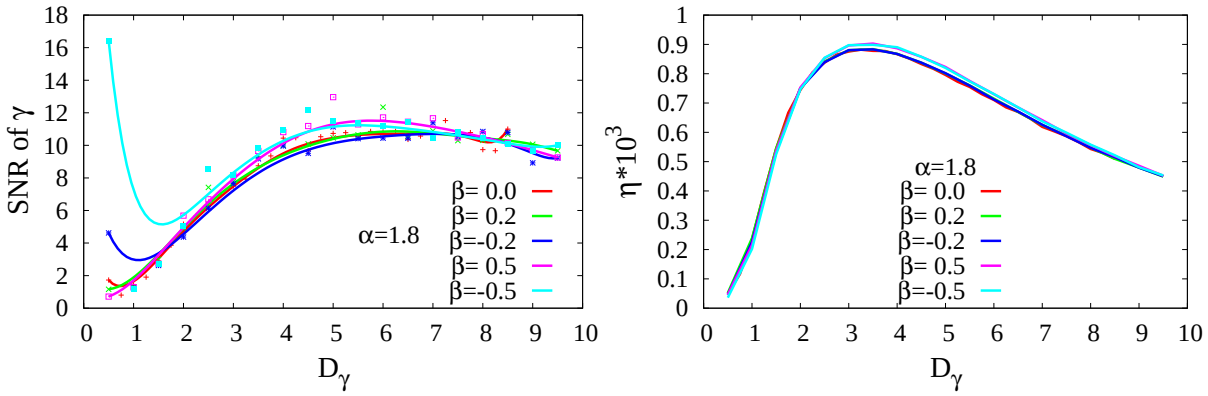

Figure 2.10: Signal-to-noise ratio and signal power amplification η of the parameter $\gamma(t)$ as a function of the noise intensity D_γ, for $\alpha = 1.8$ and different values of the index β of the stable Lévy distribution, namely $\beta = 0, \pm 0.2, \pm 0.5$. In the left panel, red plus, green cross, blue star, pink empty square and light blue full square represent the SNR values calculated by numerical integration of Eq. (2.43). The solid lines are the curves obtained by interpolating the numerical data. Each curve corresponds to the symbols with the same color. In the right panel, the solid lines have been obtained by connecting the SPA values calculated by numerical integration of Eq. (2.43).

the signal-to-noise ratio (SNR)

$$SNR = \frac{2}{S_N(\Omega)} \lim_{\Delta\omega \to 0} \int_{\Omega-\Delta\omega}^{\Omega+\Delta\omega} S(\omega) d\omega. \tag{2.51}$$

Here, $\int_{\Omega-\Delta\omega}^{\Omega+\Delta\omega} S(\omega)d\omega$ represents the power carried by the signal, while $S_N(\Omega)$ estimates the background noise level at the driving frequency Ω. The SR effect observed indicates that an optimal level of noise exists for which the response of the system undergoes resonance-like behaviour as a function of the noise level [1, 132]. In this condition, it is established a quasi-periodical switching between $\gamma = \gamma^{down} = 0.5$ and $\gamma = \gamma^{up} = 1.5$, which is responsible for an alternating coexistence/exclusion regime in the dynamics of the two populations. Because the SR phenomenon observed affects the time behaviour of $\gamma(t)$, which is a biological parameter responsible for the interaction of the two species, we name this effect "biological" stochastic resonance. In order to measure and better analyse the system response to the noise, we consider the spectral power amplification (SPA) [1, 132], indicated by η and defined as the ratio of the power of the output signal sampled at the frequency Ω of the external driving, to the power of the driving signal. In Figs. 2.8, 2.9, 2.10 we show SNR and SPA, respectively, as a function of the noise intensity D_γ. The nonmonotonic behaviour of the SNR indicates clearly the presence of stochastic resonance, characterized by a maximum whose value decreases as the index α approaches 1 (Cauchy distribution). Fixed the index α, the asymmetry parameter β slightly dirty things.

2.2.5 SR within species dynamics

In this section we analyze the dynamics of the two species densities. In particular, for different symmetrical ($\beta = 0$) α-stable Lévy distributions, we calculate the noise intensity D_γ corresponding to the regime of "biological" stochastic resonance, that is the maximum of SNR. Afterwards, in Eq. (2.43) we set D_γ at this value and solve numerically Eqs. (2.41), (2.42) for different values of the multiplicative noise intensity D. The results are shown in Figs. 2.11, 2.12, 2.13, 2.14. In particular, from panels (a), (b), (c) of these figures it is evident that, for the values of index α considered in our simulations, the multiplicative noise induces anticorrelated periodical oscillations in the time series of the two species, breaking the symmetric dynamical behaviour of the ecosystem (compare panels (a) with panels (b) and (c)

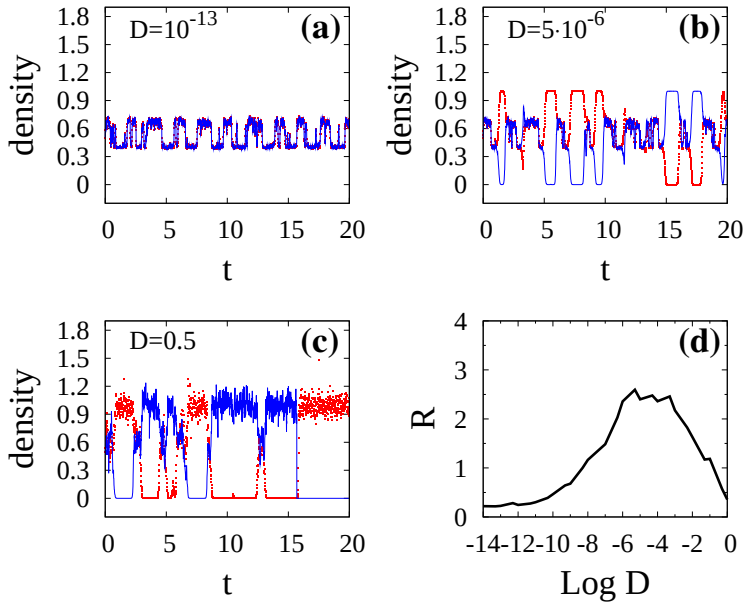

Figure 2.11:) Panels a, b, c: time series of the two species densities x (red lines) and y (blue lines) obtained from Eqs. (2.41), (2.42) with $\alpha = 1.9$, $\beta = 0$ and $D_\gamma = 5$. Panel (d): SNR of $(x-y)^2$ as a function of the noise intensity D.

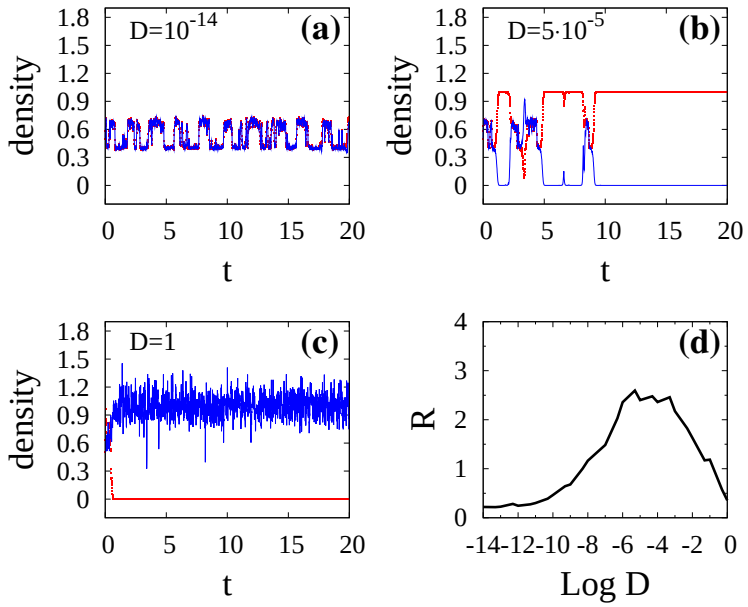

Figure 2.12: Panels a, b, c: time series of the two species densities x (red lines) and y (blue lines) obtained from Eqs. (2.41), (2.42) with $\alpha = 1.8$, $\beta = 0$ and $D_\gamma = 5.3$. Panel (d): SNR of $(x-y)^2$ as a function of the noise intensity D.

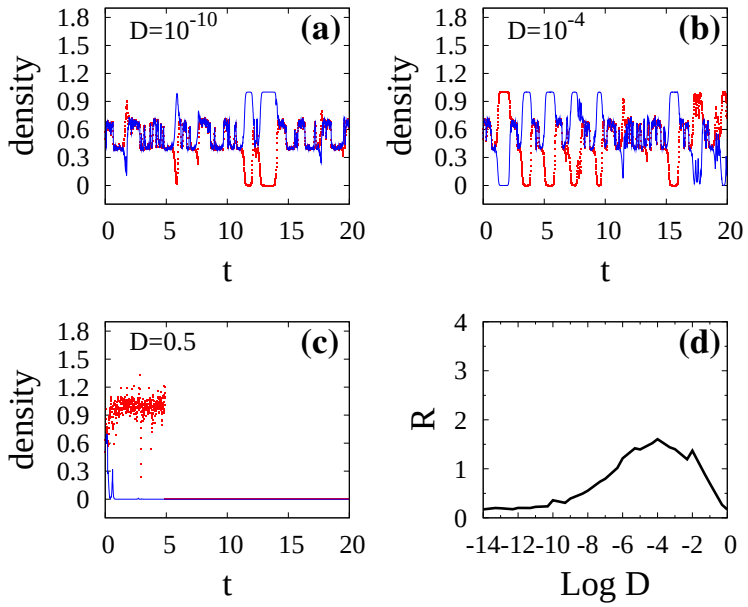

Figure 2.13: Panels a, b, c: time series of the two species x (red lines) and y (blue lines) obtained from Eqs. (2.41), (2.42) with $\alpha = 1.7$, $\beta = 0$ and $D_\gamma = 5.5$. Panel (d): SNR of $(x-y)^2$ as a function of the noise intensity D.

of Figs. 2.11, 2.12, 2.13, 2.14). Moreover, a multiplicative noise intensity exists that induces oscillating behaviour with a maximum of anticorrelation between the two species (see panel (b) of Figs. 2.11, 2.12, 2.13, 2.14). This indicates the presence of a second SR effect. We check this by calculating the SNR of $(x-y)^2$ for different values of α (see panel (d) in Figs. 2.11, 2.12, 2.13, 2.14). Here, we can observe the presence of a nonmonotonic behaviour characterized by the presence of a maximum. This confirms that the multiplicative noise is responsible for a further SR phenomenon affecting directly the dynamics of the two species. Because of this we name this effect "population" stochastic resonance. Finally, to better compare the SNR curves obtained we show them in one graph (see Fig. 2.15). Here, it is clear that the maximum of the SNR decreases as α approaches 1, according to the behaviour of SNR observed for the interaction parameter γ (see Fig. 2.8).

In Fig. 2.16 we show the SNR curves obtained, for different values of the index α and $\beta = 0$, by setting D_γ at the value that maximizes the SPA of the parameter γ.

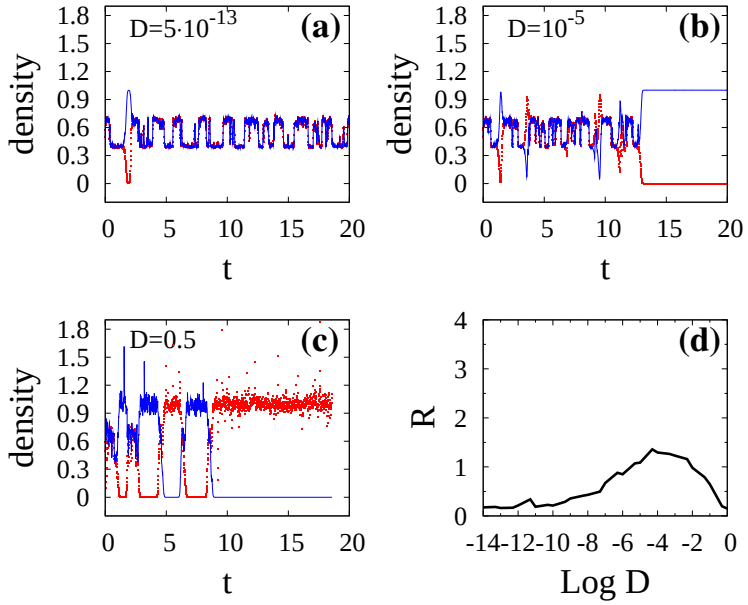

Figure 2.14: Time series of the two species x (red lines) and y (blue lines) obtained from Eqs. (2.41), (2.42) with $\alpha = 1.6$, $\beta = 0$ and $D_\gamma = 5.7$. Panel (d): SNR of $(x-y)^2$ as a function of the noise intensity D.

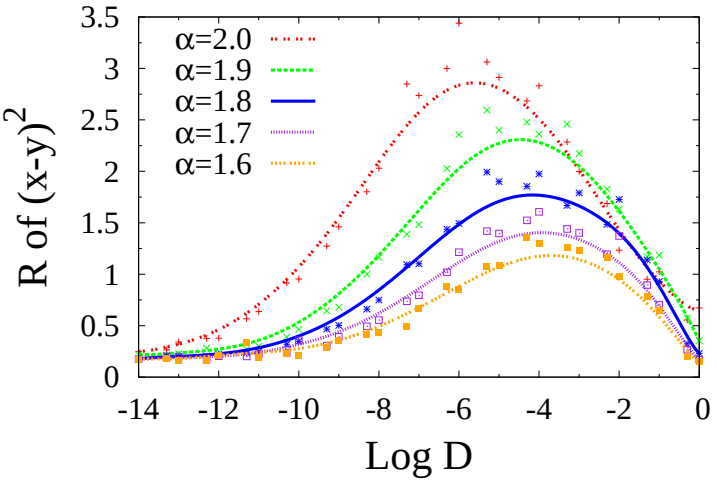

Figure 2.15: SNR of $(x-y)^2$ as a function of the noise intensity D for different values of the index α.

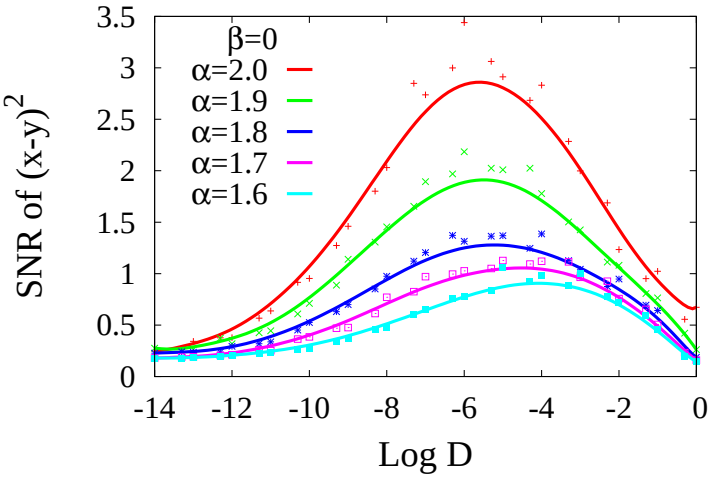

Figure 2.16: The SNR of the quantity $(x-y)^2$ as a function of the noise intensity D, for different values of the index α, namely $\alpha = 1.6, 1.7, 1.8, 1.9, 2.0$, and $\beta = 0$. Here we set D_γ at the value that maximizes the SPA curves of the parameter $\gamma(t)$. Red plus, green cross, blue star, pink empty square and light blue full square represent the SNR values calculated by numerical integration of Eqs. (2.41) - (2.43). The solid lines are the curves obtained by interpolating the numerical data. Each curve corresponds to the symbols with the same color.

2.2.6 SR with correlated noise sources

Now we want to consider symmetric Lévy stable distribution and statistically dependent noise sources. We intend to investigate the role of an interdependence between two different noise sources that influence the dynamics of the system. Motivation of this is the fact that fluctuations of food resources influence both the species concentrations through a multiplicative noise, and the interaction parameter through an additive noise. In fact, the contemporaneous presence of two noise sources, one acting directly on the species, the other one affecting the interaction parameter, can produce a "global" effect so that the effective multiplicative noise (that represents fluctuations of species concentrations) can result to be the combination of the additive noise and other noise sources. By this way, the additive noise (that mimics both fluctuations of climatic and/or atmospheric variables and food resources) affects directly not only the behaviour of the interaction parameter but also the dynamics of the two species. In particular, we consider that each source of multiplicative noise is obtained as a linear combination of the additive noise $\xi_\gamma^{\alpha,\beta}$ (see Eq. (2.43)) with a statistically independent noise source $\bar{\xi}_i^{\alpha,\beta}$ $(i = x, y)$. By this way, the multiplicative noise sources in Eqs. (2.41), (2.42) can be written as follows

$$\xi_x^{\alpha,\beta} = \rho_x \, \xi_\gamma^{\alpha,\beta} + \sqrt{1-\rho_x^2} \, \bar{\xi}_x^{\alpha,\beta}, \tag{2.52}$$

$$\xi_y^{\alpha,\beta} = \rho_y \, \xi_\gamma^{\alpha,\beta} + \sqrt{1-\rho_y^2} \, \bar{\xi}_y^{\alpha,\beta}. \tag{2.53}$$

The noise sources $\bar{\xi}_i^{\alpha,\beta}$ $(i = x, y)$ are α-stable Lévy processes. Due to Eqs. (2.52), (2.53), each multiplicative noise source $\xi_i^{\alpha,\beta}$ is statistically dependent on the additive noise source $\xi_\gamma^{\alpha,\beta}$ by a statistical dependence parameter ρ_i. To analyze the system dynamics we set $\rho_x = \rho_y = \rho$. By using Eqs. (2.52), (2.53) in the Lotka-Volterra model (see Eqs. (2.41), (2.42)), we obtain the time series and the corresponding SNR for different values both of the index α and statistical dependence parameter ρ. The results are reported in Fig. 2.17. For different combinations of the parameters α and ρ we note that the SNR of the square difference $(x-y)^2$ mantains its nonmonotonic behaviour as a function of the noise intensity. Specifically we note that the effect of the statistical dependence consists in shifting the maximum of the SNR towards higher values of the noise intensity, slightly affecting the synchronization phenomenon. For larger values of the statistical dependence between the noise sources ($\rho = 0.9$ in

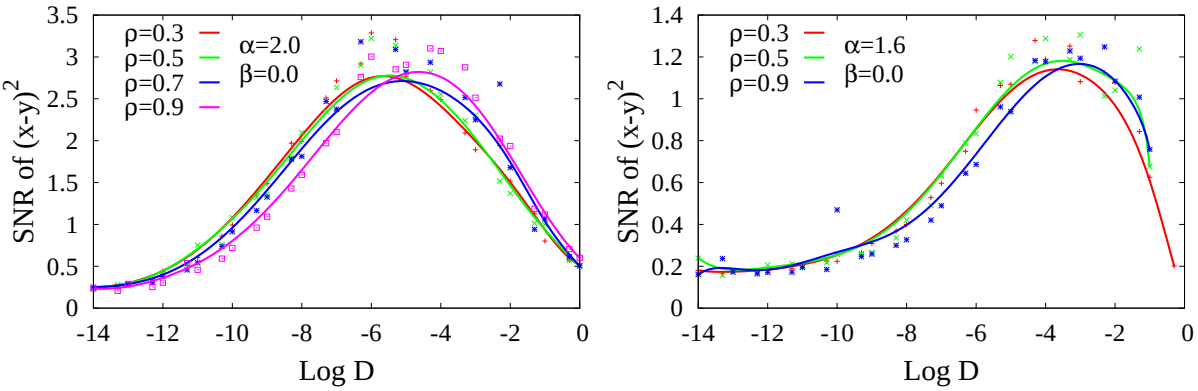

Figure 2.17: SNR of the quantity $(x-y)^2$ as a function of the noise intensity D for different values of both the index α and statistical dependence parameter ρ. In left panel: $\alpha = 2.0$, and $\rho = 0.3, 0.5, 0.7, 0.9$. In right panel: $\alpha = 1.6$, and $\rho = 0.3, 0.5, 0.9$. In both panels, red plus, green cross, blue star and (only for the top panel) pink empty square represent the SNR values calculated by numerical integration of Eqs. (2.41) - (2.43). The solid lines are the curves obtained by interpolating the numerical data. Each curve corresponds to the symbols with the same color.

Fig. 2.17) and higher noise intensity all curves, independently on the value of the index α, collapse in one curve. We can say that, in this range of noise intensity and for strong statistical dependence between noise sources, the dynamical response of the system is independent on the index α of the Lévy distribution.

Chapter 3

Open Quantum Systems

In this final chapter we present our recent results in two open quantum systems [136, 137].

First we propose a way to analyze low frequency noise in terms of fictitious correlated fluctuations of external parameters. We discuss a specific implementation, namely the Quantronium setup of a Cooper-pair box, showing that optimizing the trade-off between efficient coupling and protection against noise may allow to observe coherent population transfer in this nanodevice. Recent experiments have demonstrated coherent phenomena in three-level systems based on superconducting nanocircuits. This opens the possibility to detect Stimulated Raman Adiabatic Passage (STIRAP) in artificial atoms. Low-fequency noise (often $1/f$) is one of the main sources of decoherence in these systems, and we study its effect on the transfer efficiency.

Subsequently, we analyze the dynamics of a quantum particle subject to an asymmetric bistable potential and interacting with a thermal reservoir. We obtain the time evolution of the population distributions in both energy and position eigenstates of the particle, for different values of the coupling strength with the thermal bath. The calculation is carried out by using the Feynman-Vernon functional under the discrete variable representation.

3.1 Quantum Noise in Nanodevices

So far most of the research in this field has focused on the two lowest level of artificial atoms. In the last few years, it has been proposed that multilevel quantum coherent effects [50, 138, 139], could be observed in superconducting nanodevices: various schemes have been proposed to observe electromagnetically induced transparency [140], and selective population transfer by adiabatic passage [141]-[147]. Very recently, few experiments have demonstrated features of multilevel coherence in such devices, as the Autler-Townes effect [148, 149], coherent population trapping [150, 151], electromagnetically induced transparency [152], preparation and measurement of three-state superpositions [153].

In studying quantum optical effects in solid state devices, several differences are encountered with respect to the atomic realm: coupling between subsystems is larger, but also noise is larger, and often extends over several decades, low-frequency noise being the most important source of decoherence in many of the solid state implementations of quantum bits [154, 155]. On the other hand solid state devices offer several design solutions, and the possibility of tuning by external controls the spectral properties of the artificial atom [157]. All these elements come into play in multilevel structures [158], together with new features, as for example selection rules. Differences between specific designs may become crucial for the successful implementation of specific protocols.

Here we study coherent population transfer using the STIRAP protocol three-level artificial atoms. In Sec. 3.1.1 we introduce STIRAP, and discuss the sensitivity of the transfer efficiency to external parameters. Then we consider a specific implementation of the three-level artificial atom which is a good model for the Quantronium device [44, 60] and introduce a model for low-frequency charge noise (Sec. 3.1.4). In Sec. 3.1.7, we propose a way to characterize the effects of low-frequency noise, reducing the problem to that of the sensitivity of the transfer efficiency to fictitious correlated external parameters.

3.1.1 Coherent population transfer in three-level atoms

In quantum optics the STIRAP technique is based on a Λ configuration (Fig. 3.1) of two hyperfine ground states $|0\rangle$ and $|1\rangle$ and an excited state $|2\rangle$, with ener-

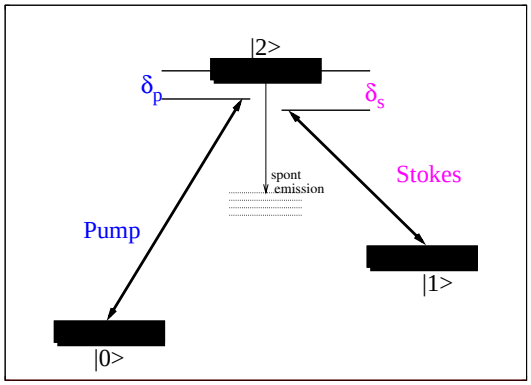

Figure 3.1: A three-level atom driven by two lasers in the Λ scheme. The state $|2\rangle$ may have a large decay probability.

gies E_0, E_1 and E_2 respectively [50, 159]. The system is driven by two classical laser fields [50, 138], called the Stokes laser $\Omega_{12} = \Omega_s \cos\omega_s t$ and the Pump laser $\Omega_{02} = \Omega_p \cos\omega_p t$. Each laser is nearly resonant with the corresponding transition. In the usual situations we can treat the laser drive fields in the Rotating-Wave Approximation (RWA) [160]. Moreover, one can introduce a phase transformation of the atomic basis and express the hamiltonian in a doubly rotating frame, with angular frequencies given by ω_i of the driving fields. The effective Hamiltonian reads

$$\tilde{H} \;=\; \delta|1\rangle\langle 1| + \delta_p|2\rangle\langle 2| + \frac{1}{2}(\Omega_s|2\rangle\langle 1| + \Omega_p|2\rangle\langle 0| + \text{h.c.}) \tag{3.1}$$

where we define the detunings $\delta_s = E_2 - E_1 - \omega_s$, $\delta_p = E_2 - E_0 - \omega_p$ and the two-photon detuning $\delta = \delta_p - \delta_s = E_2 - E_1 - (\omega_p - \omega_s)$.

At two-photon resonance, $\delta = 0$, the Hamiltonian (3.1) has an eigenstate which is a superposition of the two lowest atomic levels only

$$|D\rangle \;=\; \frac{1}{\sqrt{|\Omega_s|^2 + |\Omega_p|^2}}\,(\Omega_s|0\rangle \;-\; \Omega_p|1\rangle) \quad . \tag{3.2}$$

It is usually referred as the dark state since, despite of the presence of the lasers, the atom cannot be excited to the state $|2\rangle$ and consequently decay by spontaneous emission (Fig. 3.1). Instead, the laser fields interfere destructively and, as a result, the population is coherently trapped. A given dark state can be prepared by an

appropriate choice of both the Rabi frequencies Ω_i and the relative phase of the ac fields.

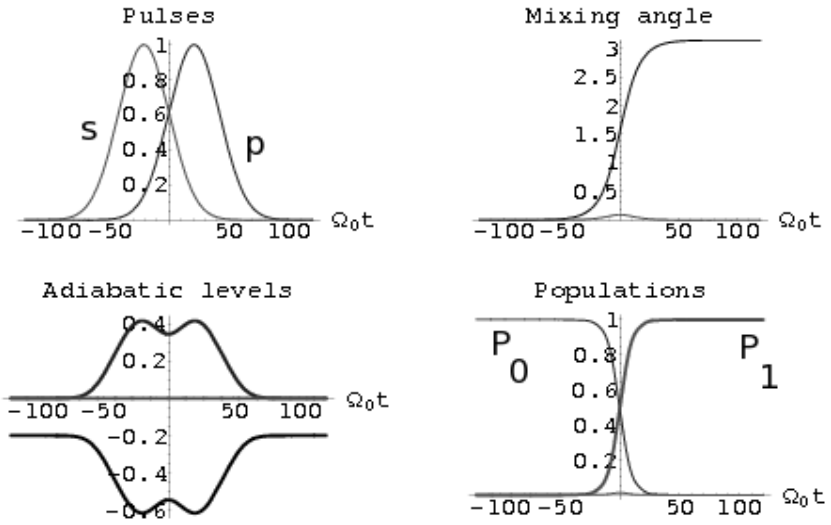

Figure 3.2: Ideal STIRAP at two-photon resonance $\delta = 0$, obtained by operating with two pulses in the counterintuitive sequence (top left panel). The system prepared in the state $|0\rangle$ follows the Hamiltonian along the zero-energy adiabatic level (left lower panel) yielding complete population tranfer (right lower panel, where $P_i = |\langle i|\psi(t)\rangle|^2$). In top right panel, the mixing angle of the dark state as a function of time for the adiabatic evolution. The pump laser is slightly detuned, $\delta_p = -0.2\Omega_0$.

3.1.2 The STIRAP protocol

From Eq. (3.2) it can be seen that by slowly varying the coupling strengths, $\Omega_s(t)$ and $\Omega_p(t)$, the dark state can be rotated in the two-dimensional subspace spanned by $|1\rangle$ and $|0\rangle$. Using adiabatic dynamics in the rotating frame, the STIRAP protocol implements coherent population transfer between the atomic states $|0\rangle \rightarrow |1\rangle$ [138].

The system can be prepared in the state $|0\rangle$ by letting $\Omega_p = 0$ and switchig on $\Omega_s(t) \neq 0$. By slowly switching Ω_s off while $\Omega_p(t)$ is switched on, the population can be transferred from state $|0\rangle$ to state $|1\rangle$. Finally also Ω_p is switched off. The mixing angle of the dark state Eq.(3.2) is defined as $\theta(t) = 2\arctan[\Omega_p(t)/\Omega_s(t)]$, and evolves from $\theta = 0$ to $\theta = 2\pi$ (Fig. 3.2, upper right panel).

This is the so-called counterintuitive scheme as opposed to the intuitive strategy where the pump pulse preceeds the Stokes pulse. In this case population transfer involves, as an intermediate step, population of the excited state $|2\rangle$, which can undergo spontaneous decay, strongly affecting the population transfer efficiency. One advantage of STIRAP is that, in the ideal procedure, the state $|2\rangle$ is never populated [138, 139], therefore it is not sensitive to spontaneuos decay. Moreover, provided adiabaticity is preserved, STIRAP is in principle insensitive to many details of the protocol, and in practice it turns out to be insensitive to the precise timing of the operations.

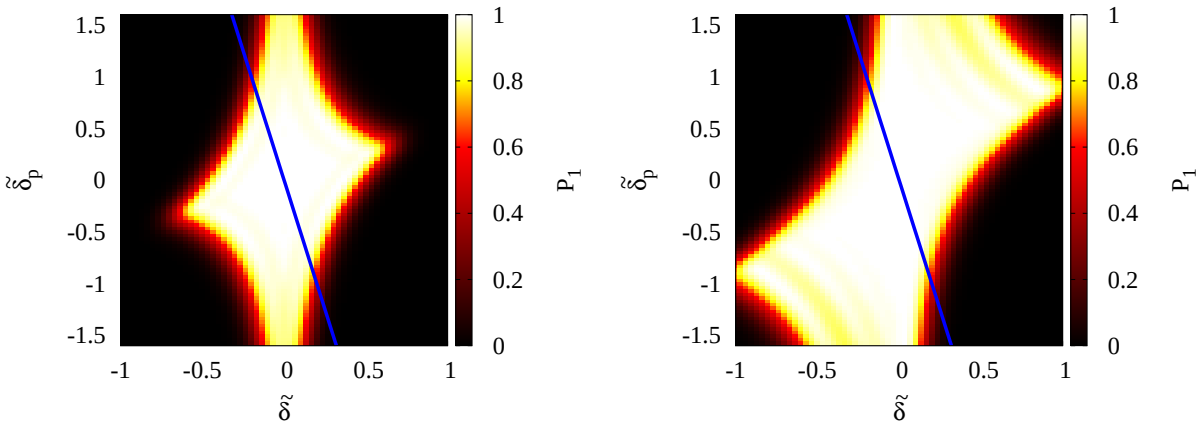

Figure 3.3: (left panel) Contour plot of the intensity of the transfer efficiency as a function of single-photon and two-photon detuning for equal peak Rabi frequencies $\kappa = \Omega_S/\Omega_P = 1$ (left panel) and $k = 2$ (right panel). In axes x, y we have $\tilde{\delta} = \delta/\Omega_0$ and $\tilde{\delta_p} = \delta_p/\Omega_0$, respectively. In both panels, the bright region corresponds to large efficiency of population transfer (more than 80%). A two-photon detuning $|\delta| \geq \Omega_0/5$ determines a substantial decrease of the efficiency. The line corresponds to correlated detunings, which give an effective description of fluctuation in the Quantronium (Sec. 3.1.7). Increasing the strength of the Stokes pulses enlarges asymmetrically the region of large transfer efficiency.

3.1.3 Sensitivity to parameters

Adiabaticity is critical to achieve high efficiency, therefore much effort has been devoted in the past to optimization of the pulse shapes [139]. A necessary condition for adiabaticity is $|\dot{\Omega}_j/\Omega_j| \ll \omega_j$ $(j = s, p)$ which suggests that efficiency can be improved by using large enough Rabi peak frequencies. Formally, they determine a large (Autler-Townes) splitting of the instantaneous eigenstates in the rotating frame [139, 138]. This splitting prevents unwanted transitions triggered by off diagonal parts (neglected in the adiabatic approximation) of the Hamiltonian in the instantaneous eigenbasis. These non-adiabatic terms are proportional to $\dot{\theta}(t)$ and tend to detrap the population, reducing the transfer efficiency. If we let $\Omega_p(t) = \Omega_0\, f[(t-\tau)/T]$ and $\Omega_s(t) = \kappa\Omega_0\, f[(t+\tau)/T]$, a positive delay τ implements the counterintuitive sequence of STIRAP. For Gaussian pulses, $f(x) = \mathrm{e}^{-\mathrm{x}^2}$, optimal choices are $\Omega_0 T > 10$ and $\tau \approx T$ [139]. In this paper we use a reduced pulse width $\Omega_0 T = 30$ and a delay $\tau = 0.7\,T$.

Sensitivity to detunings

When the two frequencies ω_s and ω_p are not exactly resonant with the respective transitions, the presence of non-zero detunings δ_s and δ_p may strongly affect the efficiency. Actually, the two-photon detuning is the crucial parameter. As it is shown in Fig. 3.3, small deviations of the two photon detuning δ lead to a substantial decrease of the efficiency, which is less sensitive to single-photon detunings at two-photon resonance $\delta = 0$. Actually, phenomena entering non-ideal STIRAP are qualitatively different according to δ vanishing or not, and their interplay leads to a rich physical picture.

Finite single photon detunings at $\delta = 0$ do not affect the formation of the dark state, because the mixing angle does not depend on it. Instead they increase the nonadiabatic terms [139]. The efficiency is insensitive to small single-photon detunings ($\delta \leq \Omega_0$, see also Fig. 3.2), while larger ones prevent the adiabatic follow on of the dark state.

The detuning from two-photon resonance is more detrimental for STIRAP, because it prevents the exclusive population of the trapped state, which is no longer an instantaneous eigenstate of the Hamiltonian. A more detailed analysis of the instan-

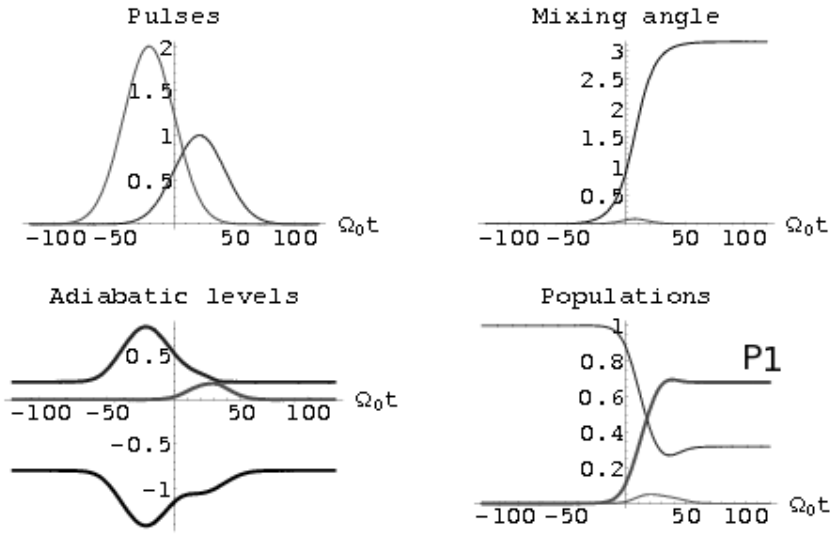

Figure 3.4: STIRAP with finite two-photon detuning $\delta = 0.2\,\Omega_0$, with the two pulses in sequence in top left panel. Population transfer occurs due to Zener transitions between crossing adiabatic levels (lower left panel), and the transfer efficiency is reduced (lower right panel). In top right panel, the mixing angle as a function of time. Here $\kappa = 2$ and $\delta_p = -4\delta$. This parametrization being appropriate for discussing effects of low-frequency noise in the Quantronium (Sec. 3.1.7).

taneous eigenstates when $\delta \neq 0$ shows that there is no adiabatic transfer state providing an adiabatic connection from the initial to the target state, as does the dark state for $\delta = 0$. In this case, the evolution leads to complete population return of the system to its initial state. The only mechanism which leads to population transfer is by non-adiabatic transitions between the adiabatic states. Actually for small values of δ, narrow avoided crossings between the instantaneous eigenvalues can occur and the population can be transferred by Landau-Zener tunneling [139, 138], as shown in Fig. 3.4.

The above considerations lead to the conclusion that the correlations between the detunings δ_s and δ_p are very important. In fact, strongly correlated fluctuating detunings, nearly preserving two-photon resonance, still allow large transfer efficiency [161, 162]. This issue becomes very important in the discussion of the effects of low-frequency noise in solid state nanodevices.

Sensitivity to Rabi frequencies

For ideal STIRAP it is better to have two nearly equal peak Rabi frequencies, i.e. $\kappa = \Omega_S/\Omega_P = 1$. Indeed if the two maximum Rabi frequencies are different, say $\kappa > 1$, while the pulse widths are about the same, the projection of the state vector onto the adiabatic transfer state is very good initially (because in our case the more intense pulse occurs first), but necessarily less good in the final stage. Consequently the transfer efficiency will be small [139].

The situation may be different if finite detuning is considered. In particular in the right panel of Fig. 3.3 it is shown that the region of great transfer efficiency enlarges asymmetrically. This happens when the larger pulse occurs during the Zener process of imperfect STIRAP (the opposite situation is illustrated in Fig. 3.4).

Of course, using large pulse areas, small deviations from the optimal conditions do not lead to significant drop in transfer efficiency, and in general increasing both the amplitudes is the convenient strategy to counteract the effect of imperfections. However, in solid state nanodevices there are restrictions on the amplitude and symmetry of the coupling to the microwave fields, playing the role of the lasers. Therefore, operating at $\kappa \neq 1$ may give room to further optimize the transfer efficiency.

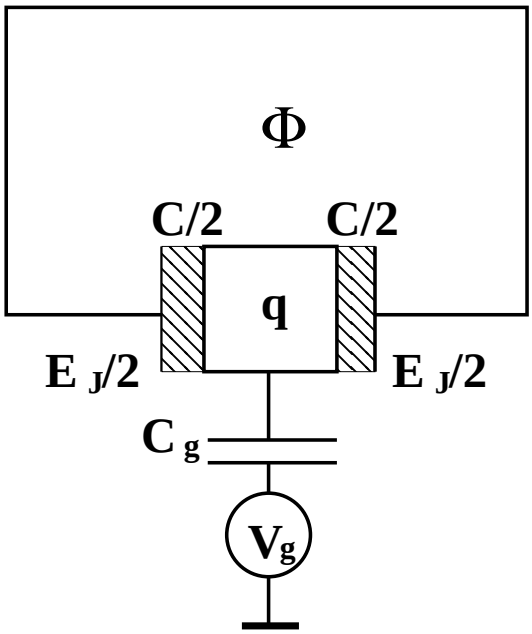

Figure 3.5: Equivalent circuit for the Quantronium. Here q and C are the charge and the capacitance of the superconducting island respectively; C_g and V_g are the capacitance and the voltage of the gate; E_g is the Josephson energy and Φ is the magnetic flux.

3.1.4 STIRAP in the Quantronium

We now discuss the implementation of the Hamiltonian (3.1) in the Quantronium [44]. The basic unit of this device consists of a Cooper pair box, namely a superconducting loop interrupted by two adjacent tunnel junctions with Josephson energies $E_J/2$ (Fig. 3.5). The two small junctions define the superconducting island of the box, whose total capacitance is C and charging energy $E_C = (2e)^2/2C$. The electrostatic energy can be modulated by a gate voltage V_g connected to the island via a capacitance $C_g \ll C$ and the Hamiltonian reads

$$H_0(q_g) = \sum_q E_C[q - q_g]^2 |q\rangle\langle q| - \frac{E_J}{2}(|q\rangle\langle q+1| + h.c.), \tag{3.3}$$

where $\{|q\rangle\}$ are eigenstates of the number operator $\hat{q}$ of extra Cooper pairs in the island. We have defined the reduced gate charge $q_g = C_g V_g/(2e)$, which is the control parameter of the system. Eigenstates of the box are superpositions of charge eigenstates. The spectrum can be modified by tuning q_g (Fig.3.6) and the device is usually operated as a qubit close to the value $q_g = 1/2$. This is a symmetry point for the device Hamiltonian (3.3) and it turns out that it is an optimal working point where the system is well protected against external noise, allowing to obtain experimental dephasing times of several hundreds nanoseconds [44, 60].

Manipulation of the quantum state is performed by adding to the dc part of the gate voltage, ac microwave pulses with small amplitudes $q_g \to q_g + q_g^{ac}(t)$. The resulting Hamiltonian can be written as

$$H_{tot}(t) = H_0(q_g) + A(t)\,\hat{q}, \tag{3.4}$$

where $A(t) = -2E_C q_g^{ac}(t)$. The effective three-level artificial atom Hamiltonian

$$H(t) = \sum_i E_i |\phi_i\rangle\langle\phi_i| + A(t) \sum_{ij} q_{ij}\, |\phi_i\rangle\langle\phi_j| \tag{3.5}$$

is obtained by projecting $H_{tot}(t)$ onto the subspace spanned by the three lowest energy eigenvectors $|\phi_i\rangle$, $i = 0, 1, 2$ of $H_0(q_g)$. In Eq. 3.5 $q_{ij} = \langle\phi_i|\hat{q}|\phi_j\rangle$. The STIRAP protocol can be carried out if we let $A(t) = A_s(t)\cos\omega_s t + A_p(t)\cos\omega_p t$. We then use the RWA, by retaining only quasi-resonant off-diagonal and co-rotating terms of the drive Hamiltonian, which simplifies to

$$A(t)\hat{q} \;\to\; H_{RWA}(t) = \frac{1}{2}\, q_{12}\, A_s(t)\, \mathrm{e}^{\mathrm{i}\omega_\mathrm{s}\mathrm{t}} |\phi_1\rangle\langle\phi_2| + \frac{1}{2}\, \mathrm{q}_{02}\, \mathrm{A_p(t)}\, \mathrm{e}^{\mathrm{i}\omega_\mathrm{p}\mathrm{t}} |\phi_0\rangle\langle\phi_2| \;+\; \mathrm{h.c.} \tag{3.6}$$

In this approximation the truncated Hamiltonian (3.5) is transformed to the doubly rotated frame, at angular frequencies ω_s and ω_p. This yields an effective Hamiltonian $\tilde{H}(q_g)$ with the structure of Eq.(3.1), which therefore implements the Λ configuration. Notice that matrix elements $q_{ij} = \langle\phi_i|\hat{q}|\phi_j\rangle$ play the same role of the dipole matrix elements in defining the Rabi frequencies, $\Omega_s = q_{12}\, A_s$ and $\Omega_p = q_{02}\, A_p$.

The RWA of Eq.(3.6) is justified in the regime where peak Rabi frequencies are much smaller than the splittings, $\Omega_i \ll |E_i - E_j|$, which is the usual experimental regime. In this case the terms neglected are rapidly oscillating in the rotating frame, and only produce a small and fast modulation in the dynamics. The approximation is supported by simulations of the full Hamiltonian (3.4), using more than ten energy levels [144, 145, 163] for the usual operating region near $q_g = 1/2$.

It is worth stressing the dependence of the effective Hamiltonian $\tilde{H}(q_g)$ on the bias charge q_g. For instance in Eq.(3.1) detunings depend on q_g via the energies E_i and peak Rabi frequencies via off diagonal matrix elements q_{ij} (see Fig. 3.6). In particular at the symmetry point, $q_g = 1/2$, the matrix element q_{02} vanishes and in general selection rules hold preventing transitions between energy states with the same parity of the label. The off-diagonal matrix elements q_{ij} shown in Fig. 3.6 play the same role of the dipole matrix elements in atoms. The largest one is q_{01}, which provides the coupling for qubit operations. Fields in STIRAP are coupled via q_{12} and q_{02}. This latter vanishes due to a parity selection rule at the symmetry point $q_g = 1/2$.

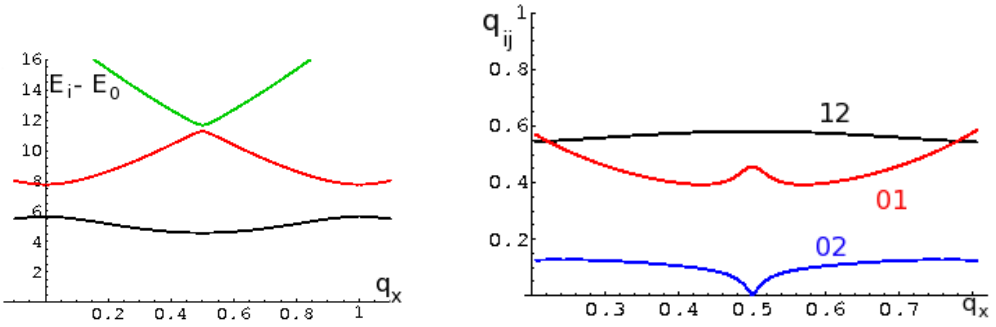

Figure 3.6: Left panel: energy spectrum of a Quantronium setup with $E_J = E_C$. The splitting $E_i - E_0$ in units of E_C is plotted as functions of q_g, The first splitting is given by $E_1(1/2) = 0.94$. Right panel: off-diagonal entries of the Cooper pair number operator, q_{01}, q_{12} and q_{02} from top to bottom.

3.1.5 Broadband noise

Since the nanocircuit is not isolated, the model has to be supplemented with noise terms. The structure of coupling to noise can be understood considering classical fluctuations of each of the parameters in the Hamiltonian of Eq. (3.3). For instance fluctuations of the gate charge can be accounted for by adding a classical stochastic term $q_g \to q_g + \delta q_x(t)$. Physical processes described by these fluctuations are those leading to a stray electrical polarization of the island, and include effects of voltage fluctuations of the circuit and effects of switching impurities [154] located in the oxides and in the substrate close to the device. Since these latter are in practice the main source of decoherence (circuit fluctuations can be reduced by careful filtering) for the Quantronium, we will only consider fluctuations of the gate charge, thus acting on the same port used to drive the system. We may write the resulting Hamiltonian as

$$H = H_0(q_g) + H_{RWA}(t) + \delta H \tag{3.7}$$

where $\delta H = -2E_C\,\delta q_x(t)\,\hat{q}$. In general, noise is due to the coupling of the device to an environment which is itself a quantum system, and the Hamiltonian is obtained by letting $\delta H = \hat{X}\,\hat{q} + H_{env}$, where H_{env} describes the environment and $\hat{X}$ is an environment operator. This model allows to treat high-frequency noise by a quantum optical master equation in the weak coupling regime. However the power spectrum of noise in the solid state has a large low-frequency component which invalidates the weak coupling approach. A multistage approach has been proposed [155, 156] where high and low-frequency noise are separtated, and the latter is treated as an adiabatic classical field. Formally $\hat{X} \to \hat{X}_f - 2E_C\,\delta q_x(t)$, where $\hat{X}_f$ describes fast environmental degrees of freedom and $\delta q_x(t)$ is now a classical slow stochastic process. We let $q_x(t) = q_g + \delta q_x(t)$ and write the Hamitonian as

$$H = H_0(q_x(t)) + H_{RWA}(t) + \hat{X}\,\hat{q} + H_{env}. \tag{3.8}$$

In many cases low-frequency noise with $1/f$ spectrum, which is the leading contribution of the slow dynamics of $q_x(t)$, is captured by a Static-Path Approximation (SPA), that is approximating the stochastic process by a suitably distributed random variable [60, 155]. In the case of many weakly coupled noise sources, the distribution of δq_x is Gaussian and is characterized by an energy width $\sigma = 2E_C\,\sigma_x$. Populations

and coherences are obtained by averaging over this distribution the entries of the reduced density matrix of the system. This approach has quantitatively explained the power law decoherence observed in Quantronium [60] and in phase qubits [164], and has been recently studied for optimal tuning of multiqubit systems [158].

This point of view provides a simple argument explaining why the symmetry point $q_g = 1/2$ is well protected against external noise. Indeed, since the energy splitting $E_1 - E_0$ depends only quadratically on the fluctuations δq_x around this point, energy fluctuations are suppressed. As a consequence, superpositions of the two lowest energy levels keep coherent, yielding a power law suppression of the signal [60, 155] and longer dephasing time.

3.1.6 Effective model for low-frequency noise in STIRAP

In order to study STIRAP we project the Hamiltonian (3.8) on the subspace spanned by the three lowest energy instantaneous eigenvectors of $H_0(q_x(t))$. In doing so we assume the adiabaticity of the dynamics induced by $\delta q_x(t)$, which allows to neglect effects of the time-dependence of the eigenvectors. Of course, if we start from the SPA version of the Hamiltonian (3.8), this condition is automatically verified. We focus on the system plus drive Hamiltonian, $H_0(q_x(t)) + H_{RWA}(t)$, which has in the rotated frame the same structure of Eq.(3.1). Parameters entering the Hamiltonian depend, of course, on the realization of the stochastic process. Fluctuations of the eigenenergies translate in fluctuations of the detunings (we let $E_0 = 0$)

$$\delta(q_x) = E_1(q_x) - \omega_p + \omega_s \quad ; \quad \delta_p(q_x) = E_2(q_x) - \omega_p. \tag{3.9}$$

Also the effective drive fluctuates due to fluctuations of the charge matrix elements, for instance $\Omega_p = q_{02}(q_x)\, A_p$.

In the regime of validity of the SPA, this analysis shows that the effect of low-frequency noise in solid-state devices, can be discussed in term of sensitivity of the transfer efficiency obtained by STIRAP to parameters characterizing an equivalent drive. This allows to apply several results known from quantum optics to solid state devices. For instance the large sensitivity to two-photon detuning, translates in the sensitivity to fluctuations of the lowest splitting, which is then the main figure to be minimized in order to achieve efficient population transfer in the solid state. Notice also that, the main steps of the analysis carried out for the Quantronium can also

be applied to other solid state implementations devices, as long as decoherence in the dynamics of the two lowest energy levels is well characterized.

3.1.7 Effects of low-frequency noise in the Quantronium

In this section we will apply the above analysis to discuss the observability of STIRAP in the Quantronium, and we will consider a device with $E_J = E_C$, whose spectral properties are given in Fig. 3.6. An important point is that while dephasing is minimized by operating at the symmetry point $q_g = 1/2$, the selection rule $q_{02} = 0$ prevents to implement STIRAP. Therefore, it has been proposed to operate slightly off the symmetry point.

In these conditions it has been shown that STIRAP allows a substantial coherent population transfer also in the presence of high-frequency noise. Notice that, while in quantum optical systems STIRAP connects two ground states, in solid state devices high-frequency noise leads to decay $1 \to 0$. These processes are well characterized experimentally [60]. In Ref. [144] it has been shown that secular dephasing between the above two states does not produce relevant effects during population transfer. A careful analysis [163] has allowed to optimize parameters for STIRAP in the presence of high-frequency noise, showing that operating at $q_g = 0.47$ already provides sufficient coupling q_{02}.

On the other hand, it is known that the effect of low-frequency noise increases when the system is operated away from the symmetry point [60, 165]. This opens the question of the trade-off between efficient coupling of the driving fields and dephasing due to slow excitations in the solid-state. In this work we focus on this issue and we neglect high-frequency noise.

Another consequence of the selection rule is that, in the vicinity of the symmetry point, coupling with the drives is asymmetric. At $q_g \approx 0.47$ we have $q_{02} \approx q_{12}/4$ (see Fig. 3.6). Since in any case it is convenient to work with the largest pump pulse Rabi peak frequency Ω_0, we will fix this value. It can be estimated by writing $\Omega_0 = (q_{02}/q_{01})\,\Omega_R \approx \Omega_R/6$, where Ω_R is the maximal angular frequency for Rabi oscillations between the lowest doublet. Frequences of approximately $\nu_R = 750 - 900\,MHz$ can be achieved in the Quantronium, corresponding to a maximum field amplitude A_p yielding $\nu_p = 100 - 150\,MHz$. The peak Rabi frequency of the Stokes field could be chosen as $\nu_s = \kappa\nu_p$, with $\kappa \leq 4$, but we will argue that $\kappa = 1$ is the

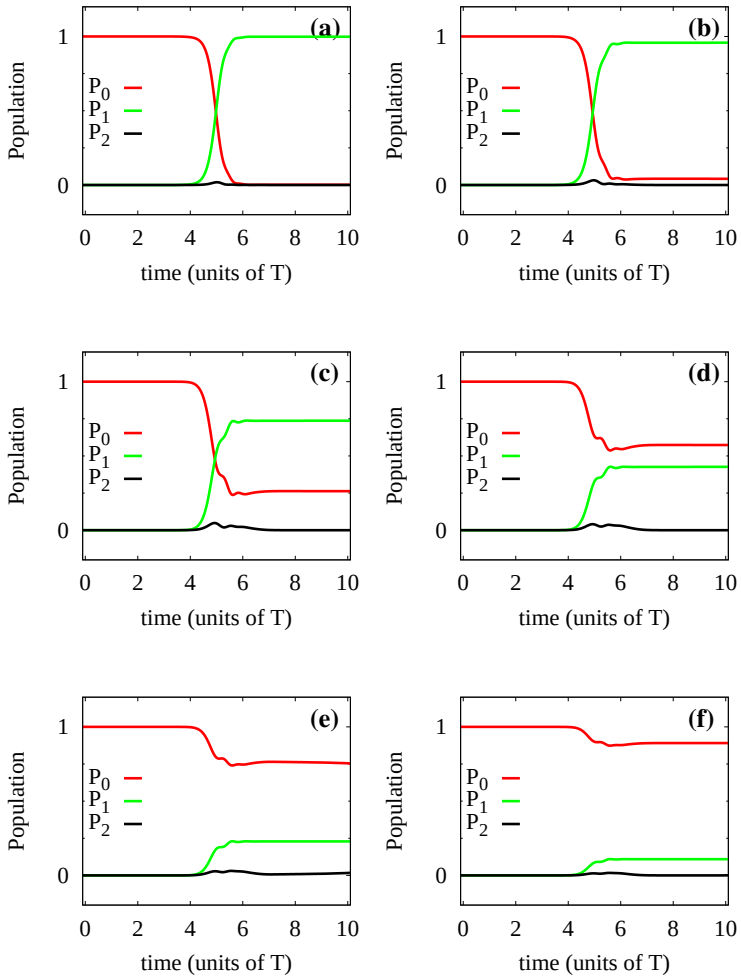

Figure 3.7: Averaged population histories for different values of the fluctuation intensity of the two-photon detuning, σ_δ. In panels (a)-(f), we have $\sigma_\delta = 0.05, 0.1, 0.2, 0.4, 0.8, 1.6$ in units of Ω_0, respectively. Here detunings are anticorrelated ($\delta_p = -5\delta$) and drives have been symmetrized ($\kappa = 1$) by using a lower amplitude A_s for the Stokes field. For $\Omega_0 = 2\pi \cdot 10^8\,\mathrm{rad/s}$ the relevant curve is $\sigma_\delta = 0.2$ and $T = 48\,ns$ yielding 60% of population transfer. Slightly increasing $\nu_p = 150MHz$ one obtains $\sigma_\delta = 0.125$ and $T = 30\,ns$.

optimal choice.

Fluctuations δq_x of the gate charge can be estimated from the dephasing time of the qubit at the symmetry point. This is due to energy fluctuations $\sigma/E_1(1/2) \sim 0.01$. Therefore fluctuations of gate charge, which are characteristic of the environment only, are estimated by $\sigma_x = \sigma/(2E_C) \approx 3 \cdot 10^{-3}$, where we used $E_C \sim 15\, GHz$. Notice that these features may depend on details of the protocol as the total measurement time, but for $1/f$ noise the dependence is logarithmic and improving the procedure does not bring essential changes of σ_x.

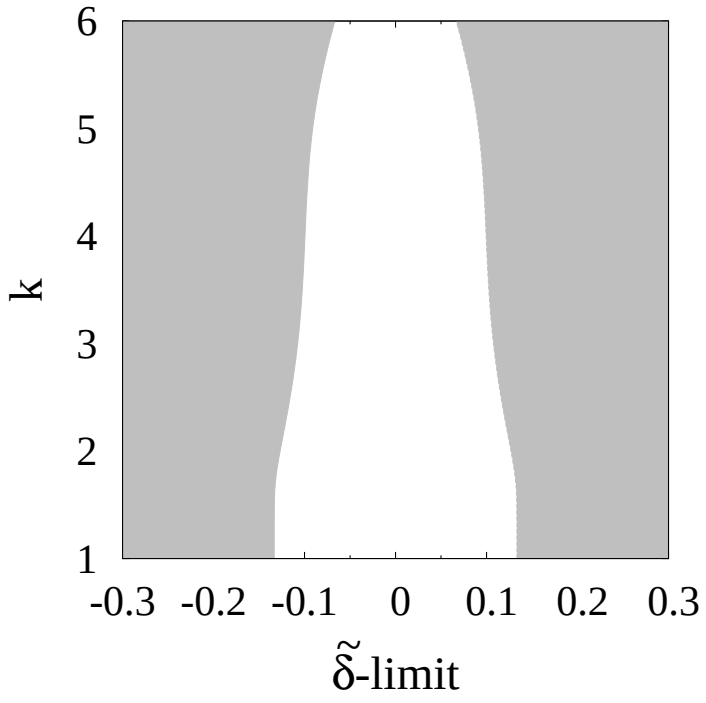

Figure 3.8: Ratio of the maximum drive amplitudes $k = \Omega_S/\Omega_P$ as a function of the two-photon detuning limits, $\tilde{\delta} = \delta/\Omega_0$, for anticorrelated noise, typical of Quantronium ($\delta_p = -5\delta$). The white zone is the region where we have more than 80% of transfer efficiency of STIRAP.

We choose to operate at single and two-photon resonance, $\delta = \delta_p = 0$ at $q_g = 0.47$. According to Eq.(3.9), fluctuations δq_x determine a distribution of the detuning. In the left panel of Fig. 3.6, we can directly read off fluctuations of the splitting, which give the estimate $\Delta\delta = \Delta E_1(q_x) \approx (\partial E_1/\partial q_x)_{q_g}\, \delta q_x$ and

$\Delta\delta_p = \Delta E_2(q_x) \approx (\partial E_2/\partial q_x)_{q_g}\, \delta q_x$.

Therefore, fluctuations of the detunings are anticorrelated, $\Delta\delta_p = a\,\Delta\delta$, where the ratio of the two derivatives is given by $a \approx -5$. This corresponds to the lines drawn in the efficiency diagrams of Fig. 3.3. Using $(\partial E_1/\partial q_x)_{q_g}\, \delta q_x \approx (E_J/4)$, we find that fluctuations of the two-photon detuning are estimated by $\sigma_\delta/\Omega_0 \approx E_J\sigma_x/(4\Omega_0) \approx \sigma/(8\Omega_0) \sim 0.1 - 0.2$, identifying the region of the efficiency diagrams explored by the system during the protocol. This estimate suggests that energy fluctuations in the Quantronium should still allow to observe coherent population.

Fluctuations of the off-diagonal elements can be estimated by the plots in Fig. 3.6 (right panel), yielding figures of $\sim (1/4)\,\sigma_x\Omega_0 \sim 10^{-3}\Omega_0$, therefore they can be neglected. The transfer efficiency is then calculated by averaging the population histories over the distribution of correlated detunings. Results are shown in Fig. 3.7 for different values of the fluctuation intensity of the two-photon detuning σ_δ in units of Ω_0. Here detunings are anticorrelated ($\delta_p = -5\delta$) and drives have been symmetrized ($\kappa = 1$), by using a lower amplitude A_s for the Stokes field. It is seen that in standard experimental conditions the low-frequency noise allows from 60% to more than 90% population transfer in the Quantronium. Notice that even for $\sigma_\delta = 0.2\,\Omega_0$ the average population of the intermediate level is very small during the whole procedure.

Finally we comment about the optimization of the laser amplitudes. In the above simulations we used $\kappa = 1$, but it would be possible to use a larger Stokes pulse, up to $\kappa = 4$. However this does not improve the efficiency if fluctuations of the detunings are anticorrelated. As shown in Fig. 3.8, in this case the region of large efficiency shrinks for increasing κ.

3.2 Asymmetric Bistable System

A feature which makes a strong difference between the behaviour of a quantum system with respect to a classical one is the quantum tunneling. This effect often occurs in condensed matter physics, such as Josephson junctions and heteronanostructures [166, 167]. In a dissipative quantum system interacting with a thermal bath, the quantum tunneling can play an important role on the relaxation time from a metastable state [168, 169]. During the last two decades the effects of environ-

ment on quantum tunneling phenomenon have been intensively studied [38],[169]-[172]. Commonly, environment is modelled as a number $\mathcal{N}$ (usually $\mathcal{N} \to \infty$) of harmonic oscillators considered at thermal equilibrium, i.e. thermal bath, interacting with the quantum system through a bilinear coupling [173]-[177]. In this context, symmetric and asymmetric quantum bistable systems are good enough to analyze superconducting quantum bits and decoherence phenomena [178, 179]. Obtaining longer coherence times in such systems, when they interact with noisy environment, is one of the major requirements in devising and manufacturing devices capable of storing quantum bits. In this respect, a main topic is to know the properties of a particle subject to an external potential, in the presence of random fluctuations. It can be also useful to study the changes occurring in the dynamics of a quantum particle affected by noisy perturbations, when different shapes of the potential profile are used. Potentials which model the interaction with laser beams have most interesting implications for quantum systems such as the coherent destruction of tunneling [180], the effect of quantum stochastic resonance [181], and the control and reduction of decoherence in open quantum systems [182]. In this work, in order to analyze the evolution of a quantum particle subject to time-independent asymmetric bistable potential and affected by environmental noise, we use the Caldeira-Leggett model [170], which allows to derive a quantum mechanical analogue of the generalized Langevin equation. The study is performed by using the approach of the Feynman-Vernon functional [183] in discrete variable representation (DVR) [168, 184].

3.2.1 The noise seen as interactions with thermal bath

Our system consists of a quantum particle with mass M, interacting with a thermal bath which plays the role of environment. The dynamics of the particle is investigated by using the Caldeira-Leggett model [170]. In our analysis $\hat{q}$ and $\hat{p}$ are one-dimensional operators for position and momentum, respectively.

The unperturbed Hamiltonian of the system is

$$\hat{H}_0 = \frac{\hat{p}^2}{2M} + \hat{V}_0(\hat{q}) \tag{3.10}$$

where

$$\hat{V}_0(\hat{q}) = \frac{M^2\omega_0^4}{64\Delta U}\hat{q}^4 - \frac{M\omega_0^4}{4}\hat{q}^2 - \hat{q}\epsilon, \tag{3.11}$$

is the asymmetric bistable potential shown in Fig. 3.9. Here, ϵ and ΔU are the asymmetry parameter and the barrier height, respectively, and ω_0 is the natural oscillation frequency. In our study we consider only 8 energy eigenstates. In Fig. 3.9

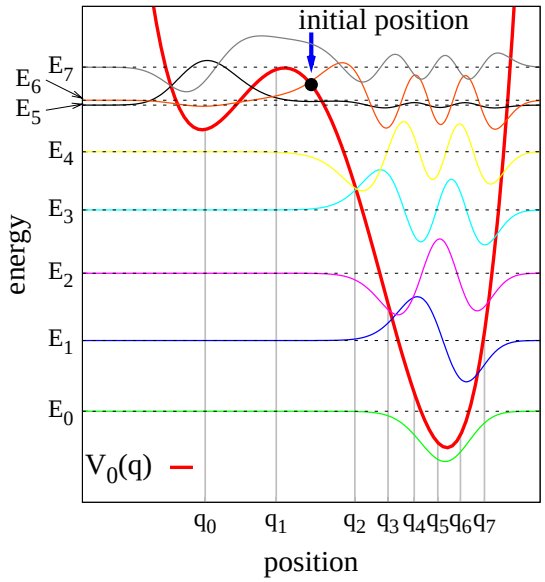

Figure 3.9: Potential profile $V_0(q)$ (see Eq. (3.11)) for $\Delta U = 3$ and $\epsilon = 0.5$. Energy levels and corresponding eigenstates considered in our analysis are indicated by horizontal lines and curves, respectively. The energy eigenvalues are $E_0 = -2.01$, $E_1 = -0.92$, $E_2 = 0.11$, $E_3 = 1.08$, $E_4 = 1.97$, $E_5 = 2.69$, $E_6 = 2.76$, $E_7 = 3.27$. By using the DVR-state $|q_\mu\rangle$, eigenvalues of the position operator are obtained and shown on the horizontal axis: $q_0 = -4.17$, $q_1 = -1.38$, $q_2 = 1.71$, $q_3 = 3.02$, $q_4 = 4.05$, $q_5 = 4.97$, $q_6 = 5.86$, $q_7 = 6.81$. The initial position is $q_{start} = 0$ (black circle).

these energy eigenvalues are shown on the vertical axis. In the same figure, on the horizontal axis we indicate the 8 position eigenvalues, obtained by using the DVR-state $|q_\mu\rangle$. The black circle marks the initial position of the particle, that is the system at $t = 0$ is in a state given by a proper linear combination of the corresponding 8 eigenstates $|q_\mu\rangle$ considered in our analysis. The curves shown in the figures are the eigenfunctions related to the 8 energy eigenvalues.

In order to describe the dynamics of the particle interacting with environment, we consider the following Hamiltonian

$$\hat{H}(t) = \hat{H}_0(t) + \hat{H}_B, \tag{3.12}$$

where

$$\hat{H}_B = \sum_{j=1}^{\mathcal{N}} \frac{1}{2} \left[\frac{\hat{p}_j^2}{m_j} + m_j \omega_j^2 \left(\hat{x}_j - \frac{c_j}{m_j \omega_j^2} \hat{q} \right)^2 \right] \tag{3.13}$$

is the Hamiltonian which describes the thermal reservoir and its interaction with the particle. As usual, the thermal bath is depicted by an ensemble of $\mathcal{N}$ harmonic oscillators with spatial coordinate $\hat{x}_j$, momentum $\hat{p}_j$, mass m_j, and frequency ω_j. The coefficients c_j are the coupling constant between system and thermal bath.

We note that, as $\mathcal{N} \to \infty$, from Eq. (3.13) a continuous spectral density is obtained.

In our study we use the Ohmic spectral density characterized by an exponential cut-off ω_c

$$J(\omega) = \eta \omega \exp\left(-\frac{\omega}{\omega_c} \right). \tag{3.14}$$

Here, $\eta = M\gamma$ with γ the strength of the coupling between system and heat bath. We note also that $\omega_c \gg \omega_0, \omega_j, \gamma$.

Because of the bilinear coupling between the coordinate $\hat{q}$ of the system and the coordinate $\hat{x}$ of the thermal bath, this model is the quantum analogue of a classical system affected by a constant random force [38]. In the next two subsections we briefly summarize the mathematical approach used in this study.

3.2.2 The Feynman-Vernon theory

In order to make our analysis independent on the properties of the heat bath, we trace out the degrees of freedom of the reservoir by using the reduced density operator

$$\rho(q_f, q_f'; t) = \int dq_0 \int dq_0' K(q_f, q_f', t; q_0, q_0', t_0) \rho_S(q_0, q_0', t_0), \tag{3.15}$$

where the propagator K is given by

$$K(q_f, q'_f, t; q_0, q'_0, t_0) = \int_{q(t_0)=q_0}^{q(t)=q_f} \mathcal{D}q \int_{q'(t_0)=q'_0}^{q'(t)=q'_f} \mathcal{D}q' \mathcal{A}[q]\mathcal{A}^*[q']\mathcal{F}_{FV}[q, q'] \tag{3.16}$$

and $\mathcal{A}[q] = \exp\left(i\frac{S_S[q]}{\hbar}\right)$ with $S_S[q]$ being the classical action functional. In Eq. (3.16), $\mathcal{F}_{FV}[q, q'] = \exp\left(-\frac{\phi_{FV}[q,q']}{\hbar}\right)$ is the Feynman-Vernon (FV) influence functional with the influence weight functional $\phi_{FV}[q, q']$ depending on the bath correlation function [38, 183].

3.2.3 Discrete Variable Representation (DVR)

By solving the eigenvalue equation connected with the Hamiltonian $\hat{H}_0$ (see Eq. (3.10)), we get the energy eigenstates (see vertical axis in Fig. 3.11). Within the framework of the discrete variable representation (DVR) [184] it is possible to obtain the basis $\{|q_\mu\rangle\}$ of eigenstates of the position operator $\hat{q}$ (see horizontal axis in Fig. 3.11).

In this representation, using Eq. (3.16), the continuous real-time path integral given in Eq. (3.15) becomes a discrete path with m transitions at times $t_1, t_2, ...t_m$

$$\dot{\rho}_{\mu_m\nu_m}(t) = \sum_{\mu_0\nu_0} \int_{\xi(t_0)=\xi_0}^{\xi(t)=\xi_m} \mathcal{D}\xi \int_{\chi(t_0)=\chi_0}^{\chi(t)=\chi_m} \mathcal{D}\chi\, \mathcal{C}[\xi, \chi]\, \mathcal{F}_{FV}[\xi, \chi]\, \rho_{\mu_0\nu_0} \tag{3.17}$$

where $\mathcal{C}[\xi, \chi] = \mathcal{A}[q]\mathcal{A}^*[q']$ and the influence weight functional of the FV functional is [185]

$$\phi_{FV}[\xi, \chi] = -\sum_{l=1}^{m}\sum_{j=0}^{l-1} \xi_l S(t_l - t_j)\xi_j - i\sum_{l=1}^{m}\sum_{j=0}^{l-1} \xi_l R(t_l - t_j)\chi_j. \tag{3.18}$$

Here, the absolute coordinates q_j are replaced by the discrete relative coordinates $\xi_j(t) = q_j(t) - q'_j(t)$ and center of mass coordinates $\chi_j = q_j(t) + q'_j(t)$.

Because we are interested in the evolution of the populations, in Eq. (3.17) we consider the diagonal terms $\rho_{\mu_m\mu_m}(t)$. Applying the non-interacting cluster approximation (NICA) [185], the following master equation (ME) is obtained [168, 169]

$$\dot{\rho}_{\mu\mu}(t) = \sum_{\nu=1}^{N} \int_{t_0}^{t} dt' \mathcal{H}_{\mu\nu}(t - t')\rho_{\nu\nu}(t'), \quad \mu = 1, \ldots, N, \tag{3.19}$$

where N is the number of eigenstates and the kernel $\mathcal{H}$, which indicates the *cluster matrix*, takes into account of all possible transitions in the DVR paths [168, 169].

According to the path integral technique based on the Feynman-Vernon theory, using ME corresponds to take into account only the paths connecting diagonal elements of the reduced density matrix of the position operator $\hat{q}$ [168, 169].

Within NICA all the *intercluster interactions* are neglected [185]. By assuming that the characteristic memory time of the matrix elements of $\mathcal{H}$ in Eq. (3.19) is the smallest time scale of the physical system, we obtain the following *Markovian approximated master equation* [168, 169, 185]

$$\dot{\rho}_{\mu\mu}(t) = \sum_{\nu=1}^{N} \Gamma_{\mu\nu}(t)\rho_{\nu\nu}(t) \tag{3.20}$$

where the time-dependent rate coefficients are expressed by

$$\Gamma_{\mu\nu}(t) = \int_0^\infty d\tau \mathcal{H}_{\mu\nu}(t, t-\tau). \tag{3.21}$$

By decoupling via a diagonalization procedure the system of equations (3.20)

$$\sum_{\kappa_1,\kappa_2=1}^{N} (S^{-1})_{\mu\kappa_1}\Gamma_{\kappa_1\kappa_2}S_{\kappa_2\nu} = \Lambda_\mu\delta_{\mu\nu}, \tag{3.22}$$

where $S_{\mu\nu}$ are the elements of the transformation matrix and Λ_μ the eigenvalues of the rate matrix [168]. The general solution of the Markov approximated ME is

$$\rho_{\mu\mu}(t) = \sum_{\nu,\kappa=1}^{N} S_{\mu\nu}(S^{-1})_{\mu\kappa}e^{\Lambda_\nu(t-t_0)}\rho_{\kappa\kappa}(t_0). \tag{3.23}$$

Because of the conservation probability, for the diagonal matrix elements we have [185]

$$\Gamma_{\nu\nu}(t) = -\sum_{\kappa\neq\nu} \Gamma_{\kappa\nu}(t), \tag{3.24}$$

and one eigenvalue is equals zero, $\Lambda_1 = 0$. The Eq. (3.23) becomes

$$\rho_{\mu\mu}(t) = \rho^\infty_{\mu\mu} + \sum_{\nu=2}^{N}\sum_{\kappa=1}^{N} S_{\mu\nu}(S^{-1})_{\mu\kappa}e^{\Lambda_\nu(t-t_0)}\rho_{\kappa\kappa}(t_0), \tag{3.25}$$

where the first term is the asymptotic population in the discrete variable representation. In asymptotic regime, the largest time-scale governing the dynamics is given by [168]

$$\Gamma \equiv \min\left\{|\Re\left(\Lambda_\nu\right)|; \nu = 2, \ldots, N\right\}, \tag{3.26}$$

where Λ_ν are the eigenvalues of the rate matrix and $|\Re(\Lambda_\nu)|$ are the non-zero absolute values of the real part of Λ_ν.

In the next section we focus our study on the medium-short time behavior of the system, using the largest Λ_ν^{-1} as timescale to analyze the non-equilibrium dynamics of the quantum particle in the presence of thermal fluctuations.

3.2.4 Relaxation Time

In this section we study the time evolution of our quantum particle taking into account the 8 energy levels shown in Fig. 3.9. We restrict the study to the 8 lowest levels of the system, because we are interested in the dynamics of a particle that can not reach energy levels higher than the relative maximum of the potential. In particular, we intend to analyze the time behaviour of the populations for different values of the coupling strength, focusing on the time behaviour of the state $|q_0\rangle$ (left side well of the potential).

By using the DVR-state $|q_\mu\rangle$, as initial condition for the particle we choose the non-equilibrium position $q_{start} = 0$. The corresponding state is given by

$$|q_{start}\rangle = c_1|q_1\rangle + c_2|q_2\rangle \tag{3.27}$$

with $c_1 = 0.745$ and $c_2 = 0.667$.

By integrating Eq. (3.19) for different values of the parameter η, which represents the intensity of the environmental noise, for each eigenstate $|q_\mu\rangle$ we obtain the time behaviour of the corresponding population $\rho_{q_\mu} \equiv \rho_{\mu\mu}$ (see Fig. 3.10). Moreover, by a simple change of basis, we calculate the time evolution of the populations also in the energy representation (see Fig. 3.11). As one can see from Eqs. (3.20), (3.22), for each value of η there are N relaxation times Λ_μ^{-1}. Here, we consider the maximum of these relaxation times, and note that this time increases rapidly for larger values of η. Therefore, to describe the time evolution of the system for different values of η, we choose as time scale τ the largest of the relaxation times obtained for $\eta = 0.01$ and calculate the evolution of the system for a maximum time $t = 600\,\tau$. This choice allows to follow the transient dynamics of the system for low and intermediate values of the coupling constant (see panels a, b, c in Figs. 3.10, 3.11). For higher values of η the system can not reach the regime condition, because of the presence of relaxation times longer than the maximum time chosen to calculate the numerical solution (see

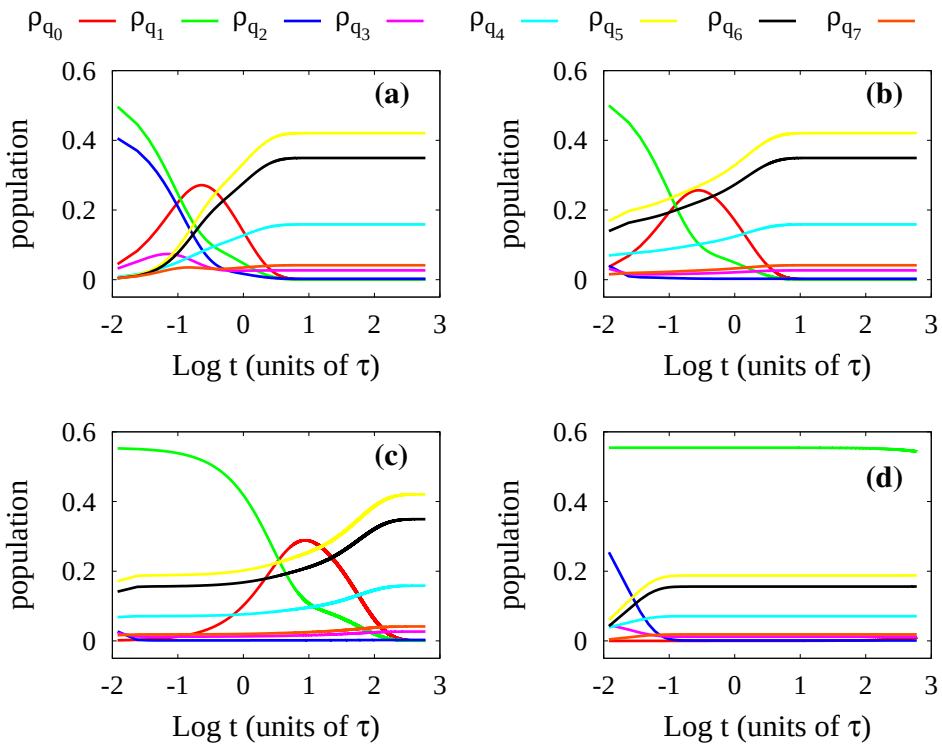

Figure 3.10: Time evolution of the diagonal elements, ρ_{q_μ} ($\mu = 0, 1, ..., 7$), of the density matrix in q-representation. The matrix elements ρ_{q_μ} are the population distributions in the eight position eigenstates considered. The time evolution is obtained for different values of the coupling strength: (a) $\eta = 0.01$, (b) $\eta = 0.4$, (c) $\eta = 1$ and (d) $\eta = 2.8$.

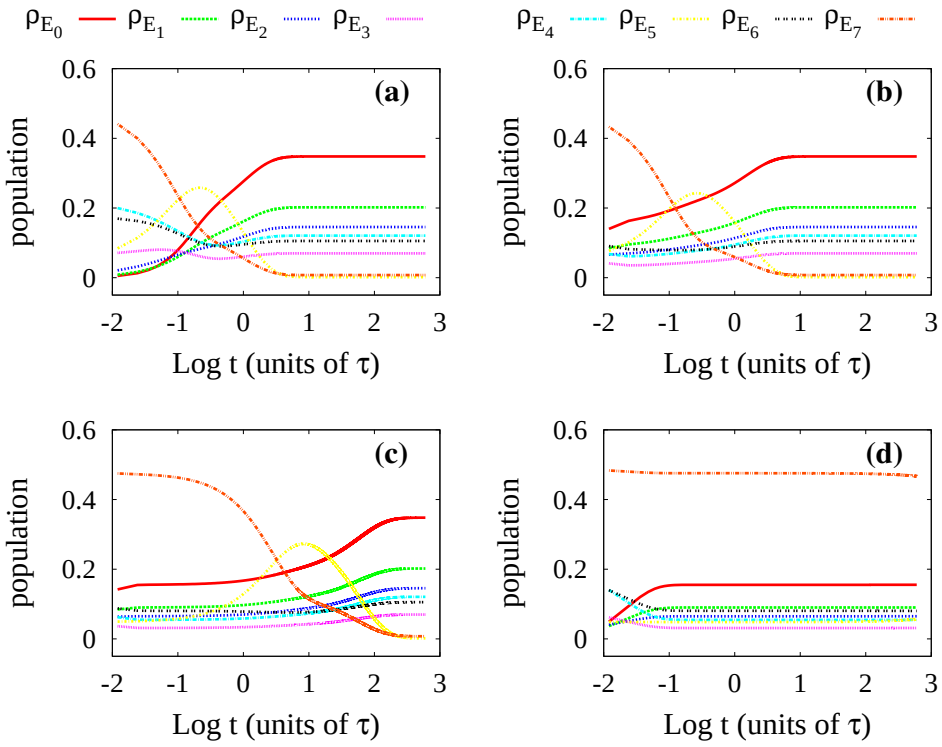

Figure 3.11: Time evolution of the diagonal elements, ρ_{E_μ} $(\mu = 0, 1, ..., 7)$, of the density matrix in energy representation. The matrix elements ρ_{E_μ} are the population distributions in the eight energy eigenstates considered. The time evolution is obtained for different values of the coupling strength: (a) $\eta = 0.01$, (b) $\eta = 0.4$, (c) $\eta = 1$ and (d) $\eta = 2.8$.

panel d in Figs. 3.10, 3.11). This delay in the system dynamics can be explained by the quantum Zeno effect, responsible for the suppression of the tunnel effect. Moreover, we observe in Fig. 3.10 a nonmonotonic behaviour of the population ρ_{q_0} as a function of the time. Finally, as a consequence of the quantum Zeno effect, the eigenstate $|q_0\rangle$ can be maximally populated at different times varying the coupling strength and, therefore, the value of η. This could be useful in view of placing a quantum particle in a given position at a fixed time.

We note that it would be interesting to compare our results with those obtained in the case of a harmonic oscillator coupled with a thermal bath without any cutoff, as studied in previous works [186, 187, 188]. On physical grounds we expect that the time behaviour of the purity of the system state is strictly connected with the relaxation rates. In our analysis the relaxation rates have been used to determine the timescale for obtaining the time evolution of the population distributions. Moreover, we found a freezing phenomenon of the state of the system due to the Zeno effect [189]. Finally, we note that the complete description of the dynamics of our initial pure state should be obtained by following the time evolution of all elements of the density matrix as expressed by Eq.(3.17). This will be subject of future investigations.

Conclusions

In the first chapter the mathematical rudiments of stochastic processes and in particular of Lévy processes, have been presented. The Lévy flights are introduced as self-similar Lévy processes. After the definition of the strictly stable random variables, the fractional differential equation for Lévy flight superdiffusion and the associated Langevin equation with symmetric α-stable Lévy noise are introduced. The general differential equation useful to calculate the nonlinear relaxation time for a particle moving in a cubic potential and with an arbitrary Lévy index α is presented in chapter two. For Cauchy noise ($\alpha = 1$) the NLRT as a function of the noise intensity and the initial position of the potential is calculated. A monotonic behavior of the NLRT as a function of the initial position of the particle was obtained in this case. For free anomalous diffusion the NLRT decreases monotonically with the noise intensity as in the presence of the cubic potential.

Moreover, in the same chapter, we presented a study on the role of the Lévy noise in population dynamics. By using the Lotka-Volterra model in the presence of two symmetrical non-Gaussian α-stable noise sources, we analyzed the time behaviour of an ecosystem consisting of two competing species and surrounding environment. In particular, an additive noise source affects the dynamics of the interaction parameter between the two species, $\gamma(t)$, which "moves" along a bistable potential in the presence of a periodical driving force. Depending on the values of the interaction parameter $\gamma(t)$, coexistence or exclusion regime takes place. By using different α-stable noise sources, stochastic resonance was always observed, with $\gamma(t)$ switching quasi-periodically between coexistence and exclusion regime. In this condition, we considered the second noise source, inserting in the Lotka-Volterra equations a term of multiplicative Lévy noise, whose intensity is indicated by D. For different values both of the index α and intensity D, we studied the time behaviour of the two

species densities, x and y, and found that noise is responsible for the generation of time series characterized by anticorrelated oscillations, whose amplitude is strictly dependent on the multiplicative noise intensity. To better analyze the response of the system to the multiplicative noise, we calculated the corresponding signal-to-noise ratio (SNR) of $(x-y)^2$. The results showed that SNR is characterized by a nonmonotonic behaviour with a maximum as a function of the noise intensity, which indicates the presence of a second stochastic resonance phenomenon. Finally, we observed that the values of this maximum in the SNR and the spectral power amplification is reduced as the Lévy index α decreases approaching 1 (more super-diffusive behaviour).

We note that our model is useful to describe physical situations in which the amplitude of periodical driving forces, such as those connected with the temperature oscillations, is weak and therefore unable to produce considerable variations in the dynamical regime of the ecosystem. The synergetic cooperation between the nonlinearity of the system and the random and periodical environmental driving forces produces, therefore, a coherent time behaviour of the ecosystem investigated. These noise-induced effects should be useful to explain the spatio-temporal behaviour of species whose dynamics is strongly affected by environmental noise characterized by Lévy distribution [122]-[125].

In the third chapter we started to study the effect of low-frequency noise on the transfer efficiency of STIRAP, proposing that low-frequency fluctuations of the spectrum can be analyzed in terms of fictitious correlated fluctuations of the detunings. For solid-state noise with large low-frequency component (e.g. for $1/f$ noise) the leading effect (static path approximation) is equivalent to consider statistically distributed detunings and can be discussed by analyzing the sensitivity to parameters of the protocol. We applied the theory to the Quantronium, showing that correlated fluctuations of the energy splittings have to be considered, and that transfer efficiency is mainly sensitive to decoherence in the subspace of the two-lowest levels, which is well characterized experimentally. Selection rules prevent to work at the symmetry point, where decoherence is minimal. Therefore, the observation of coherent population transfer requires optimization of the trade-off between increasing coupling and greater sensitivity to low-frequency noise. We have shown that this is indeed possible, given the measured figures of low-frequency noise.

Notice that we have used pulses of width $T = 48 - 30\,ns$. Therefore, the total time of the protocol $\sim 200 - 350\,ns$ is longer than the dephasing time of the qubit, as determined solely by static inhomogeneities. This dephasing time is smaller of that at the symmetry point (in the experiment of Ref. [60] the dephasing time for coherent oscillations dropped from $T_\phi \sim 600\,ns$ at the symmetry point to $T_\phi \sim 50\,ns$ at $q_g = 0.47$). This shows that STIRAP is less sensitive to low-frequency noise than coherent oscillations. Actually, accounting for high frequency noise the process will be limited by the relaxation $T_1 \geq 500\,\text{ns}$.

The analysis we illustrated applies as well to other superconducting nanodevices. In particular, it could allow to design correlations of fluctuations of the energy spectrum, which maximize the Zener channel of population transfer (see fig. 3.4).

The second topic presented in the third chapter is the dynamics of a quantum particle subject to an asymmetric bistable potential and interacting with a noisy environment. The study was performed exploiting the approach of the Feynman-Vernon functional [183] within the framework of the discrete variable representation [168, 169, 184]. By using the Caldeira-Leggett model [170], we described the transient dynamics of the system for different values of the coupling strength between the particle and the noisy environment, modelled as a thermal bath. Due to the quantum Zeno effect, responsible for the suppression of the tunnel effect, a delayed dynamics of the system was observed for higher values of the coupling strength. We found also that the metastable state inside the left side well of the potential can be populated at different times varying the value of the coupling strength.

Bibliography

[1] L. Gammaitoni , P. Hänggi, P. Jung and F. Marchesoni, *'Stochastic resonance'* Rev. Mod. Phys. **70**, 223-287 (1998).

[2] C. R. Doering and J. C. Gadoua, *'Resonant activation over a fluctuating barrier'* Phys. Rev. Lett. **69**, 2318-2321 (1992).

[3] B. Spagnolo, A. A. Dubkov, A. L. Pankratov, E. V. Pankratova, A. Fiasconaro and A. Ochab- Marcinek, *'Lifetime of metastable states and suppression of noise in Interdisciplinary Physical Models'* Acta Phys. Pol. **38**, 1925-1950 (2007).

[4] A. Fiasconaro, J. J. Mazo, and B. Spagnolo, *'Noise-induced enhancement of stability in a metastable system with damping'* Phys. Rev. E **82**, 041120 (2010).

[5] W. Horsthemke and R. Lefever, *'Noise-Induced Transition'* (Springer-Verlag, Berlin 2006).

[6] D. Valenti, A. Fiasconaro and B. Spagnolo, *'Stochastic Resonance and Noise Delayed Extinction in a Model of Two Competing Species'* Physica A **331**, 477-486 (2004).

[7] J. Garcia-Ojalvo and J. M. Sancho, *'Noise in Spatially Extended Systems'* (Springer-Verlag New York Inc. 1999).

[8] P. Hänggi and F. Marchesoni, *'100 Years of Brownian motion'* Chaos **15**, 026101 (2005).

[9] A. A. Dubkov, B. Spagnolo and V. V. Uchaikin , *Lévy Flight Supediffusion: An Introduction*, Int. J. Bifur. Chaos **18** (9), 2649-2672 (2008).

[10] P. Lévy, *'Theory de l'addition des variables Aléatoires'* (Gauthier-Villars, Paris 1937).

[11] B. V. Gnedenko and A. N. Kolmogorov,*'Limit Distributions for Sums of Independent Random Variables'*, (Addison-Wesley, Cambridge 1954).

[12] R. Metzler & J. Klafter, *'The Random Walk's Guide to Anomaluos Diffusion: A Fractional Dynamics Approach'* Phys. Rep. **339**, 1-77 (2000).

[13] Uchaikin V. V., *'Self-similar anomalous diffusion and Levy-stable laws'* Physics Uspekhi **46**, 821-849 (2003).

[14] Chechkin A V, Gonchar V Yu, Klafter J and Metzler R, *'Fundamentasls of Lévy flight processes'* Adv. Chem. Phys. **133** 439 (2006).

[15] B. Dybiec, E. Gudowska-Nowak, and I. M. Sokolov, *'Stationary states in Langevin dynamics under asymmetric Lévy noises'* Phys. Rev. E **76**, 041122 (2007).

[16] B. Dybiec and E. Gudowska-Nowak, *'Bimodality and hysteresis in systems driven by confined Lévy flights'* New J. Phys. **9**, 452-462 (2007).

[17] B. Dybiec and E. Gudowska-Nowak, *'Lévy stable noise-induced transitions: stochastic resonance, resonant activation and dynamic hysteresis'* J. Stat. Mech.: Theory Exp. **P05004**(17), (2009).

[18] L. Zhang, A. Song and J. He, *'Stochastic resonance of a subdiffusive bistable system driven by Lévy noise based on the subordination process'* J. Phys. A: Math. Theor. **42**, 475003 (2009).

[19] B. Dybiec, *'Lévy noises: Double stochastic resonance in a single-well potential'* Phys. Rev. E **80**, 041111 (2009).

[20] A. A. Dubkov and B. Spagnolo, *'Langevin approach to Lévy flights in fixed potentials: exact results for stationary probability distributions'* Acta Phys. Pol. B **38**, 1745-1758 (2007).

[21] H. A. Kramers, Physica (Amsterdam) **7**, 284 (1940).

[22] L. S. Pontryagin, A. A. Andronov, and A. A. Vitt, *'On the statistical treatment of dynamical systems'* Zh. Eksp. Teor. Fiz. **3**, 165 (1933).

[23] P. Hänggi, P. Talkner, and M. Borkovec, *'Reaction-rate theory: fifty years after Kramers'* Rev. Mod. Phys. **62** 251-341 (1990).

[24] V. I. Mel'nikov, *'The Kramers problem: Fifty years of development'* Phys. Rep. **209**, 1-2 (1991).

[25] J. Klafter and M. F. Shlesinger, *'On the Relationship Among Three Theories of Relaxation in Disordered Systems'* Proc. Natl. Acad. Sci. U.S.A. **83**, 848 (1986).

[26] A. Blumen, J. Klafter, and G. Zumofen, *'in Optical Spectroscopy of Glasses'*, edited by I. Zschokke (Reidel, Amsterdam 1986).

[27] M. O. Vlad, R. Metzler, T. F. Nonnenmacher, and M. C. Mackey, *'Universality classes for asymptotic behavior of relaxation processes in systems with dynamical disorder: Dynamical generalizations of stretched exponential'* J. Math. Phys. **37**, 2279 (1996).

[28] E.B. Davies, *'Quantum Theory of Open Systems'* (Academic Press, New York 1976).

[29] R. Alicki, *'Invitation to quantum dynamical semigroups'* Lect. Notes Phys. **597** (Springer-Verlag, Berlin 2002).

[30] F. Benatti and R. Floreanini, *'Dissipative Quantum Dynamics'* Lect. Notes Phys. **622** (Springer-Verlag, Berlin 2003).

[31] H. P. Breuer and F. Petruccione, *'The Theory of Open Quantum Systems'* (Oxford University Press, Oxford 2002).

[32] W. H. Louisell, *'Quantum Statistical Properties of Radiation'* (Wiley, New York 1973).

[33] F. Haake, *'Statistical treatment of open systems by generalized master equations'* Springer Tracts in Mod. Phys. **95**, (Springer-Verlag, Berlin 1973).

[34] C. Cohen-Tannoudji, J. Dupont-Roc and G. Grynberg, *'Atom-Photon Interactions'* (Wiley, New York 1988).

[35] D. F. Walls and G. J. Milburn, *'Quantum Optics'* (Springer-Verlag, Berlin 1994).

[36] M. O. Scully and M. S. Zubairy, *'Quantum Optics'* (Cambridge University Press, Cambridge 1997).

[37] C. W. Gardiner and P. Zoller, *'Quantum Noise'* (Springer-Verlag, Berlin 2000).

[38] U. Weiss, *'Quantum Dissipative Systems'* (World Scientific, Singapore 1999).

[39] H. Spohn, *'Kinetic equations from Hamiltonian dynamics: Markovian limits'* Rev. Mod. Phys. **52**, 569 (1980).

[40] M. A. Nielsen and I. L. Chuang, *'Quantum Computation and Quantum Information'* (Cambridge University Press, Cambridge 2002).

[41] G. Alber et al., *'Quantum Information: An Introduction to Basic Theoretical Concepts and Experiments'* Springer Tracts in Mod. Phys. **173** (Springer-Verlag, Berlin 2001).

[42] D. Bouwmeester, A. K. Ekert and A. Zeilinger, *'The Physics of Quantum Information'* (Springer- Verlag, Berlin 2000).

[43] Y. Nakamura, Yu. Pashkin, and J. S. Tsai, *'Coherent control of macroscopic quantum states in a single-Cooper-pair box'* Nature **398**, 786 (1999).

[44] D. Vion, A. Aassime, A. Cottet, P. Joyez, H. Pothier, C. Urbina, D. Esteve, and M. H. Devoret, *'Manipulating the Quantum State of an Electrical Circuit'* Science **296**, 886 (2002).

[45] I. Chiorescu, Y. Nakamura, C. J. P. M. Harmans, and J. E. Mooij, *'Coherent Quantum Dynamics of a Superconducting Flux Qubit'* Science **299**, 1869 (2003).

[46] T. Yamamoto, Yu. A. Pashkin, O. Astafiev, Y. Nakamura, and J. S. Tsai, *'Demonstration of conditional gate operation using superconducting charge qubits'* Nature **425**, 941 (2003).

[47] J. B. Majer, F. G. Paauw, A. C. J. ter Haar, C. J. P. M. Harmans, and J. E. Mooij, *'Spectroscopy on Two Coupled Superconducting Flux Qubits'* Phys. Rev. Lett. **94**, 090501 (2005).

[48] A. Wallraff, D. I. Schuster, A. Blais, L. Frunzio, R. S. Huang, J. Majer, S. Kumar, S. M. Girvin and R. J. Schoelkopf, *'Strong coupling of a single photon to a superconducting qubit using circuit quantum electrodynamics'* Nature **431**, 162 (2004).

[49] I. Chiorescu, P. Bertet, K. Semba, Y. Nakamura, C. J. P. M. Harmans, and J. E. Mooij, *'Coherent dynamics of a flux qubit coupled to a harmonic oscillator'* Nature **431**, 159 (2004).

[50] M. O. Scully and M. S. Zubairy, *'EM Quantum Optics'* (Cambridge Univ. Press, Cambridge 1997).

[51] J. M. Smith, *'Animal interactions'* (Cambridge, London 1974).

[52] M. A. Nowak and R. M. May, *'Virus Dynamics: Mathematical Principles of Immunology and Virology'* (Oxford University Press, 2000).

[53] P. Turchin, *'Complex Population Dynamics: A Theoretical/Empirical Synthesis'* (Princeton University Press, 2003).

[54] C. H. Bennett, D. P. DiVincenzo, *'Quantum information and computation'*, Nature **404**, 247-255 (2000).

[55] J. Clarke, F. K. Wilhelm, *'Superconducting quantum bits'*, Nature **453**, 1031-1042 (2008).

[56] F. Brauer and C. Castillo-Chavez, *'Mathematical Models in Population Biology and Epidemiology'* (Springer-Verlag, 2000).

[57] J. M. Smith, *'Mathematical Ideas in Biology'* (Cambridge University Press, 1968).

[58] O. G. Pybus and A. Rambaut, *'Evolutionary analysis of the dynamics of viral infectious disease'*, Nature Reviews Genetics **10**, 540-550 (2009).

[59] A. Houston, C. Clark, J. McNamara, M. Mangel, *'Dynamic models in behavioural and evolutionary ecology'*, Nature **332**, 29-34 (1988).

[60] G. Ithier, E. Collin, P. Joyez, P. J. Meeson, D. Vion, D. Esteve1, F. Chiarello, A. Shnirman, Y. Makhlin4, J. Schriefl and G. Schön , *'Decoherence in a superconducting quantum bit circuit'* Phys. Rev. B **72**, 134519 (2005).

[61] B. Øksendal, *'Stochastic Differential Equations: An Introduction with Applications'* (Springer, Berlin 2003).

[62] R. Durrett, *'Stochastic calculus. A practical introduction. Probability and Stochastics Series'* (Richard Durrett Editor, 1996).

[63] L. Richardson, *'Atmospheric diffusion shown on a distance neighbour graph'*, Proc. Roy. Soc. A **110**, 709-737 (1926).

[64] A. Ya. Khintchine, *'Limit Distributions for the Sum of Independent Random Variables'*, (O.N.T.I., Moscow 1938) [in Russian].

[65] W. Feller, *'An Introduction to Probability Theory and its Applications'*, Vol. 2 (John Wiley & Sons, Inc., NY 1971).

[66] R. Weron, *'On the Chambers-Mallows-Stuck method for simulating skewed stable random variables'* Statistics & Probability Letters **28** 165-171 (1996).

[67] J. Bertoin, *'Lévy Processes'* (Cambridge University Press, Cambridge 1996).

[68] K. I. Sato, *'Lévy Processes and Infinitely Divisible Distributions'* (Cambridge University Press, Cambridge 1999).

[69] B. Fristedt and L. Gray, *'A modern approach to probability theory'* (Birkäuser, Berlin 1997).

[70] R. N. Mantegna and H. E. Stanley, *'Stochastic Process with Ultraslow Convergence to a Gaussian: The Truncated Lvy Flight'* Phys. Rev. Lett. **73**, 2946-2949 (1994).

[71] R. N. Mantegna and H. E. Stanley, *'Stock market dynamics and turbulence: parallel analysis of fluctuation phenomena'* Physica A **239**, 255-266 (1997).

[72] R. N. Mantegna and H. E. Stanley, *'Turbulence and financial markets'* Nature **383**, 587-588 (1996).

[73] R. N. Mantegna and H. E. Stanley, *'An Introduction to Econophysics, Correlations and Complexity in Finance'* (Cambridge University Press, Cambridge, 2000).

[74] I. Podlubny, *'Fractional Differential Equations'* (Academic Press, San Diego USA 1999).

[75] A. I. Saichev & G. M. Zaslavsky, *'Fractional kinetic equations: Solutions and applications'*, Chaos **7**, 753-764 (1997).

[76] V. V. Uchaikin, *'Evolution equations for Lévy stable processes'*, Int. J. Theor. Phys. **38**, 2377-2388 (1999).

[77] F. Mainardi, Yu. Luchko & G. Pagnini, *'The fundamental solution of the space-time fractional diffusion equation'*, Fract. Cal. Appl. Anal. **4**, 153-192 (2001).

[78] R. Metzler & T. F. Nonnenmacherc, *'Spaceand time-fractional diffusion and wave equations, fractional Fokker-Planck equations, and physical motivation'*, Chem. Phys. **284**, 67-90 (2002).

[79] E. K. Lenzi, R. S. Mendes, K. S. Fa, L. C. Malacarne, & L. R. da Silva, *'Anomalous diffusion: Fractional Fokker-Planck equation and its solutions'*, J. Math. Phys. **44** 2179-2185 (2003).

[80] R. Gorenflo & F. Mainardi, *'Simply and multiply scaled diffusion limits for continuous time random walks'*, J. Phys., Conf. Series (JPCS) **7**, 1-16 (2005).

[81] I. M. Sokolov & A. V. Chechkin, *'Anomalous diffusion and generalized diffusion equations'*, Fluct. Noise Lett. **5**, L275-L282 (2005).

[82] G. M. Zaslavsky, *'Hamiltonian Chaos and Fractional Dynamics'*, Oxford University Press (2005).

[83] A. A. Dubkov and B. Spagnolo, *'Generalized Wiener Process and Kolmogorov's Equation for Diffusion Induced by Non-Gaussian Noise Source'* Fluct. Noise Lett. **5**, L267-L274 (2005).

[84] A. A. Dubkov, A. La Cognata and B. Spagnolo *'The problem of analytical calculation of barrier crossing characteristics for Lévy flights'* J. Stat. Mech.: Theo Exp **P01002** (2009).

[85] A. La Cognata, D. Valenti, A. A. Dubkov and B. Spagnolo, *'Dynamics of two competing species in the presence of Lévy noise sources'* Phys. Rev. E **82**, 011121, (2010).

[86] A. La Cognata, D. Valenti, B. Spagnolo and A. A. Dubkov, *'Two competing species in super-diffusive dynamical regimes'* Eur. Phys. J. B **77**, 273-279, (2010).

[87] A. Fiasconaro, B. Spagnolo, and S. Boccaletti, *'Signatures of noise-enhanced stability in metastable states'* Phys. Rev. E **72**, 061110 (2005).

[88] P. D. Ditlevsen, *'Anomalous jumping in a double-well potential'* Phys. Rev. E **60**, 172-179 (1999).

[89] S. Ratynskaia, G. Regnoli, K. Rypdal, B. Klumov, and G. Morfill, *'Critical fluctuations and anomalous transport in soft Yukawa-Langevin systems'* Phys. Rev. E **80**, 046404 (2009).

[90] J. Fajans and A. Schmidt, *'Malmberg-Penning and minimum-B trap compatibility: the advantages of higher-order multipole traps'* Nucl. Instrum. & Methods A **521**, 318 (2004).

[91] M. Gitterman, *'Mean first passage time for anomalous diffusion'* Phys. Rev. E **62** 6065 (2000).

[92] S. B. Yuste and K. Lindenberg, *'Comment on mean first passage time for anomalous diffusion'* Phys. Rev. E **69**, 033101 (2004).

[93] G. Rangarajan and M. Ding, *'Anomalous diffusion and the first passage time problem'* Phys. Rev. E **62**, 120 (2000).

[94] S. V. Buldyrev, S. Havlin, A. Ya. Kazakov, M. G. E. da Luz, E. P. Raposo, H. E. Stanley and G. M. Viswanathan, *'Average time spent by Lévy flights and walks on an interval with absorbing boundaries'* Phys. Rev. E **64**, 041108 (2001).

[95] J. D. Bao, H. Y. Wang, Y. Jia and Y. Zh. Zhuo , *'Cancellation phenomenon of barrier escape driven by a non-Gaussian noise'* Phys. Rev. E **72**, 051105 (2005).

[96] A. V. Chechkin , R. Metzler, V. Yu. Gonchar, J. Klafter and L. V. Tanatarov, *'First Passage and Arrival Time Densities for Lévy Flights and the Failure of the Method of Images'* J. Phys. A: Math. Gen. **36**, L537 (2003).

[97] A. V. Chechkin, V. Yu. Gonchar, J. Klafter and R. Metzler, *'Natural cutoff in Lévy flights caused by dissipative nonlinearity'* Phys. Rev. E. **72**, 010101 (2005).

[98] A. V. Chechkin, O. Yu. Sliusarenko, R. Metzler and J. Klafter, *'Barrier crossing driven by Levy noise: Universality and the role of noise intensity'* Phys. Rev. E **75**, 041101(11) (2007).

[99] B. Dybiec, E. Gudowska-Nowak and P. Hänggi, *'Escape driven by alpha-stable white noises'* Phys. Rev. E **75**, 021109 (2007).

[100] B. Dybiec, E. Gudowska-Nowak and P. Hänggi, *'Lévy-Brownian motion on finite intervals: Mean first passage time analysis'* Phys. Rev. E **73**, 046104 (2006).

[101] P. Imkeller and I. Pavlyukevich, *'Lévy flights: transitions and meta-stability'* J. Phys. A: Math. Gen. **39**, L237 (2006).

[102] P. Imkeller, I. Pavlyukevich and T. Wetzel, *'First exit times for Lévy-driven diffusions with exponentially light jumps'* The Annals of Probability **37**, 530564 (2009).

[103] T. Koren, A. V. Chechkin and J. Klafter, *'On the First Passage Time and Leapover Properties of Lévy Motions '* Physica A **379**, 10 (2007).

[104] E. Sparre-Andersen, *'On the fluctuations of sums of random variables'* Math. Scand. **1**, 263 (1953).

[105] E. Sparre-Andersen, Math. Scand. **2**, 195 (1954).

[106] A. J. F. Siegert, *'On the first passage time probability problem'* Phys. Rev. **81** 617 (1951).

[107] C. W. Gardiner, *'Handbook of stochastic methods'* (Springer, Berlin 1993).

[108] J. R. Krebs, and N. B. Davies, *'Behavioural Ecology: An Evolutionary Approach'* (Blackwell, Oxford, 1997).

[109] D. Tilman and P. M. Kareiva, *'Spatial Ecology : The Role of Space in Population Dynamic and Interspecific Interactions'* (Princeton University Press, Princeton 1997).

[110] J. Bascompte and R. Sole, *'Modelling Spatiotemporal Dynamics in Ecology'* (Springer, Berlin 1998).

[111] A. C. Maddison, J. Holt, M. J. Jeger, *'Spatial dynamics of a monocyclic disease in a perennial crop'* Ecol. Mod. **88**, 45 (1996).

[112] J. R. Anderson, *'A spreading activation theory of memory'* J. Verb. Learn. Verb. Behav. **22**, 261 (1983).

[113] H. J. de Knegt , G. M. Hengeveld, F. van Langevelde, W. F. de Boer and K. P. Kirkman, *'Patch density determines movement patterns and foraging efficiency of large herbivores'* Behav. Ecol. **18**, 1065 (2007).

[114] G. M. Viswanathan, V. Afanasyev, S. V. Buldyrev, E. J. Murphy, P. A. Prince, and H. E. Stanley, *'Lévy flight search patterns of wandering albatrosses'* Nature **381**, 413 (1996).

[115] A. M. Edwards, R. A. Phillips, N. W. Watkins, M. P. Freeman, E. J. Murphy, V. Afanasyev, S. V. Buldyrev, M. G. E. da Luz, E. P. Raposo, H. E. Stanley and G. M. Viswanathan, *'Revisiting Lévy flight search patterns of wandering albatrosses, bumblebees and deer'* Nature **449**, 1044 (2007).

[116] A. M. Reynolds, A. D. Smith, R. Menzel, U. Greggers, D. R. Reynolds, J. R. Riley, *'Displaced honey bees perform optical scale-free search flights'* Ecology **88**, 1955 (2007).

[117] G. M. Viswanathan, S. V. Buldyrev, S. Havlin, M. G. E. da Luz, E. P. Raposo, H. E. Stanley, *'Optimizing the success of random searches'* Nature **401**, 911 (1999).

[118] J. C. Stout, D. Goulson, *'The use of conspecific and interspecific scent marks by foraging bumblebees and honeybees'* Anim. Behav. **62**, 183 (2001).

[119] A. M. Reynolds, *'Deterministic walks with inverse-square power-law scaling are an emergent property of predators that use chemotaxis to locate randomly distributed prey'* Phys. Rev. E **78**, 011906 (2008).

[120] G. Ramos-Fernandz, J. L. Mateos, O. Miramontes, G. Cocho, G. Larralde and B. Ayala-Orozco, *'Lévy walk patterns in the foraging movements of spider monkeys (Ateles geoffroyi)'* Behav. Ecol. Sociobiol. **55**, 223 (2004).

[121] S. Bertrand, J. M. Burgos, F. Gerlotto and J. Atiquipa, *'Lévy trajectories of fishers as an indicator of pelagic fish spatial distribution: the case of the Peruvian anchovy (Engraulis ringens) fishery'* J. Mar. Sci. **62**, 477 (2005).

[122] A. B. Medvinsky, D. A. Tikhonov, J. Enderlein, and H. Malchow, *'Fish and plankton interplay determines both plankton spatio-temporal pattern formation and fish school walks: a theoretical study'* Nonlin. Dyn. Psychology Life Sciences **4** (2), 135-152 (2000).

[123] R. Nathan, G. G. Katul, H. S. Horn, S. M. Thomas, R. Oren, R. Avissar, S. W. Pacala and S. A. Levin, *'Mechanisms of long-distance dispersal of seeds by wind'* Nature **418**, 409 (2002);

[124] S. Bertrand, E. Díaz, M. Lengaigne, *'Patterns in the spatial distribution of Peruvian anchovy (Engraulis ringens) revealed by spatially explicit fishing data'* Progress in Oceanogr. **79**, 379 (2008);

[125] M. Gutiérrez, G. Swartzman, A. Bertrand and S. Bertrand, *'Anchovy and sardine spatial dynamics and aggregation patterns in the Humboldt Current ecosystem, Peru, from 1983-2003'* Fish. Oceanogr. **16**, 155 (2007).

[126] A. A. Dubkov and B. Spagnolo, *'Verhulst model with Lévy white noise excitation'* Eur. Phys. J. B **65**, 361 (2008).

[127] G. Nicolis and C. Nicolis, *'Foundations of Complex Systems'* (World Scientific, Singapore 2007).

[128] A. J. Lotka, *'Analytical Note on Certain Rhythmic Relations in Organic Systems'* Proc. Nat. Acad. Sci USA **6**, 410 (1920);

[129] V. Volterra, *'Variazioni e fluttuazioni del numero d'individui in specie animali conviventi'* Mem. R. Accad. Nazionale Lincei (Ser. VI) **2**, 31-113 (1926).

[130] T. Srokowski, *'Multiplicative Lévy processes: Itö versus Stratonovich interpretation'* Phys. Rev. E **80**, 051113 (2009).

[131] A. D. Bazykin, *Nonlinear dynamics of interacting populations* (World Scientific, Singapore 1998).

[132] V. S. Anishchenko, A. B. Neiman, F. Moss and L. Schimansky-Geier, *'Stochastic resonance as noise induced phenomenon increasing order'* Sov. Phys. Usp. **42**, 7 (1999).

[133] P. Jung, P. Hänggi, *'Amplification of small signals via stochastic resonance'* Phys. Rev. A **44**, 8032 (1991)

[134] P. Jung, P. Hänggi, *'Stochastic nonlinear dynamics modulated by external periodic forces'* Europhys. Lett. **8**, 505 (1989).

[135] P. Talkner et al, *'Statistics of transition times, phase diffusion and synchronization in periodically driven bistable systems'* New J. Phys. **7**, 14 (2005).

[136] A. La Cognata, P. Caldara, D. Valenti, B. Spagnolo, E. Palladino, A. D'Arrigo, G. Falci, *'Effect of low-frequency noise on adiabatic passage in a superconducting nanocircuit'* Int. J. of Quantum Information, in press (2011).

[137] P. Caldara, A. La Cognata, D. Valenti, B. Spagnolo, E. Palladino, M. Berritta, G. Falci, *'Dynamics of a quantum particle in asymmetric bistable potential with environmental noise'* Int. J. of Quantum Information, in press (2011).

[138] K. Bergmann, H. Theuer and B. W. Shore, *'Coherent population transfer among quantum states of atoms and molecules'* Rev. Mod. Phys. **70**, 1003 (1998).

[139] N. V. Vitanov, T. Halfmann, B. W. Shore and K. Bergmann, *'Laser-induced population transfer by adiabatic passage techniques'* Annu. Rev. Phys. Chem. **52**, 763-809 (2001).

[140] K. V. R. M. Murali, Z. Dutton, W. D. Oliver, D. S. Crankshaw and T. Orlando, *'Evidence for Entangled States of Two Coupled Flux Qubits'* Phys. Rev. Lett. **93**, 087003 (2004).

[141] M. H. S. Amin, A. Yu. Smirnov and A. Maassen v.d. Brink, *'Josephson-phase qubit without tunneling'* Phys. Rev. B **67**, 100508(R) (2003).

[142] J. Siewert and T. Brandes, *'Applications of Adiabatic Passage in Solid-State Devices'* Adv. Solid State Phys. **44**, 181 (2004).

[143] Y. X. Liu, J. Q. You, L. F. Wei, C. P. Sun, and F. Nori, *'Optical Selection Rules and Phase-Dependent Adiabatic State Control in a Superconducting Quantum Circuit'* Phys. Rev. Lett. **95**, 087001 (2005).

[144] J. Siewert, T. Brandes and G. Falci, *'Adiabatic passage with superconducting nanocircuits'* Opt. Comm. **264**, 435 (2006)

[145] J. Siewert, T. Brandes and G. Falci, *'Advanced control with a Cooper-pair box: Stimulated Raman adiabatic passage and Fock-state generation in a nanomechanical resonator'* Phys. Rev. B **79**, 024504 (2009).

[146] M. Mariantoni, M.J. Storcz, F.K. Wilhelm, W.D. Oliver, A. Emmert, A. Marx, R. Gross, H. Christ, and E. Solano, *'On-Chip Microwave Fock States and Quantum Homodyne Measurements'* arXiv:cond-mat/0509737 (unpublished).

[147] A. S. Parkins, P. Marte, P. Zoller, H. J. Kimble, *'Synthesis of arbitrary quantum states via adiabatic transfer of Zeeman coherence'* Phys. Rev. Lett. **71**, 3095 (1993).

[148] M.A. Sillanpää, J. Li, K. Cicak, F. Altomare, J.I. Park, R.W. Simmonds, G.S. Paraoanu, P.J. Hakonen, *'Autler-Townes Effect in a Superconducting Three-Level System'* Phys. Rev. Lett. 103, 193601 (2009).

[149] M. Baur, S. Filipp, R. Bianchetti, J. M. Fink, M. Göppl, L. Steffen, P. J. Leek, A. Blais and A. Wallraff, *'Measurement of Autler-Townes and Mollow Transitions in a Strongly Driven Superconducting Qubit'* Phys. Rev. Lett. 102, 243602 (2009).

[150] P. Caldara and E. Fiordilino, *'High-order harmonic emission from a three-level atom in a laser field'* J. Mod. Opt. **46**, 5 743-754 (1999).

[151] W. R. Kelly, Z. Dutton, J. Schlafer, B. Mookerji, T. A. Ohki, J.S. Kline, D.P. Pappas, *'Direct Observation of Coherent Population Trapping in a Superconducting Artificial Atom'* Phys. Rev. Lett. 104, 163601 (2010).

[152] A. A. Abdumalikov Jr., O. Astafiev1, A. M. Zagoskin, Yu. A. Pashkin, Y. Nakamura, and J. S. Tsai, *'Electromagnetically Induced Transparency on a Single Artificial Atom'* Phys. Rev. Lett. **104**, 193601(4) (2010).

[153] R.Bianchetti, S.Filipp, M. Baur, J. M. Fink, C. Lang, L. Steffen, M. Boissonneault, A. Blais, A. Wallraff, *'Control and Tomography of a Three Level Superconducting Artificial Atom'* Phys. Rev. Lett. **105**, 223601 (2010).

[154] E. Paladino, L. Faoro, G. Falci and R. Fazio, *'Decoherence and 1/f Noise in Josephson Qubits'* Phys. Rev. Lett. **88**, 228304 (2002).

[155] G. Falci, A. D'Arrigo, A. Mastellone, and E. Paladino , *'Initial Decoherence in Solid State Qubits'* Phys. Rev. Lett. **94**, 167002 (2005).

[156] E. Paladino et al., *'Broadband noise decoherence in solid-state complex architectures'* Phys. Scr. **T137**, 014017 (2009).

[157] G. Falci and R. Fazio, *Quantum computation with Josephson junctions*, Proceedings of the International School of Physics "Enrico Fermi" on "Quantum Computers, Algorithms and Chaos", G. Casati, D.L. Shepelyansky, and P. Zoller Eds. (2006).

[158] E. Paladino, A. Mastellone, A. DArrigo, and G. Falci, *'Optimal tuning of solid-state quantum gates: A universal two-qubit gate'* Phys. Rev. B **81**, 052502 (2010).

[159] M. Henrich, T. Legero, A. Kuhn, and G. Rempe, *'Vacuum-Stimulated Raman Scattering Based on Adiabatic Passage in a High-Finesse Optical Cavity'* Phys. Rev. Lett. **85**, 4872 (2000).

[160] M. A. Kmetic, R. A. Thuraisingham, and W. J. Meath, *'Two-level rotating-wave approximations for molecules in a static electric field with an application to rotationally averaged spectra'* Phys. Rev. A **33**, 1688 (1986).

[161] L.P. Yatsenko, V.I. Romanenko, B.W. Shore and K. Bergmann, *'Stimulated Raman adiabatic passage with partially coherent laser fields'* Phys. Rev. A **65**, 043409 (2002).

[162] P. A. Ivanov, N. V. Vitanov and K. Bergmann, *'Effect of dephasing on stimulated Raman adiabatic passage'* Phys. Rev. A **70**, 063409 (2004).

[163] G. Mangano, J. Siewert and G. Falci, *'Sensitivity to parameters of STIRAP in a Cooper Pair Box'* Eur. Phys. Journ. ST **160**, 259 (2008).

[164] S. Poletto, F Chiarello, M. G. Castellano, J. Lisenfeld, A. Lukashenko, C. Cosmelli, G. Torrioli, P. Carelli and A. V. Ustinov, *'Coherent oscillations in a superconducting tunable flux qubit manipulated without microwaves'* New Jour. Phys. **11**, 013009 (2009).

[165] G. Falci, A. Mastellone, A. D'Arrigo and E. Paladino, *'Low-Frequency Noise Characterization in Charge-Based Coherent Nanodevice'* Open Sys. & Inf. Dyn. **13**, 323 (2006).

[166] Y. Nakamura, Yu. A. Pashkin & J. S. Tsai, *'Coherent control of macroscopic quantum states in a single-Cooper-pair box'* Nature **398**, 786-788 (1999).

[167] D. Rakoczy, R. Heer, G. Strasser and J. Smoliner, *'High-energy ballistic transport in hetero- and nano-structures'* Physica E **16**, 129-136 (2003).

[168] M. Thorwart, M. Grifoni and P. Hänggi, *'Strong Coupling Theory for Tunneling and Vibrational Relaxation in Driven Bistable Systems'* Ann. Phys. **293**, 15-66 (2001).

[169] M. Thorwart, M. Grifoni and P. Hänggi, *'Strong Coupling Theory for Driven Tunneling and Vibrational Relaxation'* Phys. Rev. Lett. **85**, 860-863 (2000).

[170] A. O. Caldeira and A. J. Leggett, *'Influence of Dissipation on Quantum Tunneling in Macroscopic Systems'* Phys. Rev. Lett. **46** 211-214 (1981).

[171] A. J. Leggett, S. Chakravarty, A. T. Dorsey, M. Fisher, A. Garg, and W. Zwerger, *'Dynamics of the dissipative two-state system'* Rev. Mod. Phys. **59**, 1-85 (1987).

[172] M. Grifoni and P. Hänggi, *'Driven Tunneling'* Phys. Rep. **304**, 229-354 (1998).

[173] A. J. Leggett, *'Quantum tunneling in the presence of an arbitrary linear dissipation mechanism'* Phys. Rev. B **30**, 1208-1218 (1984).

[174] C. H. Chou, T. Yu and B. L. Hu, *'Exact master equation and quantum decoherence of two coupled harmonic oscillators in a general environment'* Phys. Rev E **77**, 011112 (2008).

[175] M. Rosenau da Costa, A. O. Caldeira, S. M. Dutra and H. Westfahl Jr., *'Exact diagonalization of two quantum models for the damped harmonic oscillator'* Phys Rev A **61**, 022107 (2000).

[176] N. V. Prokofev and P. C. E. Stamp, *'Theory of the Spin Bath'* Rep. Prog. Phys. **63**, 669726 (2000).

[177] H. P. Breuer and F. Petruccione, *The Theory of Open Quantum Systems* (Claredon Press, Oxford, 2006).

[178] J. R. Friedman, V. Patel, W. Chen, S. K. Tolpygo & J. E. Lukens et al., *'Quantum superposition of distinct macroscopic states'* Nature **406**, 43-46 (2000).

[179] J. M. Martinis, S. Nam, J. Aumentado, C. Urbina et al., *'Rabi Oscillations in a Large Josephson-Junction Qubit'* Phys. Rev. Lett. **89**, 117901 (2002).

[180] F. Grossmann, T. Dittrich, P. Jung and P. Hänggi, *'Coherent destruction of tunneling'* Phys. Rev. Lett. **67**, 516-519 (1991).

[181] R. Löfstedt and S. N. Coppersmith, *'Quantum stochastic resonance'* Phys. Rev. Lett. **72**, 1947-1950 (1994).

[182] L. Viola, E. Knill and S. Lloyd, *'Dynamical Decoupling of Open Quantum Systems'* Phys. Rev. Lett. **82**, 2417-2421 (1999).

[183] R. P. Feynman and F. L. Vernon Jr., *'The theory of a generalized quantum system interacting with a linear dissipative system'* Ann. Phys. **24**, 118-173 (1963).

[184] D. O. Harris, G. G. Engerholm and W. D. Gwinn, J. Chem. Phys. **43**, 1515-1517 (1965).

[185] R. Egger, C. H. Mak and U. Weiss, *'Rate concept and retarded master equations for dissipative tight-binding models'* Phys. Rev. E **50**, 2 (1994).

[186] M. G. A. Paris, F. Illuminati, A. Serafini and S. De Siena, *'Purity of Gaussian states: Measurement schemes and time evolution in noisy channels'* Phys. Rev. A **68**, 012314 (2003).

[187] A. Serafini, F. Illuminati, M. G. A. Paris and S. De Siena, *'Entanglement and purity of two-mode Gaussian states in noisy channels'* Phys. Rev. A **69**, 022318 (2004).

[188] A. Serafini, M. G. A. Paris, F. Illuminati and S. De Siena, *'Quantifying decoherence of continuous variable systems'* J. Opt. B **7**, R19-R36 (2005).

[189] P. Facchi, S. Tasaki, S. Pascazio, H. Nakazato, A. Tokuse and D. A. Lidar, *'Control of decoherence: Analysis and comparison of three different strategies'* Phys. Rev. A **71**, 022302 (2005).

Appendix A

Pubblications

A.1 Papers in ISI Journals

A. A. Dubkov, A. La Cognata and B. Spagnolo *'The problem of analytical calculation of barrier crossing characteristics for Lévy flights'* J. Stat. Mech.: Theo Exp P01002 (2009).

A. La Cognata, D. Valenti, B. Spagnolo and A. A. Dubkov, *'Two competing species in super-diffusive dynamical regimes'* Eur. Phys. J. B **77** 273-279 (2010).

A. La Cognata, D. Valenti, A. A. Dubkov and B. Spagnolo, *'Dynamics of two competing species in the presence of Lévy noise sources'* Phys. Rev. E **82** 011121 (2010).

A. La Cognata, P. Caldara, D. Valenti, B. Spagnolo, E. Palladino, A. D'Arrigo, G. Falci, *'Effect of low-frequency noise on adiabatic passage in a superconducting nanocircuit'* International Journal of Quantum Information, IN PRESS (2011).

P. Caldara, A. La Cognata, D. Valenti, B. Spagnolo, E. Palladino, M. Berritta, G. Falci, *'Dynamics of a quantum particle in asymmetric bistable potential with environmental noise'* International Journal of Quantum Information, IN PRESS (2011).

A.2 Proceedings

B. Spagnolo, A. Augello, P. Caldara, A. Fiasconaro, A. La Cognata, N. Pizzolato, D. Valenti, A. A. Dubkov and P. L. Pankratov, *'Noise stabilization effects in models of interdisciplinary physics'* Journal of Physics: Conference Series, IOP pubblishing **174**, 012037(13) (2009).